

2

WAVEGUIDE FOUR-WAVE MIXING

Thomas B. Simpson
Jia-ming Liu

JAYCOR
San Diego, CA 92186-5154

October 1991

Final Report

DTIC
ELECTE
NOV 26 1991
S B D

APPROVED FOR PUBLIC RELEASE; DISTRIBUTION UNLIMITED.



PHILLIPS LABORATORY
Directorate of Lasers and Imaging
AIR FORCE SYSTEMS COMMAND
KIRTLAND AIR FORCE BASE, NM 87117-6008

91-16434



91 1125 059

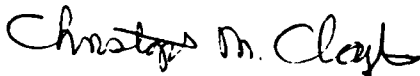
This report was prepared by JAYCOR, San Diego, California, under Contract F29601-88-C-0023, Job Order 33261B17 with the Phillips Laboratory, Kirtland Air Force Base, New Mexico. The Laboratory Project Officer-in-Charge was Christopher M. Clayton (LITN).

When Government drawings, specifications, or other data are used for any purpose other than in connection with a definitely Government-related procurement, the United States Government incurs no responsibility or any obligation whatsoever. The fact that the Government may have formulated or in any way supplied the said drawings, specifications, or other data, is not to be regarded by implication, or otherwise in any manner construed, as licensing the holder, or any other person or corporation; or as conveying any rights or permission to manufacture, use, or sell any patented invention that may in any way be related thereto.

This report has been authored by a contractor of the United States Government. Accordingly, the United States Government retains a nonexclusive, royalty-free license to publish or reproduce the material contained herein, or allow others to do so, for the United States Government purposes.

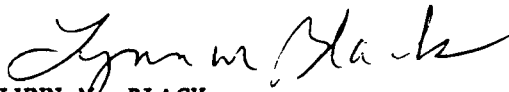
If your address has changed, or if your organization no longer employs the addressee, please notify PL/LITN, Kirtland AFB, NM 87117-6008, to help us maintain a current mailing list.

This report has been reviewed and is approved for publication.



CHRISTOPHER M. CLAYTON
Project Officer

FOR THE COMMANDER



LYNN M. BLACK
Major, USAF
Ch, Nonlinear Optics
Center of Technology



BRUCE A. CONWAY
Major, USAF
Chief, Technology Division

DO NOT RETURN COPIES OF THIS REPORT UNLESS CONTRACTUAL OBLIGATIONS OR NOTICE ON A SPECIFIC DOCUMENT REQUIRES THAT IT BE RETURNED.

REPORT DOCUMENTATION PAGE

Form Approved

OMB No. 0704-0188

Public reporting burden for this collection of information is estimated to average 1 hour per response, including the time for reviewing instructions, searching existing data sources, gathering and maintaining the data needed, and completing and reviewing the collection of information. Send comments regarding this burden estimate or any other aspect of this collection of information, including suggestions for reducing this burden, to Washington Headquarters Services, Directorate for Information Operations and Reports, 1215 Jefferson Davis Highway, Suite 1204, Arlington, VA 22202-4302, and to the Office of Management and Budget, Paperwork Reduction Project (0704-0188), Washington, DC 20503

1. AGENCY USE ONLY (Leave blank)		2. REPORT DATE 1991 October	3. REPORT TYPE AND DATES COVERED Final Report; May 88 - Mar 91	
4. TITLE AND SUBTITLE WAVEGUIDE FOUR-WAVE MIXING			5. FUNDING NUMBERS C: F29601-88-C-0023 PE: 62601F PR: 3326 TA: 1B WU: 17	
6. AUTHOR(S) Thomas B. Simpson and *Jia-ming Liu				
7. PERFORMING ORGANIZATION NAME(S) AND ADDRESS(ES) JAYCOR PO Box 85154 San Diego, CA 92186-5154			8. PERFORMING ORGANIZATION REPORT NUMBER J200-91-0080/7208	
9. SPONSORING / MONITORING AGENCY NAME(S) AND ADDRESS(ES) Phillips Laboratory Kirtland AFB, NM 87117-6008			10. SPONSORING / MONITORING AGENCY REPORT NUMBER PL-TR--91-1045	
11. SUPPLEMENTARY NOTES *Prof Jia-ming Liu is with the Electrical Engineering Department at the University of California, Los Angeles, CA 90024-159410.				
12a. DISTRIBUTION / AVAILABILITY STATEMENT Approved for public release; distribution unlimited.			12b. DISTRIBUTION CODE	
13. ABSTRACT (Maximum 200 words) This program has investigated four-wave mixing (4-wm) in non-linear waveguides, with particular emphasis on waveguides with gain and a resonant enhancement. To understand the basic physical processes which determine the formation, duration, tunability, and fidelity of the scattered optical signal, a general analytical framework was developed for studying nonlinear optical processes in waveguides based on the coupled-mode formalism. The influence of diffusion on those media where the nonlinearity is dominated by mobile particles, such as free carriers in a semiconductor under current injection, can be incorporated through a Lorentzian dependence on spatial and temporal frequency of the interacting modes. The theoretical analysis shows that there are strict limits on the speed and spatial fidelity of the phase conjugation process in a multimode waveguide. However, these limits can be relaxed through the use of an array of single-mode waveguides. Laser diodes are a particularly interesting nonlinear waveguide due to the simultaneous combination of strong nonlinearity, resonant gain, and a Fabry-Perot cavity. It is demonstrated that the action of a nearly-degenerate, weak signal beam is to phase modulate the output of a laser diode through 4-wm.				
14. SUBJECT TERMS Nonlinear Optics Waveguide Phase Conjugation Four Wave Mixing			15. NUMBER OF PAGES 112	
			16. PRICE CODE	
17. SECURITY CLASSIFICATION OF REPORT UNCLASSIFIED	18. SECURITY CLASSIFICATION OF THIS PAGE UNCLASSIFIED	19. SECURITY CLASSIFICATION OF ABSTRACT UNCLASSIFIED	20. LIMITATION OF ABSTRACT	

ACKNOWLEDGEMENTS

The authors have benefitted from many useful discussions with Dr. Chris Clayton and Dr. Tom Gavrielides of the Nonlinear Optics Group at the Phillips Laboratory. In addition, Mr. Frank Doft of JAYCOR, San Diego, CA, and Mr. Don Gianardi of Rockwell Power Systems, Albuquerque, NM, provided expert assistance in the experimental work.

Accession For	
NTIS GRA&I	<input checked="checked" type="checkbox"/>
DTIC TAB	<input type="checkbox"/>
Unannounced	<input type="checkbox"/>
Justification	
By	
Distribution/	
Availability Codes	
Dist	Avail and/or Special
A-1	



CONTENTS

	<u>Page</u>
1.0 SUMMARY	1
2.0 INTRODUCTION	3
2.1 BACKGROUND	4
3.0 COUPLED-MODE THEORY FOR NONLINEAR WAVEGUIDES	6
3.1 INTRODUCTION	6
3.2 WAVE EQUATIONS	7
3.3 NORMAL MODES OF THE LINEAR WAVEGUIDE	10
3.4 NONLINEAR COUPLED-MODE EQUATIONS	17
3.5 DISCUSSION	23
4.0 EFFECT OF CARRIER DIFFUSION ON PHASE CONJUGATE FOUR-WAVE MIXING IN SEMICONDUCTOR WAVEGUIDES	27
4.1 INTRODUCTION	27
4.2 CARRIER-INDUCED POLARIZATIONS	29
4.3 EFFECT OF CARRIER DIFFUSION	36
4.4 DEGENERATE FOUR-WAVE MIXING	47
4.5 CONCLUSIONS	50
5.0 CONJUGATE GENERATION REQUIREMENTS IN MULTIMODE WAVEGUIDES AND THE UTILITY OF WAVEGUIDE ARRAYS	53
5.1 INTRODUCTION	53
5.2 MULTIMODE WAVEGUIDE PHASE-CONJUGATION REQUIREMENTS	53
5.3 FOUR-WAVE MIXING IN A WAVEGUIDE ARRAY	57
6.0 EXPERIMENTS ON OPTICAL FIBERS AND LASER DIODES	64
6.1 INTRODUCTION	64
6.2 FIBER NONLINEAR BIREFRINGENCE EXPERIMENT	64
6.3 LASER DIODE EXPERIMENTS	73
7.0 CONCLUSIONS	95
REFERENCES	98
APPENDIXES	
A. DOT PRODUCT ORTHOGONALITY RELATIONS	101
B. ITERATIVE PROCEDURE FOR E WHEN $P_z^{NL} \neq 0$	103

FIGURES

<u>Figure</u>	<u>Page</u>
1. Schematic illustrations of two arrangements for generating an optical beam, E, which is PC to an input beam by 4-wm with pump beams G and H (Ref. 11).	5
2. Schematic diagram of PC 4-wm with a multimode waveguide.	30
3. Waveguide cross section.	30
4. Geometry for 4-wm in a waveguide array with incident pump beams E_1 and E_2 , signal beam E_s , and generated beam E_c .	57
5. Schematic of the experimental configuration investigating polarization effects in single-mode fibers.	65
6. The polarization ratio as a function of output power from the fiber for the p-polarized input light.	67
7. The polarization ratio, the maximum to minimum transmitted intensity ratio determined by rotating a polarizer, as a function of input power.	68
8. The ellipse rotation as a function of output power for orthogonally polarized inputs.	69
9. A schematic of the modified experimental apparatus used to illustrate the effects of polarization scrambling on interference measurements.	70
10. Oscilloscope trace of the fast photodiode output using the apparatus shown in Figure 9. Average power through the fiber is 100 mW.	71
11. Oscilloscope trace of the fast photodiode output using the apparatus shown in Figure 9. Average power through the fiber is 300 mW.	72
12. Schematic of the experimental arrangement for 4-wm in laser diodes.	75
13. Optical spectrum analyzer trace using the apparatus shown in Figure 12. The upper trace is an offset, 100x expansion of the lower trace.	77
14. Optical spectrum analyzer trace using the apparatus shown in Figure 12, except that the direct optical path from laser diode #1 to the beamsplitter has been blocked. The upper trace is an offset, 100x expansion of the lower trace.	78

FIGURES (CONTINUED)

	<u>Page</u>
15. Radio frequency spectrum analyzer trace using the apparatus shown in Figure 12.	79
16. Radio frequency spectrum analyzer trace using the apparatus shown in Figure 12 when the two laser diodes are phase locked.	81
17. Radio frequency spectrum analyzer trace using the apparatus shown in Figure 12 when the two laser diodes have a frequency difference of ~80 MHz.	82
18. Radio frequency spectrum analyzer trace using the apparatus shown in Figure 12 when laser diode #2 operates at a higher frequency than laser diode #1.	83
19. Optical spectrum analyzer trace of the output from laser diode #2 when the injection frequency is offset by ~8 GHz. The upper trace is a 50x expansion of the lower trace.	84
20. Optical spectrum analyzer trace of the output from laser diode #2 when the injection frequency is offset by the relaxation resonance frequency. The upper trace is a 10x expansion of the lower trace.	85
21. Optical spectrum analyzer trace of the output from laser diode #2 when the injection frequency is offset by ~3 GHz. The upper trace is a 25x expansion of the lower trace.	86
22. Optical spectrum analyzer trace of the output from laser diode #2 when the injection frequency is offset by ~1 GHz. The upper trace is a 10x expansion of the lower trace.	87
23. Optical spectrum analyzer trace of the output from laser diode #2 when it is phase locked. The upper trace is a 10x expansion of the lower trace.	88
24. Optical spectrum analyzer trace showing the free-running output of the Sharp LT015 laser diode with its relatively strong resonance sidebands at $\sim \pm 3$ GHz.	90
25. Optical spectrum analyzer trace showing the Sharp LT015 laser diode under strong optical injection ~10 GHz below the main peak.	91
26. Optical spectrum analyzer trace showing the LT015 laser diode under strong optical injection ~6 GHz below the free-running frequency.	92

FIGURES (CONCLUDED)

	<u>Page</u>
27. Optical spectrum analyzer trace showing the LT015 laser diode under strong optical injection ~3 GHz below the free-running frequency.	93
28. Optical spectrum analyzer trace showing the LT015 laser diode under strong optical injection ~3 GHz above the free-running frequency.	94

1.0 SUMMARY

This program has investigated four-wave mixing (4-wm) in nonlinear waveguides, with particular emphasis on waveguides with gain and a resonant enhancement. In 4-wm a signal or probe beam is scattered off of a grating induced in a nonlinear medium due to interaction with two pump beams. Under appropriate conditions, the scattered beam will be an amplified phase-conjugate (PC) or frequency-shifted replica of the signal beam. Such a scattered beam has applications in laser device phase locking, beam steering, and optical computing. Phase conjugation by 4-wm in nonlinear waveguide with gain and/or a resonant enhancement has the potential to be a high-speed process requiring only modest power levels.

To understand the basic physical processes which determine the formation, duration, tunability, and fidelity of the scattered optical signal, a general analytical framework has been developed for studying nonlinear optical processes in waveguides based on the coupled-mode formalism. This approach has the advantage of developing a model of 4-wm which is similar to the coupled-wave formalism used to describe nonlinear optics in bulk media. The influence of diffusion on those media where the nonlinearity is dominated by mobile particles, such as free carriers in a semiconductor under current injection, can be incorporated through a Lorentzian dependence on spatial and temporal frequency of the interacting modes. Our theoretical analysis shows that there are strict limits on the speed and spatial fidelity of the phase conjugation process in a multimode waveguide. However, these limits can be relaxed by using an array of single-mode waveguides.

The theoretical framework gives as a requirement for maximum possible fidelity in conjugate generation, that there be no degeneracy among the guided modes. An experiment using an optical fiber showed that the degeneracy between the two orthogonal polarizations in the circularly symmetric medium leads to polarization scrambling through both linear inhomogeneities as well as nonlinear interaction. Polarization scrambling reduces fidelity and complicates the analysis of the nonlinear interaction.

Laser diodes are a particularly interesting nonlinear waveguide due to the simultaneous combination of strong nonlinearity, resonant gain, and a Fabry-Perot cavity. Previous work has shown conjugate signal generation with intensities 1,000-fold larger than the input signal intensity. It has been demonstrated that the action of a nearly-degenerate, weak signal beam is to phase modulate the output of a laser diode through 4-wm. To be a phase modulation, the 4-wm signal must be essentially equal in amplitude with the amplified input signal and maintain a specific phase relationship with respect to the input signal and the counterpropagating pump beams. In the semiconductor medium under current injection, the nonlinearity acts to minimize carrier fluctuations induced by the probe beam through the generation of a conjugate beam, oppositely shifted in frequency with respect to the free-running diode.

2.0 INTRODUCTION

Nonlinear optical processes using 4- μm in bulk media have been demonstrated and studied in a variety of applications (Ref. 1). Recently, much of the scientific work has gone into the investigation of photorefractive materials such as BaTiO_3 . Four-wave mixing in photorefractive materials can be achieved at low intensities relative to media using other nonresonant properties or stimulated Raman or Brillouin scattering (Ref. 1). There have been a variety of studies showing application of 4- μm in BaTiO_3 to the multiple coupling and locking of lasers (Refs. 2, 3, and 4), beam steering (Ref. 5), and optical computing (Refs. 6 and 7). However, there are stringent bounds on the speed of photorefractive materials at low laser intensity (Ref. 8) due to the time required for the photo-generated carriers to achieve sufficient density and separation to create the internal electric field. Since many applications demand high speed and modest power levels, there are limitations on the utility of bulk materials in 4- μm applications.

Phase conjugation by 4- μm in waveguides containing a nonlinear medium with gain and/or a resonantly enhanced nonlinearity would not be limited by these considerations. Four-wave mixing in waveguides was originally investigated to take advantage of the waveguide's capability to maintain high intensity over a long interaction length and the guide's reduced alignment requirements (Refs. 9-12). Following these initial reports, there was no further activity for several years because there were no suitable nonlinear materials (Ref. 13). Recently, there has been a report of 4- μm in a semiconductor laser (Ref. 14) and an observation of large optical nonlinearities in GaAs/AlGaAs multiple quantum wells (MQW) (Ref. 15). Subsequent analysis of the 4- μm in the semiconductor laser has not included the effects of the guided-wave structure (Refs. 16-19) and there have been no studies of 4- μm using the MQW excitonic resonance in waveguides. A theoretical study is proposed to make the connection between the new semiconductor materials, with gain and resonant enhancement, and the particular requirements and advantages imposed by multi-mode waveguides, as outlined by Hellwarth (Ref. 11), on the problem of 4- μm . The goal of this study is to understand the basic physics involved, with attention to the feasibility of the system to applications such as laser coupling and phase locking.

2.1 BACKGROUND

Hellwarth's article was the first to show the general utility of "generation of a PC of a free wave at the entrance of a waveguide" (Ref. 11). The system is depicted schematically in Figure 1. His analysis pointed out that as long as the pump and probe beams occupy many modes and are well guided, the output of the 4-wm process will be the PC beam. Further, beam alignment is not critical; it is only necessary to inject the beams into the guiding modes. Simultaneously, experimental work demonstrated the advantages of the long path length, high intensity interaction region possible in waveguides (Refs. 10 and 12). Lower pump levels relative to bulk media were possible, but the ratio of conjugate beam power to input beam power was less than unity. The waveguide medium, CS_2 , did not have a sufficiently strong nonlinearity to produce stronger outputs. For this reason, the theoretical analysis was limited to the regime of small conjugate reflectivities. Subsequent work showed equally small conjugate reflectivities in waveguides where CS_2 was used as the cladding, rather than guiding, medium (Ref. 20).

The recent observation of 4-wm in an AlGaAs semiconductor laser showed conjugate reflectivities approaching 10^4 due to the resonant enhancement and gain in the laser medium (Ref. 14). The nonlinearity, created by carrier-density modulated index gratings, has a response time governed by carrier spontaneous lifetimes, independent of excitation intensity (Ref. 18). These lifetimes are on the order of 1 ns in III-V semiconductors. Recent calculations show that response times as short as 10 ps are possible in semiconductor lasers (Ref. 19). The theoretical modeling of the single-mode laser diode structures has focused on the nonlinear semiconductor medium without considering the waveguiding aspects of the interaction (Refs. 16-19). Therefore, the connection remained to be made between these recent materials studies and the issues of 4-wm in multimode waveguides raised by Hellwarth.

This program has addressed the issue of conjugate generation through 4-wm in waveguides containing both nonlinearity and resonant amplification. A general formalism for studying waveguide nonlinear optics is developed in Section 3.0. The effects of carrier diffusion are analyzed in Section 4.0. These topics have been summarized in two publications (Refs. 21 and 22). Section 5.0 reviews some of the factors which limit the speed and fidelity of conjugate

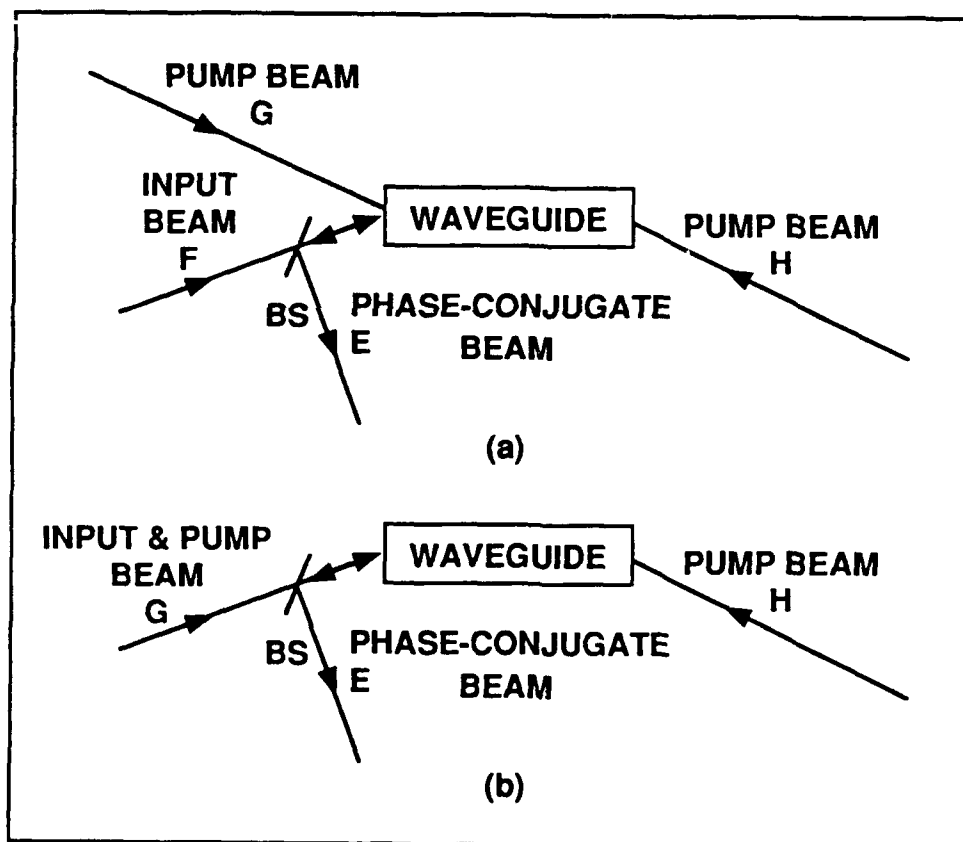


Figure 1. Schematic Illustrations of two arrangements for generating an optical beam, E, which is PC to an input beam by 4-wm with pump beams G and H (Ref. 11). a) Three-beam configuration with F being phase conjugated. If the waveguide is a laser, G and H are the intracavity oscillating beams (Ref. 14). b) Two beam configuration where one of the pump beams, G, is phase conjugated.

formation in a nonlinear waveguide. An array of multimode waveguides is proposed as a way to overcome these limits (Ref. 23). The array format shows that the nonlinearity in laser diodes can be used for conjugate formation. The results of experimental investigations of 4-wm in laser diodes are described in Section 6.0, along with experiments on optical fibers. The laser diode work shows that the action of an injected, nearly-degenerate signal is to phase modulate the optical output in a way that works to minimize the fluctuations of free carriers in the device. The fiber work illustrates some complicating effects of polarization on the nonlinear interaction in a system where the two orthogonal polarizations yield nearly degenerate modes. Section 7.0 summarizes the results of the program and suggests directions for future research.

3.0 COUPLED-MODE THEORY FOR NONLINEAR WAVEGUIDES

3.1 INTRODUCTION

The unique nonlinear optical effects in waveguides have recently become an area of intensive research (Ref. 24). Because of the optical confinement in a waveguide, guided optical waves can maintain high-power densities over a long distance for efficient nonlinear optical interactions at relatively low total power levels. Many important optical systems, such as optical communications and signal processing systems, involve guided-wave optics. Many desirable optical operations, such as optical PC, optical bistability, and optical switching, require nonlinear optical interactions. It is therefore important to understand the nonlinear optical wave behavior, including the propagation and coupling of the optical fields, in the waveguides.

There has been some recent work on the propagation and coupling of optical waves in nonlinear waveguides (Refs. 24-26) and nonlinear couplers (Refs. 27 and 28). Usually the techniques used are coupled-mode theory (Refs. 29-31) and beam-propagation method (Refs. 32-34). Strictly speaking, the concept of normal modes is applicable only for linear waveguides. The extension of the coupled-mode theory to nonlinear waveguides is a good approximation only when the nonlinear polarization is relatively small compared to the input fields. On the other hand, the beam-propagation method is not limited by this restriction and can be a more accurate approach for nonlinear waveguides. However, the beam-propagation method is formulated in terms of a scalar field (Refs. 32-34). This restricts the method to cases in which the electromagnetic (EM) fields can be separated into linearly polarized components, such as the transverse electric (TE) and transverse magnetic (TM) modes in slab waveguides, so that scalar-wave equations can be used to describe the problem. In many practical cases, such as optical-fiber waveguides with a circular or elliptical cross section and waveguides with a strong confinement, the polarization of the guided fields can become very complicated. Then the beam-propagation method becomes limited while the coupled-mode approach may still be good so long as the nonlinearity is not very large. It appears that each of these two methods has its own advantages and limitations and should be used in different situations.

Past work applying the coupled-mode formalism to nonlinear waveguides has assumed a real, isotropic dielectric constant and negligible contribution to the nonlinear polarization from the longitudinal field components (Refs. 24-27). However, many practical optical waveguides are fabricated with anisotropic materials, such as LiNbO_3 . Because of the tensorial nature of nonlinear susceptibilities, the longitudinal component of the nonlinear polarization can be significant in a nonlinear waveguide. Recently, there is also much interest in nonlinear waveguides with an active gain, i.e., with a complex dielectric constant, such as III-V semiconductor waveguides under current injection (Refs. 14, 17, and 35). This report considers the coupled-mode approach for nonlinear waveguides formally for various conditions of interest, including anisotropic waveguides and waveguides with a gain or loss.

3.2 WAVE EQUATIONS

The EM fields in a nonlinear waveguide are governed by the following Maxwell's equations,

$$\nabla \times \mathbf{E} = - \frac{1}{c} \frac{\partial \mathbf{H}}{\partial t} \quad (1)$$

$$\nabla \times \mathbf{H} = \frac{1}{c} \frac{\partial \mathbf{E}}{\partial t} + \frac{4\pi}{c} \frac{\partial \mathbf{P}}{\partial t} \quad (2)$$

$$\nabla \cdot (\mathbf{E} + 4\pi \mathbf{P}) = 0 \quad (3)$$

$$\nabla \cdot \mathbf{H} = 0 \quad (4)$$

where the material is assumed nonmagnetic so that $\mathbf{B} = \mathbf{H}$. The total polarization is given by the sum of the linear and nonlinear polarizations (Ref. 25)

$$\mathbf{P}(\mathbf{r}, t) = \mathbf{P}^L(\mathbf{r}, t) + \mathbf{P}^{NL}(\mathbf{r}, t) \quad (5)$$

where

$$\mathbf{P}^L(\mathbf{r}, t) = \int_{-\infty}^{\infty} \chi^{(1)}(\mathbf{r} - \mathbf{r}', t - t') \cdot \mathbf{E}(\mathbf{r}', t') d\mathbf{r}' dt' \quad (6)$$

$$\begin{aligned} \mathbf{P}^{NL}(\mathbf{r}, t) = & \int_{-\infty}^{\infty} \chi^{(2)}(\mathbf{r} - \mathbf{r}_1, t - t_1; \mathbf{r} - \mathbf{r}_2, t - t_2) \\ & : \mathbf{E}(\mathbf{r}_1, t_1) \mathbf{E}(\mathbf{r}_2, t_2) d\mathbf{r}_1 d\mathbf{r}_2 dt_1 dt_2 \\ & + \int_{-\infty}^{\infty} \chi^{(3)}(\mathbf{r} - \mathbf{r}_1, t - t_1; \mathbf{r} - \mathbf{r}_2, t - t_2; \mathbf{r} - \mathbf{r}_3, t - t_3) \\ & : \mathbf{E}(\mathbf{r}_1, t_1) \mathbf{E}(\mathbf{r}_2, t_2) \mathbf{E}(\mathbf{r}_3, t_3) d\mathbf{r}_1 d\mathbf{r}_2 d\mathbf{r}_3 dt_1 dt_2 dt_3 + \dots \end{aligned} \quad (7)$$

At a given frequency ω , the electric and magnetic fields are

$$\mathbf{E}(\mathbf{r}, t) = \mathbf{E}(\mathbf{r}, \omega) \exp(-i\omega t) + \mathbf{E}^*(\mathbf{r}, \omega) \exp(i\omega t) \quad (8)$$

$$\mathbf{H}(\mathbf{r}, t) = \mathbf{H}(\mathbf{r}, \omega) \exp(-i\omega t) + \mathbf{H}^*(\mathbf{r}, \omega) \exp(i\omega t) \quad (9)$$

and the complex polarization, $\mathbf{P}(\mathbf{r}, \omega)$, is similarly defined. In case the linear and nonlinear electric susceptibilities are temporally nonlocal but spatially local functions, they depend on the light frequency but not on the wave propagation constants. Then, one can write the nonlinear Maxwell's equations in terms of $\mathbf{E}(\mathbf{r}, \omega)$, $\mathbf{H}(\mathbf{r}, \omega)$, and $\mathbf{P}^{NL}(\mathbf{r}, \omega)$ in the frequency domain,

$$\nabla \times \mathbf{E} = \frac{i\omega}{c} \mathbf{H} \quad (10)$$

$$\nabla \times \mathbf{H} = -\frac{i\omega}{c} \epsilon \cdot \mathbf{E} - \frac{i4\pi\omega}{c} \mathbf{P}^{NL} \quad (11)$$

$$\nabla \cdot (\epsilon \cdot \mathbf{E} + 4\pi \mathbf{P}^{NL}) = 0 \quad (12)$$

$$\nabla \cdot \mathbf{H} = 0 \quad (13)$$

The linear and nonlinear polarizations in the frequency domain are given by

$$\mathbf{P}^L(\mathbf{r}, \omega) = \chi^{(1)}(\mathbf{r}, \omega) \cdot \mathbf{E}(\mathbf{r}, \omega) \quad (14)$$

$$\begin{aligned} \mathbf{P}^{NL}(\mathbf{r}, \omega) = & \chi^{(2)}(\mathbf{r}, \omega = \omega_1 + \omega_2) : \mathbf{E}(\mathbf{r}, \omega_1) \mathbf{E}(\mathbf{r}, \omega_2) \\ & + \chi^{(3)}(\mathbf{r}, \omega = \omega_1 + \omega_2 + \omega_3) : \mathbf{E}(\mathbf{r}, \omega_1) \mathbf{E}(\mathbf{r}, \omega_2) \mathbf{E}(\mathbf{r}, \omega_3) \\ & + \dots \end{aligned} \quad (15)$$

The linear dielectric constant is in general a 3 x 3 tensor defined by

$$\epsilon(\mathbf{r}, \omega) = 1 + 4\pi\chi^{(1)}(\mathbf{r}, \omega) \quad (16)$$

so that

$$\mathbf{E} + 4\pi\mathbf{P}^L = \epsilon \cdot \mathbf{E} \quad (17)$$

in the frequency domain. Here the *local* spatial dependence of χ and ϵ accounts for the spatial variation of material properties in the waveguide structure.

In what follows, take the z -coordinate as the longitudinal direction of the waveguide. The fields can be separated into the transverse components in the cross-sectional xy -plane and the longitudinal components parallel to the z -direction of wave propagation in the waveguide,

$$\mathbf{E} = \mathbf{E}_T + \mathbf{E}_z \quad (18)$$

$$\mathbf{H} = \mathbf{H}_T + \mathbf{H}_z \quad (19)$$

and the operator ∇ can be written as $\nabla = \nabla_T + \partial/\partial z$. Notice that the third and fourth Maxwell's equations (Eqs. 12 and 13) can be obtained by taking the divergence of the second and first Maxwell's equations (Eqs. 11 and 10), respectively, and do not provide more information than that obtained from the first two Maxwell's equations alone. Therefore, in most situations do not invoke them in the formulation of the problem.

3.3 NORMAL MODES OF THE LINEAR WAVEGUIDE

Without the nonlinearity, there exists a complete set of normal modes of the waveguide structure. When $\epsilon(r, \omega)$ does not have z -dependence, at frequency ω each normal mode is characterized by a set of mode fields,

$$\mathbf{E}_a(\mathbf{r}, t) = \boldsymbol{\Psi}_a(x, y) \exp(i\beta_a z - i\omega t) + \boldsymbol{\Psi}_a^*(x, y) \exp(-i\beta_a^* z + i\omega t) \quad (20)$$

$$\mathbf{H}_a(\mathbf{r}, t) = \boldsymbol{\Phi}_a(x, y) \exp(i\beta_a z - i\omega t) + \boldsymbol{\Phi}_a^*(x, y) \exp(-i\beta_a^* z + i\omega t) \quad (21)$$

where β_a is the propagation constant of the a th mode. These normal mode fields propagate in the z -direction and satisfy the linear Maxwell's equations, which are obtained by setting $\mathbf{P}^{NL} = 0$ in Equations 1-4, with appropriate boundary conditions determined by the waveguide structure.

The complex mode fields of the a th mode at the frequency ω are

$$\begin{aligned} \mathbf{E}_a(\mathbf{r}, \omega) &= \boldsymbol{\Psi}_a(x, y) \exp(i\beta_a z) = \boldsymbol{\Psi}_{aT}(x, y) \exp(i\beta_a z) \\ &+ \boldsymbol{\Psi}_{aZ}(x, y) \exp(i\beta_a z) \end{aligned} \quad (22)$$

$$\begin{aligned} \mathbf{H}_a(\mathbf{r}, \omega) &= \boldsymbol{\Phi}_a(x, y) \exp(i\beta_a z) = \boldsymbol{\Phi}_{aT}(x, y) \exp(i\beta_a z) \\ &+ \boldsymbol{\Phi}_{aZ}(x, y) \exp(i\beta_a z) \end{aligned} \quad (23)$$

where $\boldsymbol{\Psi}_{aT} = \psi_{ax}\hat{x} + \psi_{ay}\hat{y}$ and $\boldsymbol{\Psi}_{aZ} = \psi_{az}\hat{z}$. These complex-mode fields satisfy Equations 10-13 with $\mathbf{P}^{NL} = 0$. With the complex normal mode fields in Equations 22 and 23 and from the first two linear Maxwell's equations decomposed into longitudinal and transverse components, one has

$$\boldsymbol{\Psi}_{aZ} = -\frac{c}{i\omega\epsilon_{zz}} \nabla_T \times \boldsymbol{\Phi}_{aT} - \frac{1}{\epsilon_{zz}} \epsilon_z \cdot \boldsymbol{\Psi}_{aT} \quad (24)$$

$$\epsilon_T \cdot \boldsymbol{\Psi}_{aT} + \epsilon_T \cdot \boldsymbol{\Psi}_{aZ} = -\frac{c}{i\omega} (\nabla_T \times \boldsymbol{\Phi}_{aZ} + i\beta_a \hat{z} \times \boldsymbol{\Phi}_{aT}) \quad (25)$$

$$\varphi_{az} = \frac{c}{i\omega} \nabla_T \times \psi_{aT} \quad (26)$$

$$\varphi_{aT} = \frac{c}{i\omega} (\nabla_T \times \psi_{az} + i\beta_a \hat{z} \times \psi_{aT}) \quad (27)$$

In Equations 24-27, $\epsilon = \epsilon_x + \epsilon_y + \epsilon_z = \epsilon_T + \epsilon_z$ was used with the following definition

$$\epsilon_x \cdot \mathbf{E} = \hat{x} (\epsilon_{xx} E_x + \epsilon_{xy} E_y + \epsilon_{xz} E_z) \quad (28)$$

$$\epsilon_y \cdot \mathbf{E} = \hat{y} (\epsilon_{yx} E_x + \epsilon_{yy} E_y + \epsilon_{yz} E_z) \quad (29)$$

$$\epsilon_z \cdot \mathbf{E} = \hat{z} (\epsilon_{zx} E_x + \epsilon_{zy} E_y + \epsilon_{zz} E_z) \quad (30)$$

Since the coupled-mode theory is based upon the linear normal modes of the waveguide, the properties of these normal modes will be examined before using them to formulate the problem involving nonlinearity in the waveguide.

3.3.1 Backward-Propagating Modes

For each normal mode, a backward-propagation mode can be constructed by time-reversal or space-inversion in the z-direction or both, depending on the property of the waveguide material, i.e., the property of ϵ . Since only nonmagnetic (reciprocal) materials are considered in this report, the dielectric tensor is symmetric, $\epsilon_{kj} = \epsilon_{jk}$ (Ref. 36), but it can be anisotropic as well as complex. In the following, the subscript -a will be used to represent the mode propagating in the backward direction with respect to the mode with the subscript a which propagates in the positive z-direction. Certain useful properties of the modes can be obtained by considering the relationship between the forward- and backward-propagating modes.

CASE 1. ϵ is real, $\epsilon(\omega) = \epsilon^*(\omega)$, but it can be a general 3 x 3 tensor with nonvanishing real elements. This includes the case when the waveguide material is real but anisotropic.

In this case, time-reversal can be used, but not z-inversion, to construct the backward-propagating modes from the forward-propagating modes. By replacing time t with $-t$ for time-reversal in the linear Maxwell's equations for the normal modes, the following relations are obtained

$$\psi_{-a} = \psi_a^* \quad (31)$$

$$\varphi_{-a} = -\varphi_a^* \quad (32)$$

and

$$\beta_{-a} = -\beta_a^* \quad (33)$$

For the propagating modes, β_a is real and there is a corresponding backward-propagating mode with $\beta_{-a} = -\beta_a$. For the evanescent modes, $\beta_{-a} = \beta_a = i\beta_a''$ is purely imaginary and there is no separate backward evanescent modes.

CASE 2. $\epsilon(z) = \epsilon(-z)$ or ϵ is cylindrically symmetric with respect to the z-axis. The tensor elements of $\epsilon(\omega)$ can be complex, i.e., the waveguide has gain or loss.

In this case, the longitudinal z-axis of the waveguide is along one of the principal axes of the material, or the tensor ϵ can be transformed to a form of cylindrical symmetry

$$\epsilon = \begin{pmatrix} \epsilon_{xx} & \epsilon_{xy} & 0 \\ \epsilon_{yx} & \epsilon_{yy} & 0 \\ 0 & 0 & \epsilon_{zz} \end{pmatrix} \quad (34)$$

Then, z-inversion can be used, but not time-reversal, to construct the backward-propagating modes from the forward-propagating modes by replacing z with $-z$ in the linear Maxwell's equations for the normal modes. The following relations are obtained

$$\psi_{-aT} = \psi_{aT}, \quad \psi_{-az} = -\psi_{az} \quad (35)$$

$$\varphi_{-aT} = -\varphi_{aT}, \quad \varphi_{-az} = \varphi_{az} \quad (36)$$

and

$$\beta_{-a} = -\beta_a \quad (37)$$

where ψ_a , φ_a , and $\beta_a = \beta'_a + i\beta''_a$ are all complex in general.

CASE 3. ϵ is both real and cylindrically symmetrical with respect to the waveguide longitudinal z -axis, i.e., $\epsilon(\omega) = \epsilon^*(\omega)$ and $\epsilon(z) = \epsilon(-z)$. This includes the simplest situation when ϵ is real and isotropic.

In this case, both time-reversal and z -inversion apply and the results in CASE 1 and CASE 2 can be combined to obtain the following relations

$$\psi_{aT} = \psi_{aT}^* = \psi_{-aT} = \psi_{-aT}^* = \text{real} \quad (38)$$

$$\psi_{az} = -\psi_{az}^* = -\psi_{-az} = \psi_{-az}^* = \text{purely imaginary} \quad (39)$$

$$\varphi_{aT} = \varphi_{aT}^* = -\varphi_{-aT} = -\varphi_{-aT}^* = \text{real} \quad (40)$$

$$\varphi_{az} = -\varphi_{az}^* = \varphi_{-az} = -\varphi_{-az}^* = \text{purely imaginary} \quad (41)$$

and

$$\beta_{-a} = -\beta_a = \text{real for propagating modes} \quad (42)$$

$$\beta_{-a} = \beta_a = \text{purely imaginary for evanescent modes} \quad (43)$$

CASE 4. $\epsilon(\omega) \neq \epsilon^*(\omega)$ and $\epsilon(z) \neq \epsilon(-z)$.

The material has a linear loss or gain and does not have a cylindrically-symmetrical optical property with respect to the waveguide z -direction. In

this case, both time-reversal and z-inversion do not apply and no simple relations can be obtained for the mode fields and propagation constants between the forward- and backward-propagating modes.

3.3.2 Orthogonality and Normalization

The linear normal modes of a waveguide form a complete orthonormal set. However, the orthogonality relations between the normal modes depend on the property of the waveguide material. The orthogonality and normalization conditions can be derived for each case discussed earlier using the results in Equations 31-43 and the reciprocity of the fields in a nonmagnetic medium where ϵ is symmetric. The *Lorentz reciprocity theorem* states that at any point for which the fields are source-free there is the relation (Ref. 37)

$$\nabla \cdot (\mathbf{E}_1 \times \mathbf{H}_2 - \mathbf{E}_2 \times \mathbf{H}_1) = 0 \quad (44)$$

for any two sets of EM fields at the same frequency existing in the same linear, reciprocal medium. Taking $\mathbf{E}_1 = \psi_1 \exp(i\beta_1 z)$, $\mathbf{H}_1 = \varphi_1 \exp(i\beta_1 z)$, and $\mathbf{E}_2 = \psi_2 \exp(i\beta_2 z)$, $\mathbf{H}_2 = \varphi_2 \exp(i\beta_2 z)$ for the fields of any two normal modes and integrating Equation 44 over the waveguide structure, one gets (Ref. 38)

$$(\beta_1 + \beta_2) \iint dx dy \hat{z} \cdot (\psi_{1T} \times \varphi_{2T} - \psi_{2T} \times \varphi_{1T}) = 0 \quad (45)$$

in terms of the transverse-mode field components.

CASE 1. $\epsilon(\omega) = \epsilon^*(\omega)$, real but anisotropic.

Taking 1 = a and 2 = -b for Equation 45 and using Equations 31-33, one gets

$$(\beta_a - \beta_b) \iint dx dy \hat{z} \cdot (\psi_{aT} \times \varphi_{bT}^* + \psi_{bT}^* \times \varphi_{aT}) = 0 \quad (46)$$

If both modes are propagating modes, β_a and β_b are both real and $\beta_b^* = \beta_b$. The following orthogonality relation is obtained

$$\iint dx dy \hat{z} \cdot (\psi_{aT} \times \phi_{bT}^* + \psi_{bT}^* \times \phi_{aT}) = \pm 2 \delta_{ab} \quad (47)$$

The factor 2 in the above equation is introduced to give the modes the following normalization,

$$\iint dx dy \hat{z} \cdot \text{Re}(\psi_{aT} \times \phi_{aT}^*) = \iint dx dy \hat{z} \cdot \text{Re}(\psi_a \times \phi_a^*) = \pm 1 \quad (48)$$

In Equations 47 and 48, the positive sign is used if mode a propagates in the positive z -direction and the negative sign corresponds to mode a propagating backward. Notice that $\delta_{ab} = 0$ if $a = -b$ in Equation 47. The backward-propagating mode is orthogonal to its corresponding forward-propagating mode in this case with anisotropic media.

For the evanescent modes, β becomes purely imaginary. From Equation 46, if one or both of the modes are evanescent, the integral in Equation 47 vanishes even when $a = b$. This is because both terms in the integrand of Equation 47 become purely imaginary and are complex conjugate of each other when $a = b$ for evanescent modes. Therefore, the normalization condition for the evanescent modes is

$$\iint dx dy \hat{z} \cdot \psi_{aT} \times \phi_{aT}^* = \iint dx dy \hat{z} \cdot \psi_a \times \phi_a^* = i \quad (49)$$

The integral in Equation 48 vanishes for evanescent modes since the evanescent modes cannot propagate and do not carry power (Ref. 37).

CASE 2. $\epsilon(z) = \epsilon(-z)$, cylindrically symmetric but complex.

Taking 1 = a and 2 = $-b$ for Equation 45 and using Equations 35-37, one gets

$$(\beta_a - \beta_b) \iint dx dy \hat{z} \cdot (\psi_{aT} \times \phi_{bT} + \psi_{bT} \times \phi_{aT}) = 0 \quad (50)$$

Taking $1 = a$ and $2 = b$, one obtains

$$(\beta_a + \beta_b) \iint dx dy \hat{z} \cdot (\psi_{aT} \times \phi_{bT} - \psi_{bT} \times \phi_{aT}) = 0 \quad (51)$$

Multiplying Equations 50 and 51 by $\beta_a + \beta_b$ and $\beta_a - \beta_b$, respectively, and summing the results, the orthogonality relation obtained is

$$\iint dx dy \hat{z} \cdot \psi_{aT} \times \phi_{bT} = 0, \text{ if } \beta_a \neq \pm \beta_b \quad (52)$$

If one takes mode a to propagate in the positive z -direction and uses Equations 35-37, one can normalize the mode fields to get

$$\begin{aligned} \iint dx dy \hat{z} \cdot \psi_{aT} \times \phi_{aT} &= - \iint dx dy \hat{z} \cdot \psi_{aT} \times \phi_{-aT} \\ &= \iint dx dy \hat{z} \cdot \psi_{-aT} \times \phi_{aT} \\ &= - \iint dx dy \hat{z} \cdot \psi_{-aT} \times \phi_{-aT} = 1 \end{aligned} \quad (53)$$

Since the mode fields ψ and ϕ are complex in this case, normalization to yield Equation 53 will involve complex normalization constants. Notice that different from the orthogonality relations in CASE 1, the forward and corresponding backward-propagating modes are not orthogonal in this case and the orthogonality and normalization relations in Equations 52 and 53 are in terms of ψ_{aT} and ϕ_{bT} , instead of ψ_{aT} and ϕ_{bT}^* .

CASE 3. $\epsilon(\omega) = \epsilon^*(\omega)$ and $\epsilon(z) = \epsilon(-z)$.

In this case, both ψ_{aT} and ϕ_{aT} are real and Equations 47 and 52 are equivalent. Also, Equation 48 is equivalent to Equation 53. Then the orthogonality and normalization relations are the same as those in Equations 52 and 53, but with

$$\iint dx dy \hat{z} \cdot \psi_{aT} \times \phi_{bT} = \iint dx dy \hat{z} \cdot \psi_{aT} \times \phi_{bT}^* \quad (54)$$

Equation 49 applies for evanescent modes in this case, too.

CASE 4. $\epsilon(\omega) \neq \epsilon^*(\omega)$ and $\epsilon(z) \neq \epsilon(-z)$.

In this case, there are no simple relations between the field components between the forward- and backward-propagating modes. The orthogonality relations can only be derived directly from Equation 45.

The orthogonality relations derived in this section are in terms of the cross products of the transverse-mode fields. Orthogonality relations can also be obtained in terms of the dot products of the mode fields in CASES 2 and 3 and are given in Appendix A.

3.4 NONLINEAR COUPLED-MODE EQUATIONS

The nonlinear fields are solutions of the nonlinear Maxwell's equations (Eqs. 10-13). Since Equations 12 and 13 are not independent of Equations 10 and 11, only Equations 10 and 11 have to be used, which can be decomposed into longitudinal and transverse components,

$$\mathbf{E}_z = -\frac{c}{i\omega\epsilon_{zz}} \nabla_T \times \mathbf{H}_T - \frac{1}{\epsilon_{zz}} \epsilon_z \cdot \mathbf{E}_T - \frac{4\pi}{\epsilon_{zz}} \mathbf{P}_z^{NL} \quad (55)$$

$$\epsilon_T \cdot \mathbf{E}_T + \epsilon_T \cdot \mathbf{E}_z = -\frac{c}{i\omega} \left(\nabla_T \times \mathbf{H}_z + 2 \times \frac{\partial \mathbf{H}_T}{\partial z} \right) - 4\pi \mathbf{P}_T^{NL} \quad (56)$$

$$\mathbf{H}_z = \frac{c}{i\omega} \nabla_T \times \mathbf{E}_T \quad (57)$$

$$\mathbf{H}_T = \frac{c}{i\omega} \left(\nabla_T \times \mathbf{E}_z + 2 \times \frac{\partial \mathbf{E}_T}{\partial z} \right) \quad (58)$$

3.4.1 Normal Mode Expansion

Strictly speaking, the linear normal modes form a complete basis only within the space of solutions for the linear Maxwell's equations. The solutions of the nonlinear Maxwell's equations in Equations 10-13 do not span the same

solution-space as that for the solutions of the linear Maxwell's equations and cannot be precisely represented as linear combinations of the linear normal modes. However, if the nonlinearity is not large so that

$$|4\pi\mathbf{P}^{\text{NL}}| \ll |\epsilon \cdot \mathbf{E}| \quad (59)$$

the nonlinear polarization \mathbf{P}_{NL} may be treated as a perturbation to the linear polarization. Then, expansion of the fields in the nonlinear waveguide as linear combinations of the linear normal modes of the waveguide structure can be considered as a good approximation to represent the fields in a nonlinear waveguide. If Equation 59 is not satisfied, the coupled-mode approach fails for the nonlinear waveguide and beam-propagation method can be used if the fields are sufficiently linearly polarized so that the wave equations can be reduced to scalar-field equations.

When expanding the EM fields in terms of linear combinations of normal modes, the same set of expansion coefficients are normally used for all the electric and magnetic-field components to keep the mode identity,

$$\mathbf{E}(\mathbf{r}, \omega) = \sum_a A_a(z) \psi_a(x, y) \exp(i\beta_a z) \quad (60)$$

$$\mathbf{H}(\mathbf{r}, \omega) = \sum_a A_a(z) \varphi_a(x, y) \exp(i\beta_a z) \quad (61)$$

where \sum_a sums over all forward and backward discrete guided propagating modes and integrates over the continuum of radiation modes. The evanescent modes should also be included in these expansions for completeness. However, since the evanescent modes do not propagate and are important only near sources or discontinuities of a waveguide, these fields will not be considered in the coupled-mode equations.

The nonlinear waveguide fields are described by Equations 55-58, while the normal mode fields satisfy Equations 24-27. The field expansion in Equations 60 and 61, with the same expansion coefficients for all field components to retain the mode identity, forces \mathbf{P}_z^{NL} to vanish in order for Equations 24 and 55 to be satisfied simultaneously. However, in general, $\mathbf{P}_z^{\text{NL}} \neq 0$ in

nonlinear waveguides, particularly when the waveguide has a strong confinement in which \mathbf{E}_z is significant or when the waveguide material is anisotropic in which \mathbf{P}_z^{NL} can be induced by \mathbf{E}_T . When $\mathbf{P}_z^{\text{NL}} \neq 0$, the linear mode identity cannot be completely retained in the expansion of the nonlinear-guided fields. The mode identity has to be relaxed and the coefficients for the six electric and magnetic-field components cannot all be the same. This is consistent with the observation that the solutions for the nonlinear system do not necessarily span the same solution-space as that for the linear system. However, there is no unique choice to relax the mode identity. In principle, all the expansion coefficients for the six field components can be different once the mode identity is not retained. It appears that the choice depends on how well the nonlinear fields can be approximated and whether the expansion coefficients can be easily solved. The linear mode field components are then used solely as a mathematically convenient function set to approximate the nonlinear-guided fields.

One simple choice is to relax \mathbf{E}_z when $\mathbf{P}_z^{\text{NL}} \neq 0$. By assuming a different set of expansion coefficients, say $B_a(z)$, for \mathbf{E}_z while maintaining the same set of expansion coefficients $A_a(z)$, for the other five field components, Equations 55-58 can be satisfied while simultaneously fulfilling the requirements of Equations 24-27. Therefore, when $\mathbf{P}_z^{\text{NL}} \neq 0$, one can choose the following expansion,

$$\mathbf{E}_T = \sum_a A_a(z) \psi_{aT}(x, y) \exp(i\beta_a z) \quad (62)$$

$$\mathbf{E}_z = \sum_a A_a(z) \psi_{az}(x, y) \exp(i\beta_a z) - \frac{4\pi}{\epsilon_{zz}} \mathbf{P}_z^{\text{NL}} \quad (63)$$

$$\mathbf{H}_T = \sum_a A_a(z) \varphi_{aT}(x, y) \exp(i\beta_a z) \quad (64)$$

$$\mathbf{H}_z = \sum_a A_a(z) \varphi_{aT}(x, y) \exp(i\beta_a z) \quad (65)$$

From the definition \mathbf{P}^{NL} in Equation 15, it is clear that \mathbf{E}_z cannot be solved directly from the amplitude coefficients, $A_a(z)$, but that Equations 62-65 must be solved by iteration. When $\mathbf{P}_z^{NL} = 0$, Equations 62-65 reduce to those in Equations 60 and 61 which can be solved directly.

3.4.2 Coupled-Mode Equations

The fields in the nonlinear waveguide satisfy Equations 55-58. For generality, assume $\mathbf{P}_z^{NL} \neq 0$ and substitute the field expansion given by Equations 62-65 in Equations 55-58. Then, using Equations 24-27, the following are obtained

$$\sum_a \frac{dA_a}{dz} \exp(i\beta_a z) \hat{z} \times \phi_{aT} = - \frac{i4\pi\omega}{c} \left(\mathbf{P}_T^{NL} - \frac{1}{\epsilon_{zz}} \epsilon_T \cdot \mathbf{P}_z^{NL} \right) \quad (66)$$

$$\sum_a \frac{dA_a}{dz} \exp(i\beta_a z) \hat{z} \times \psi_{aT} = 4\pi \nabla_T \times \frac{\mathbf{P}_z^{NL}}{\epsilon_{zz}} \quad (67)$$

Using these two equations and the orthogonality relations obtained in Subsection 3.3, the coupled-mode equations will be derived for the nonlinear waveguide in each case discussed earlier.

CASE 1. $\epsilon(\omega) = \epsilon^*(\omega)$, real but anisotropic.

Taking the sum of the dot product of $-\psi_{bT}^*$ with Equation 66 and that of ϕ_{bT}^* with Equation 67, integrating the resultant equation over space, and using the orthogonality relation for CASE 1 in Equation 47, one gets

$$\begin{aligned} \frac{dA_a}{dz} = 2\pi \exp(-i\beta_a z) \iint dx dy \left\{ \phi_{aT}^* \cdot \nabla_T \times \frac{\mathbf{P}_z^{NL}}{\epsilon_{zz}} \right. \\ \left. + \frac{i\omega}{c} \psi_{aT}^* \cdot \mathbf{P}_T^{NL} - \frac{i\omega}{c\epsilon_{zz}} \psi_{aT}^* \cdot \epsilon_T \cdot \mathbf{P}_z^{NL} \right\} \end{aligned} \quad (68)$$

Using vector identities and Equations 24-27, it can be shown that

$$\varphi_{aT}^* \cdot \nabla_T \times \frac{\mathbf{P}_z^{NL}}{\epsilon_{zz}} = \frac{i\omega}{c} \psi_{az}^* \cdot \mathbf{P}_z^{NL} + \frac{i\omega}{c\epsilon_{zz}} \psi_{aT}^* \cdot \epsilon_T \cdot \mathbf{P}_z^{NL} + \nabla_T \cdot \left(\frac{\mathbf{P}_z^{NL}}{\epsilon_{zz}} \times \varphi_{aT}^* \right) \quad (69)$$

Substituting Equation 69 into Equation 68 for the first term of the integrand, the following coupled-mode equation for a nonlinear waveguide is obtained

$$\begin{aligned} \frac{dA_a}{dz} = & \frac{i2\pi\omega}{c} \exp(-i\beta_a z) \iint dx dy \mathbf{P}_z^{NL} \cdot \psi_a^* \\ & + 2\pi \exp(-i\beta_a z) \iint dx dy \nabla_T \cdot \left(\frac{\mathbf{P}_z^{NL}}{\epsilon_{zz}} \times \varphi_{aT}^* \right) \end{aligned} \quad (70)$$

Since every realistic waveguide is transversely bounded by vacuum in which $\mathbf{P}_z^{NL} = 0$, the last in integral Equation 70 can be shown to vanish by converting it into a closed line integral at transverse infinity. Therefore, one gets

$$\frac{dA_a}{dz} = \pm \frac{i2\pi\omega}{c} \exp(-i\beta_a z) \iint dx dy \mathbf{P}_z^{NL} \cdot \psi_a^* \quad (71)$$

where the plus sign is chosen if mode a is a forward-propagating mode in the positive z -direction and the minus sign is chosen if mode a is a backward-propagating mode.

According to the normalization with Equation 48, the power in each guided propagating mode a is

$$P_a(z) = \frac{c}{2\pi} |A_a(z) \exp(i\beta_a z)|^2 = \frac{c}{2\pi} |A_a(z)|^2 \quad (72)$$

where β_a is real for any propagation mode a in this case.

CASE 2. $\epsilon(z) = \epsilon(-z)$, cylindrically symmetric but complex.

In this case, $\epsilon_T \cdot \mathbf{P}_z^{NL} = 0$ and Equations 66 and 67 become

$$\sum_a \frac{dA_a}{dz} \exp(i\beta_a z) \hat{z} \times \boldsymbol{\varphi}_{aT} = - \frac{i4\pi\omega}{c} \mathbf{P}_T^{NL} \quad (73)$$

$$\sum_a \frac{dA_a}{dz} \exp(i\beta_a z) \hat{z} \times \boldsymbol{\psi}_{aT} = 4\pi \nabla_T \times \frac{\mathbf{P}_z^{NL}}{\epsilon_{zz}} \quad (74)$$

where $\beta_a = \beta'_a + i\beta''_a$ is a complex propagation constant. In this case, the forward and corresponding backward-propagating modes are not independent. Using the orthogonality relations in Equations 52 and 53, one finds

$$\frac{dA_a}{dz} \exp(i\beta_a z) - \frac{dA_{-a}}{dz} \exp(-i\beta_a z) = \frac{i4\pi\omega}{c} \iint dx dy \mathbf{P}_T^{NL} \cdot \boldsymbol{\psi}_{aT} \quad (75)$$

$$\frac{dA_a}{dz} \exp(i\beta_a z) + \frac{dA_{-a}}{dz} \exp(-i\beta_a z) = - \frac{i4\pi\omega}{c} \iint dx dy \mathbf{P}_z^{NL} \cdot \boldsymbol{\psi}_{az} \quad (76)$$

Combining these two equations, one gets

$$\frac{dA_a}{dz} = \frac{i2\pi\omega}{c} \exp(-i\beta_a z) \iint dx dy (\mathbf{P}_T^{NL} \cdot \boldsymbol{\psi}_{aT} - \mathbf{P}_T^{NL} \cdot \boldsymbol{\psi}_{az}) \quad (77)$$

$$\frac{dA_{-a}}{dz} = - \frac{(i2\pi\omega)}{c} \exp(i\beta_a z) \iint dx dy \mathbf{P}_z^{NL} \cdot \boldsymbol{\psi}_a \quad (78)$$

Notice the difference between Equation 70, where the components of $\boldsymbol{\psi}_a^*$ are used, and Equation 77, where $\boldsymbol{\psi}_a$ has to be used, because of the difference in the orthogonality relations, Equations 47 and 52, respectively, for the two cases.

The total power in the guided field is

$$P = \frac{c}{2\pi} \sum_{a,b} |A_a(z) A_b^*(z) \exp(i(\beta_a + \beta_b^*)z) \iint dx dy z \cdot \text{Re}(\psi_{aT} \times \phi_{bT}^*)| \quad (79)$$

Since the orthogonality relation and the normalization condition are given by Equations 52 and 53, respectively, in terms of ψ_{aT} and ϕ_{bT} , mode power is not a well-defined concept here. However, when the gain or loss in the waveguide is small such that $\beta_a' \ll \beta_a$, ψ_{aT} and ϕ_{aT} are approximately real functions according to Equations 38 and 40. Then the power in each guided mode can be approximated by

$$P_{\pm a} = \frac{c}{2\pi} |A_{\pm a}(z)|^2 \exp(\mp 2\beta_a'' z) \quad (80)$$

CASE 3. $\epsilon(\omega) = \epsilon^*(\omega)$ and $\epsilon(z) = \epsilon(-z)$.

In this case, following the same procedure in CASE 2, Equations 75 and 76 and Equations 77 and 78 are still obtained, but with real propagation constants $\beta_a = -\beta_{-a}$ for propagating modes. The power in each guided mode is given by Equation 72.

CASE 4. $\epsilon(\omega) \neq \epsilon^*(\omega)$ and $\epsilon(z) \neq \epsilon(-z)$.

In this case, a simple coupled-mode equation cannot be obtained because there are no simple relations between the mode field components and no simple orthogonality relations.

3.5 DISCUSSION

In Subsection 3.4, the coupled-mode equations have been written for the amplitude coefficients, A_a , using the electric-field pattern of the corresponding mode. This is the general practice used in the literature (Refs. 24, 25, 27, and 29), where real and isotropic nonlinear waveguides with negligible P_z^{NL} have been considered. Because the mode orthogonality relations depend on

waveguide material properties, our equations for more complicated materials have different forms. Equation 71 (for the case of an anisotropic, real dielectric tensor), contains Ψ_a^* , while Equation 77 (for cylindrically symmetric, complex dielectric tensors), contains Ψ_{aT} and Ψ_{az} . The coupled-mode equations can be written in a general form using the electric-field patterns of the counterpropagating modes

$$\frac{dA_a}{dz} = \pm \frac{i2\pi\omega}{c} \exp(-i\beta_a z) \iint dx dy P^{NL} \cdot \Psi_{-a} \quad (81)$$

The plus sign is used when mode a propagates in the positive z -direction, while the minus sign is used when mode a propagates in the negative z -direction. This equation applies to all the cases where the orthogonality relations can be derived.

Most of the commonly used waveguide materials, including nonlinear dielectric crystals such as LiNbO_3 and all III-V semiconductors such as GaAs, have anisotropic nonlinear optical properties. In this case, depending on the waveguide geometry with respect to the crystal optical axes, the TE-field components, E_T , can induce a large longitudinal nonlinear polarization, P_z^{NL} . In addition, to increase the power density for efficient nonlinear interaction, a strong optical confinement is usually needed in nonlinear waveguides. The strong confinement can result in a large longitudinal electric-field component, E_z , which can contribute to P_z^{NL} in the third-order process even if the material is isotropic. Therefore, in general, the longitudinal nonlinear polarization, P_z^{NL} , does not vanish and can become very important in waveguides of special geometry.

Subsection 3.4 shows that when $P_z^{NL} \neq 0$, the linear mode identity cannot be retained in the expansion of the nonlinear waveguide fields. In this case, there is no unique way of doing the expansion. In Subsection 3.4, the choice was to relax E_z only. Another simple possibility is to choose one set of expansion coefficients, say $A_a(z)$, for all three electric-field components and a different set, $B_a(z)$, for all three magnetic-field components. By doing so, the coupled-mode equations become substantially more complicated and can be reduced to a simple form only under certain special conditions. This is

because the orthogonality relations, as given in Subsection 3.3, are all in terms of TE and TM mode fields, ψ_{aT} and ϕ_{aT} , together. Therefore, using different expansion coefficients for \mathbf{E}_T and \mathbf{H}_T makes it mathematically complicated. It is more convenient to choose the same coefficients for \mathbf{E}_T and \mathbf{H}_T . In general terms, when the mode identity cannot be retained, it probably does not matter how the fields are expanded so long as the fields and the nonlinear polarization can be *approximated* as accurately as possible and the resulting equations are mathematically as simple as possible. It appears that the choice used in Subsection 3.4 does this better than other possible choices. If the material is magnetic with a nonvanishing longitudinal nonlinear magnetization, then \mathbf{H}_z has to be relaxed and be expanded similar to \mathbf{E}_z in Equation 63.

When $\mathbf{P}_z^{\text{NL}} = 0$, the coupled-mode equations can be solved as coupled simultaneous equations for $A_a(z)$ directly since \mathbf{P}_T^{NL} can be expressed explicitly in terms of products of $A_a(z)$ through Equations 15 and 60. When $\mathbf{P}_z^{\text{NL}} \neq 0$, \mathbf{P}^{NL} cannot be explicitly expressed in terms of products or combinations of $A_a(z)$ any more because of Equation 63. Then, the coupled-mode equations cannot be reduced to simple and direct simultaneous equations for $A_a(z)$. In this case, the nonlinear fields can only be solved *iteratively* using the coupled-mode equations together with Equation 15 and Equations 62 and 63. $A_a(z)$ and \mathbf{P}_z^{NL} can be solved successively using the procedure outlined in Appendix B until a self-consistent solution is obtained.

The contribution of \mathbf{P}_z^{NL} to the coupled-mode equation becomes important when \mathbf{P}_z^{NL} and ψ_{az} are both significant, as can be seen from Equations 71, 77 and 78. This can happen when the waveguide material is anisotropic and the fields are tightly guided. When this contribution is negligible because \mathbf{P}_z^{NL} vanishes or because ψ_{az} is very small such as in weakly guiding system, one has

$$\frac{dA_a}{dz} \exp(i\beta_a z) + \frac{dA_{-a}}{dz} \exp(-i\beta_a z) = 0 \quad (82)$$

for CASES 2 and 3. In this case, taking a *slowly varying amplitude approximation* for the forward-propagating wave is equivalent to neglecting the backward-propagating wave (Refs. 25 and 40). This does not apply to CASE 1

since the forward and backward modes are independent in CASE 1. When the contribution \mathbf{P}_z^{NL} is not negligible, Equation 82 is not valid. Then the relation between the forward- and backward-propagating waves can become more complicated.

The linear and nonlinear electric susceptibilities, χ , and the dielectric constant, ϵ , are assumed all *spatially local* functions so that $\mathbf{P}^{\text{L}}(\mathbf{r},\omega)$ and $\mathbf{P}^{\text{NL}}(\mathbf{r},\omega)$ can be written in the forms given by Equations 14 and 15, respectively. However, in certain cases of interest, such as in a semiconductor waveguide under carrier injection and the carriers have a diffusion length longer than the wavelength of the guided wave, χ and ϵ are *nonlocal* spatially as well as temporally. Then $\mathbf{P}^{\text{L}}(\mathbf{r},\omega)$ and $\mathbf{P}^{\text{NL}}(\mathbf{r},\omega)$ have to be expressed as spatial convolution integrals of χ and \mathbf{E} . In this case, the z -dependent expansion coefficients, $A_n(z)$, are also involved in the convolution integrals when the field expansion is substituted into the nonlinear wave equations. It seems that there is no simple coupled-mode approach in this situation.

4.0 EFFECT OF CARRIER DIFFUSION ON PHASE CONJUGATE FOUR-WAVE MIXING IN SEMICONDUCTOR WAVEGUIDES

4.1 INTRODUCTION

Four-wave mixing in a nonlinear optical waveguide has the advantage of long nonlinear interaction length and high field intensities due to the optical confinement of the waveguide. Phase conjugation by 4-wm in optical fibers was proposed by Yariv, *et al.* (Ref. 9). They showed that if a multimode optical fiber is excited with two counterpropagating single-mode pump beams both coupled into the lowest-order transverse mode, a third probe beam launched in the waveguide can be replicated with high fidelity through the PC 4-wm process in the waveguide. The multimode fiber has to accommodate a number of propagating modes equal to the number of resolution elements contained in the probe field for sufficient image resolution (Ref. 9). Subsequently, Hellwarth (Ref. 11) carried out a more detailed analysis on the generation of a PC replica of a free wave at the entrance plane of a multimode waveguide by 4-wm in the waveguide. The pump power required in the waveguide is orders of magnitude less than that needed for phase conjugation with unguided beams in a bulk medium. Furthermore, unlike for unguided waves, beam alignment is not critical (Ref. 11). It is only necessary to sufficiently couple the beams into the guided modes.

Hellwarth's analysis also showed that the two counterpropagating pump beams can be multimode without spoiling the fidelity of the PC replica, as long as the nonlinear coupling between the pump beams and the probe beam does not vary from mode to mode (Ref. 11). It is also possible to replicate the image carried by a multimode pump beam in the presence of a counterpropagating pump beam at the same frequency in the waveguide. In this two-beam configuration, the first pump serves as both the pump and the image beam. Both the three-beam and two-beam arrangements for phase conjugation were simultaneously demonstrated by Jensen and Hellwarth with a multimode glass waveguide filled with liquid CS₂ (Ref. 10). The pump powers required were nearly an order of magnitude lower than that required in the bulk medium. However, the conjugate reflectivity was less than unity because of the small optical nonlinearity of CS₂.

Recently, there have been a series of experimental (Refs. 14, 17, 35, 39 and 40) and theoretical (Refs. 16 and 41) studies of nearly degenerate 4-wm in semiconductor lasers and amplifiers. A large signal gain of 30 to 40 dB, which corresponds to a conjugate reflectivity of 10^3 to 10^4 , has been observed (Refs. 14 and 17). This is caused by the optical gain and the resonant enhancement in addition to the large optical nonlinearity in the semiconductor laser medium (Ref. 35). Using a noncollinear phase conjugation geometry in a broad-area diode laser, Lucente, *et al.* (Refs. 42 and 43) showed that the 4-wm signal is emitted in the PC direction.

It becomes obvious that if the semiconductor waveguide can be used for the generation of optical PC signals, a very large PC reflectivity could be realized, in addition to the various advantages of using a dielectric waveguide demonstrated by Hellwarth (Refs. 10 and 11). Since it is relatively easy to control the optical gain in a semiconductor waveguide by current injection, the signal intensity can also be easily varied without changing the pump intensity. So far, the experimental and theoretical investigations on the nearly degenerate 4-wm in semiconductor waveguides have focused on the nonlinear properties of the semiconductor medium without much consideration on the waveguiding and mode properties of the interaction (Refs. 14, 16, 17, 35 and 39-42). Most of these studies have considered only single-mode semiconductor waveguides. However, as has been pointed out by Yariv, *et al.* (Ref. 9) and by Hellwarth (Ref. 11) for the generation of a PC image a multimode waveguide with a large number of guided modes is necessary for sufficient resolution of the image. In addition, the nonlinear coupling between modes has to be uniform for high-fidelity phase conjugation (Ref. 11).

In a semiconductor waveguide under current injection for an optical gain, carrier diffusion can affect the efficiency of nonlinear wave coupling in a 4-wm process (Refs. 41 and 43). In fact, using a noncollinear arrangement Lucente, *et al.* (Ref. 43) were able to measure the ambipolar carrier diffusion constant directly by measuring the spatial and frequency dependence of the conjugate signal efficiency in a broad-area laser diode. Carrier diffusion can also degrade the mode identity in a multimode waveguide. The effect of carrier diffusion on PC 4-wm in semiconductor waveguides is studied for the possibility and limitations of using semiconductor waveguides under current injection for efficient generation of PC image signals.

4.2 CARRIER-INDUCED POLARIZATIONS

The 4-wm process is considered with two counterpropagating pump beams in a multimode semiconductor waveguide under current injection. The generic scheme is shown in Figure 2 where the z-direction is taken to be along the waveguide axis. The waveguide is assumed to be index-guided with a rectangular cross section of dimensions w and d in the x- and y-directions, respectively, as is shown in Figure 3. The intrinsic refractive index of the guiding core is n and that of the surrounding clad is $n_0 < n$ for index guiding. The forward- and backward-propagating pump fields are \mathbf{E}_p and $\mathbf{E}_{p'}$, respectively. \mathbf{E}_i is the input image (probe) field and \mathbf{E}_s is the returned signal (conjugate) field. Here a prime is used in the field indices for the backward-propagating fields, i.e., those propagating in the -z direction. The forward-propagating fields are indexed without a prime. For generality, consider nearly degenerate, but nondegenerate, 4-wm with degenerate pump frequency, $\omega_p = \omega_{p'} = \omega$, and detuned probe frequency, $\omega_i = \omega - \Omega$. The returned signal is then at frequency $\omega_s = \omega + \Omega$. The degenerate case when $\omega_p = \omega_{p'} = \omega_i = \omega_s$ will be discussed in Subsection 4.4.

The complex field at a particular frequency ω_j is given by

$$\mathbf{E}_j(\mathbf{r}, t) = \mathbf{E}_j(\mathbf{r}, \omega_j) \exp(-i\omega_j t) \quad (83)$$

where $\mathbf{E}_j(\mathbf{r}, \omega_j)$ contains the spatial information, and the real field can be obtained from $\mathbf{E}_j(\mathbf{r}, t) + \mathbf{E}_j^*(\mathbf{r}, t)$. In a multimode waveguide, the spatially dependent parts of the fields can be expanded in terms of the normal mode fields of the waveguide. In a nonlinear waveguide where the longitudinal component of the nonlinear polarization, P_z^{NL} , does not vanish, the longitudinal z-component of the electric field can, in general, have different expansion coefficients from those for the transverse field components. In addition, the backward-propagating modes, ψ_{-a} , are not generally identical to the forward-propagating modes, ψ_a . However, for the discussions in this report, these differences will be ignored for simplicity in the formulation. Therefore, the spatially-dependent parts of the fields can be expanded as follows

$$\mathbf{E}_p(\mathbf{r}) = \sum_a A_a^{(p)}(z) \psi_a(x, y) \exp(i\beta_a z) \quad (84)$$

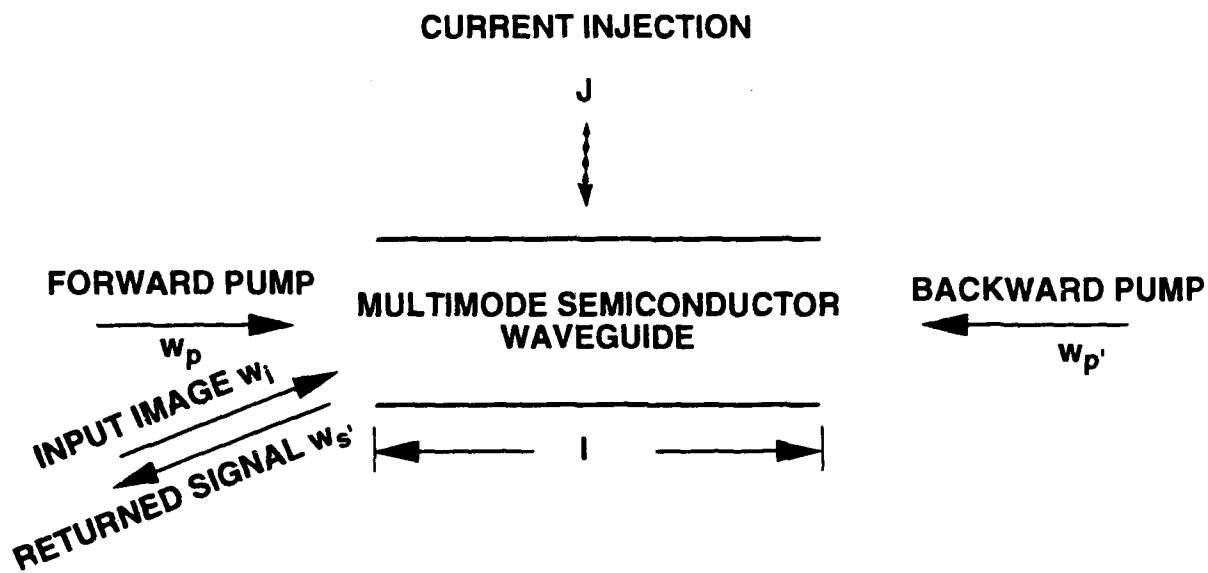


Figure 2. Schematic diagram of PC 4-wm with a multimode waveguide.

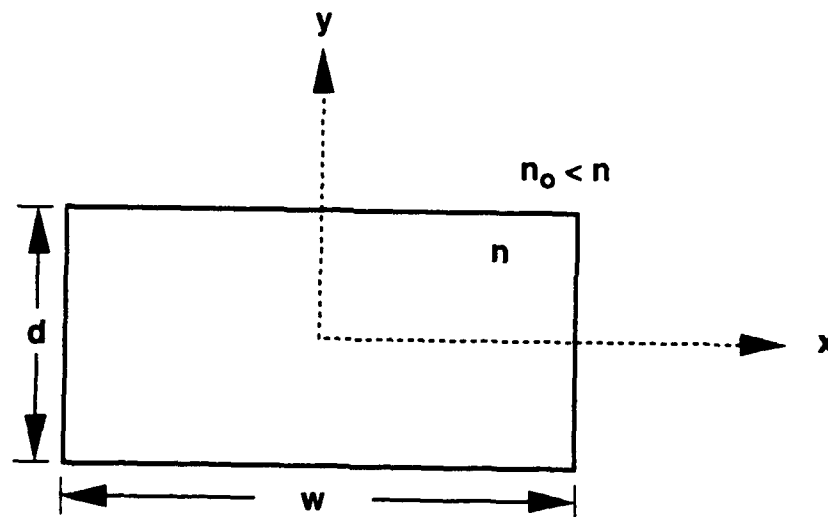


Figure 3. Waveguide cross section.

$$\mathbf{E}_p(\mathbf{r}) = \sum_a A_a^{(p')} (z) \psi_a(x, y) \exp(-i\beta_a z) \quad (85)$$

$$\mathbf{E}_i(\mathbf{r}) = \sum_a A_a^{(i)} (z) \psi_a(x, y) \exp((i\beta_a - \delta\beta_a) z) \quad (86)$$

$$\mathbf{E}_s(\mathbf{r}) = \sum_a A_a^{(s')} (z) \psi_a(x, y) \exp(-i(\beta_a + \delta\beta_a) z) \quad (87)$$

where β_a is the propagation constant of mode a . Here, ψ_a is assumed the normal mode of the intrinsic waveguide structure without current injection. Therefore, β_a is approximately real since the imaginary part, β_a' , contributed by the intrinsic waveguide loss is generally very small in comparison to real part, β_a'' . In this case, the optical gain contributed by the injected current is not included in β_a . The contributions of the carrier-induced gain and optical nonlinearities are described by the total carrier-induced polarization \mathbf{P} with linear and nonlinear components. The mode field pattern $\psi_a(x, y)$ depends only on the transverse coordinates and are characterized by two wave numbers, ξ_a and η_a , which describe the transverse spatial frequencies of ψ_a in the x - and y -directions, respectively. For guided modes, these constants satisfy the following conditions

$$\xi_a^2 + \eta_a^2 + \beta_a^2 = k^2 \quad (88)$$

and

$$k_0 < \beta_a < k \quad (89)$$

where $k_0 = n_0\omega/c$ and $k = n\omega/c$.

To obtain the carrier-induced polarization, one has to calculate the linear and nonlinear susceptibilities of the semiconductor medium in the presence of the injected current and the multimode optical fields. A formal and rigorous approach is to calculate the carrier distribution with the band structure of the semiconductor and then to employ the density-matrix formalism for the interaction of the optical fields and the medium (Ref. 44). This approach

will enable a more accurate accountability for the microscopic properties of the semiconductor medium, such as the band structure and the crystal symmetry. However, it is mathematically much more involved. Since the interest is primarily in the effect of carrier diffusion in this report, the microscopic nature of the semiconductor medium will not be considered. Instead, a phenomenological approach will be taken with the rate-equation approximation. In this approach (Refs. 41-43), the carrier diffusion is described by an ambipolar diffusion constant, D , and the intensity gain, $g(N)$, as a function of the carrier density, N , as approximated by (Ref. 41).

$$g(N) = a(N - N_0) \quad (90)$$

where a is the gain coefficient and N_0 is the minimum carrier density needed for optical transparency in the semiconductor medium. The total carrier-induced susceptibility can then be approximated by (Ref. 41).

$$\chi(N) = - \frac{cn}{4\pi\omega} (b + i) g(N) \quad (91)$$

where b is the antiguidance factor (Refs. 45 and 46). Since the interest is also in the possibility of a large signal gain, only the situation of small pump-probe detuning is considered (Ref. 41), $|\Omega|\tau \leq 1$, where τ is the carrier recombination lifetime. The 4-wm efficiency is much higher in this case, when compared to the case of a large detuning such that $|\Omega|\tau \gg 1$ (Refs. 41-47), and the rate-equation approximation is valid.

A procedure similar to that outlined by Agrawal (Ref. 41) is followed for a single-mode waveguide. However, because the 4-wm is being considered in a multimode waveguide, the mode properties (including intermode coupling) must be taken into account in the formulation. Begin by considering the spatial and temporal variations of the carrier density, $N(\mathbf{r}, t)$ described by the rate equation (Refs. 41 and 43)

$$\frac{dN(\mathbf{r}, t)}{dt} = \frac{J}{ed} - \frac{N(\mathbf{r}, t)}{\tau} - \frac{cn}{2\pi\hbar\omega} g(N(\mathbf{r}, t)) |\mathbf{E}(\mathbf{r}, t)|^2 + D\nabla^2 N(\mathbf{r}, t) \quad (92)$$

where J is the injection current density, e is the electronic charge, and D is the ambipolar diffusion constant. The total field in the waveguide is

$$\mathbf{E}(\mathbf{r}, t) = \mathbf{E}_p \exp(-i\omega t) + \mathbf{E}_{p'} \exp(-i\omega t) + \mathbf{E}_i \exp(-i(\omega - \Omega)t) + \mathbf{E}_{s'} \exp(-i(\omega + \Omega)t) \quad (93)$$

where $\mathbf{E}_p, \mathbf{E}_{p'}, \mathbf{E}_i$ and $\mathbf{E}_{s'}$ are given by Equations 2-5, respectively. Taking the strong-pump approximation that $|\mathbf{E}_p + \mathbf{E}_{p'}| \gg |\mathbf{E}_i|$ and $|\mathbf{E}_{s'}|$, one can write

$$|\mathbf{E}(\mathbf{r}, t)|^2 = |\mathbf{E}_p + \mathbf{E}_{p'}|^2 + \{[(\mathbf{E}_p + \mathbf{E}_{p'}) \cdot \mathbf{E}_i^* + (\mathbf{E}_p + \mathbf{E}_{p'})^* \cdot \mathbf{E}_{s'}] \exp(-i\Omega t) + c.c.\} \quad (94)$$

where the first term is time-independent but can be strongly spatially dependent, as are the time-dependent terms in the equation, because of the multimode mixing. To solve Equation 92, one writes (Ref. 41)

$$N(\mathbf{r}, t) = N_s(\mathbf{r}) + [N_m(\mathbf{r}) \exp(-i\Omega t) + c.c.] \quad (95)$$

where N_s contains the effect of gain saturation due to the pump fields and N_m accounts for the contributions from the wave mixing with the probe image and conjugate signal fields. Substituting Equations 94 and 95 in Equation 92, one obtains

$$L^2 \nabla^2 N_s = (1 + |\mathbf{E}_p + \mathbf{E}_{p'}|^2 / I_s) N_s - (N^{(1)} + N_0 |\mathbf{E}_p + \mathbf{E}_{p'}|^2 / I_s) \quad (96)$$

$$L^2 \nabla^2 N_m = (1 - i\Omega\tau + |\mathbf{E}_p + \mathbf{E}_{p'}|^2 / I_s) N_m + (N_s - N_0) [(\mathbf{E}_p + \mathbf{E}_{p'}) \cdot \mathbf{E}_i^* + (\mathbf{E}_p + \mathbf{E}_{p'})^* \cdot \mathbf{E}_{s'}] / I_s \quad (97)$$

where $L = \sqrt{D\tau}$ is the carrier diffusion length and $I_s = 2\pi\hbar\omega/(cn\tau a)$ is the saturation intensity scaled to the unit of $|E|^2$. The carrier density in the absence of the optical fields is $N^{(1)} = J\tau/ed$, which gives the unsaturated and unperturbed linear gain

$$g^{(1)} = a(N^{(1)} - N_0) \quad (98)$$

The corresponding unsaturated linear susceptibility is

$$\chi^{(1)} = -\frac{cn}{4\pi\omega}(b + i)g^{(1)} \quad (99)$$

In the presence of optical fields and carrier diffusion, Equations 96 and 97 are usually approximated by spatially averaging the fields to account for the carrier diffusion and then by dropping the diffusion terms (Ref. 48). To more accurately trace the effect of carrier diffusion, this approach has not been taken. Instead, Equations 96 and 97 were solved by expanding $N_s(\mathbf{r})$ and $N_m(\mathbf{r})$ in spatially-dependent Fourier series containing terms of longitudinal and transverse spatial frequencies corresponding to those generated by mixing between field modes. The effect of carrier diffusion is to include in the wave-mixing efficiency a Lorentzian lineshape function

$$\begin{aligned} \mathcal{L}(\xi_a \pm \xi_b, \eta_a \pm \eta_b, \beta_a \pm \beta_b; \Omega) = & \{1 + [(\xi_a \pm \xi_b)^2 \\ & + (\eta_a \pm \eta_b)^2 + (\beta_a \pm \beta_b)^2] L^2 \\ & - i\Omega\tau\}^{-1} \end{aligned} \quad (100)$$

which depends on the spatial and temporal beat frequencies of the mixing modes. Therefore, each term in the Fourier series will have a different Lorentzian multiplier depending on the beat frequencies. With this understanding, the Fourier-series solutions can be written for N_s and N_m in the following concise forms,

$$N_s = N_s^{(1)} - \frac{(N_s^{(1)} - N_0) \mathcal{L}(0) |\mathbf{E}_p + \mathbf{E}_p'|^2 / I_s}{1 + \mathcal{L}(0) \sum_a (I_a^{(p)} + I_a^{(p')}) / I_s} \quad (101)$$

$$N_m = - \frac{(N_s^{(1)} - N_0) \mathcal{L}(\Omega) [(\mathbf{E}_p + \mathbf{E}_{p'}) \cdot \mathbf{E}_i^* + (\mathbf{E}_p^* + \mathbf{E}_{p'}^*) \cdot \mathbf{E}_s]}{1 + \mathcal{L}(\Omega) \sum_a (I_a^{(p)} + I_a^{(p')}) / I_s} \quad (102)$$

where $\mathcal{L}(0) = \mathcal{L}(\Omega = 0)$ and

$$N_s^{(1)} = \frac{N^{(1)} + N_0 \sum_a (I_a^{(p)} + I_a^{(p')}) / I_s}{1 + \sum_a (I_a^{(p)} + I_a^{(p')}) / I_s} \quad (103)$$

is the background carrier saturation which does not depend on the mixing spatial frequencies of the modes. $I_a^{(p)} = |A_a^{(p)}|^2$ and $I_a^{(p')} = |A_a^{(p')}|^2$ are the spatial-frequency-independent average intensities in individual pump modes. The spatial-frequency dependencies of $\mathcal{L}(0)$ and $\mathcal{L}(\Omega)$ vary with the mixing modes and can only be determined after the fields are expanded using Equations 84-87.

Using Equations 101-103 and Equations 90 and 91, one can write

$$\chi_s = \chi_s^{(1)} - \frac{\chi_s^{(1)} \mathcal{L}(0) |\mathbf{E}_p + \mathbf{E}_{p'}|^2 / I_s}{1 + \mathcal{L}(0) \sum_a (I_a^{(p)} + I_a^{(p')}) / I_s} \quad (104)$$

$$\chi_m = - \frac{\chi_s^{(1)} \mathcal{L}(\Omega) [(\mathbf{E}_p + \mathbf{E}_{p'}) \cdot \mathbf{E}_i^* + (\mathbf{E}_p^* + \mathbf{E}_{p'}^*) \cdot \mathbf{E}_s]}{1 + \mathcal{L}(\Omega) \sum_a (I_a^{(p)} + I_a^{(p')}) / I_s} \quad (105)$$

where χ_s is the susceptibility corresponding to the saturated gain and χ_m is the susceptibility responsible for the wave mixing. The saturated carrier-induced background susceptibility is

$$\chi_s^{(1)} = \frac{\chi^{(1)}}{1 + \sum_a (I_a^{(p)} + I_a^{(p')}) / I_s} \quad (106)$$

In the strong-pump approximation, one can then write the total carrier-induced polarizations at the pump, image, and signal frequencies,

$$P(\omega) = P_F(\omega) + P_B(\omega) = \chi_s(E_p + E_{p'}) \quad (107)$$

$$P(\omega - \Omega) = P_F(\omega - \Omega) + P_B(\omega - \Omega) = \chi_s E_i + \chi_m^*(E_p + E_{p'}) \quad (108)$$

$$P(\omega + \Omega) = P_F(\omega + \Omega) + P_B(\omega + \Omega) = \chi_s E_{s'} + \chi_m(E_p + E_{p'}) \quad (109)$$

where P_F and P_B are polarizations containing forward- and backward-propagating wave vectors, respectively, i.e.,

$$P_F \sim \text{sum of } \exp(i\beta z), \exp(i3\beta z), \dots \text{ terms} \quad (110)$$

$$P_B \sim \text{sum of } \exp(-i\beta z), \exp(-i3\beta z), \dots \text{ terms} \quad (111)$$

4.3 EFFECT OF CARRIER DIFFUSION

The total carrier-induced polarizations given in Equations 107-109 contain the linear and nonlinear polarizations. In general, the total pump intensity can easily be comparable to or larger than the saturation intensity, I_s , in a semiconductor waveguide, which is typically of the order of 3 to 5 mW/ μm^2 (Ref. 49). Therefore, the wave-mixing process has to be described by Equations 107-109 together with the total χ_s and χ_m given in Equations 104 and 105, respectively. One can expand χ_s and χ_m ,

$$\chi_s = \chi_s^{(1)} + \chi_s^{(3)} (\langle E_p \cdot E_p^* \rangle + \langle E_{p'} \cdot E_{p'}^* \rangle + \langle E_p \cdot E_{p'}^* \rangle + \langle E_{p'} \cdot E_p^* \rangle) \quad (112)$$

$$\chi_m = \chi_m^{(3)} (\langle E_p \cdot E_i^* \rangle + \langle E_{p'} \cdot E_i^* \rangle + \langle E_p^* \cdot E_{s'} \rangle + \langle E_{p'}^* \cdot E_{s'} \rangle) \quad (113)$$

where

$$\chi_s^{(3)} = - \frac{\mathcal{Q}(0) \chi_s^{(1)} / I_s}{1 + \mathcal{Q}(0) \sum_a (I_a^{(p)} + I_a^{(p')}) / I_s} \quad (114)$$

$$\chi_m^{(3)} = - \frac{\mathcal{Q}(\Omega) \chi_s^{(1)} / I_s}{1 + \mathcal{Q}(\Omega) \sum_a (I_a^{(p)} + I_a^{(p')}) / I_s} \quad (115)$$

The symbol $\langle \mathbf{E}_p \cdot \mathbf{E}_i^* \rangle$, for example, indicates that the spatial-frequency dependencies of $\mathcal{Q}(\Omega)$ in $\chi_m^{(3)}$ for the first term in Equation 113, $\chi_m^{(3)} \langle \mathbf{E}_p \cdot \mathbf{E}_i^* \rangle$, depends on the spatial beat frequencies of the mode components of the multimode fields \mathbf{E}_p and \mathbf{E}_i^* . It does not mean that spatial averaging has been taken for $\mathbf{E}_p \cdot \mathbf{E}_i^*$. Using Equations 112 and 113, one can expand $\mathbf{P}(\omega)$, $\mathbf{P}(\omega - \Omega)$, and $\mathbf{P}(\omega + \Omega)$ in Equations 107-109, respectively. Since the phase-matched or nearly phase-matched nonlinear are the only interested processes, keep only terms $\sim \exp(i\beta z)$ for \mathbf{P}_F and those $\sim \exp(-i\beta z)$ for \mathbf{P}_B and drop terms with higher-harmonic propagation constants. Then one has

$$\mathbf{P}_F(\omega) = \chi_s^{(1)} \mathbf{E}_p + \chi_s^{(3)} (\langle \mathbf{E}_p \cdot \mathbf{E}_p^* \rangle \mathbf{E}_p + \langle \mathbf{E}_{p'} \cdot \mathbf{E}_{p'}^* \rangle \mathbf{E}_p + \langle \mathbf{E}_p \cdot \mathbf{E}_{p'}^* \rangle \mathbf{E}_{p'}) \quad (116)$$

$$\begin{aligned} \mathbf{P}_F(\omega - \Omega) = & \chi_s^{(1)} \mathbf{E}_i + \chi_s^{(3)} (\langle \mathbf{E}_p \cdot \mathbf{E}_p^* \rangle \mathbf{E}_i + \langle \mathbf{E}_{p'} \cdot \mathbf{E}_{p'}^* \rangle \mathbf{E}_i) \\ & + \chi_m^{(3)} (\langle \mathbf{E}_p^* \cdot \mathbf{E}_i \rangle \mathbf{E}_p + \langle \mathbf{E}_{p'}^* \cdot \mathbf{E}_i \rangle \mathbf{E}_{p'} + \langle \mathbf{E}_p \cdot \mathbf{E}_{s'}^* \rangle \mathbf{E}_{p'} \\ & + \langle \mathbf{E}_{p'} \cdot \mathbf{E}_{s'}^* \rangle \mathbf{E}_p) \end{aligned} \quad (117)$$

$$\mathbf{P}_F(\omega + \Omega) = \chi_s^{(3)} \langle \mathbf{E}_p \cdot \mathbf{E}_{p'}^* \rangle \mathbf{E}_{s'} + \chi_m^{(3)} (\langle \mathbf{E}_p \cdot \mathbf{E}_i^* \rangle \mathbf{E}_p + \langle \mathbf{E}_{p'}^* \cdot \mathbf{E}_{s'} \rangle \mathbf{E}_p) \quad (118)$$

and

$$\mathbf{P}_B(\omega) = \chi_s^{(1)} \mathbf{E}_{p'} + \chi_s^{(3)} (\langle \mathbf{E}_p \cdot \mathbf{E}_p^* \rangle \mathbf{E}_{p'} + \langle \mathbf{E}_{p'} \cdot \mathbf{E}_{p'}^* \rangle \mathbf{E}_{p'} + \langle \mathbf{E}_p^* \cdot \mathbf{E}_{p'} \rangle \mathbf{E}_p) \quad (119)$$

$$\mathbf{P}_B(\omega - \Omega) = \chi_s^{(3)} \langle \mathbf{E}_p^* \cdot \mathbf{E}_{p'} \rangle \mathbf{E}_i + \chi_m^{(3)} (\langle \mathbf{E}_p^* \cdot \mathbf{E}_i \rangle \mathbf{E}_{p'} + \langle \mathbf{E}_{p'} \cdot \mathbf{E}_{s'}^* \rangle \mathbf{E}_{p'}) \quad (120)$$

$$\begin{aligned}
P_B(\omega + \Omega) = & \chi_s^{(1)} E_{s'} + \chi_s^{(3)} (\langle E_p \cdot E_p^* \rangle E_{s'} + \langle E_{p'} \cdot E_{p'}^* \rangle E_{s'}) \\
& + \chi_m^{(3)} (\langle E_p \cdot E_i^* \rangle E_{p'} + \langle E_{p'} \cdot E_i^* \rangle E_p + \langle E_p^* \cdot E_{s'} \rangle E_p \\
& + \langle E_{p'}^* \cdot E_{s'} \rangle E_{p'})
\end{aligned} \tag{121}$$

Here $P_F(\omega)$ and $P_B(\omega)$ contribute to the forward and backward pumps, respectively, $P_F(\omega - \Omega)$ and $P_B(\omega + \Omega)$ and contribute to the probe image and returned signal fields, respectively. The other two polarizations $P_F(\omega + \Omega)$ and $P_B(\omega - \Omega)$ generate, in addition, a forward-propagating field at $\omega + \Omega$ and a backward-propagating field at $\omega - \Omega$ through the 4-wm process. In the nondegenerate case, these two additional fields can be easily separated from the image and signal. In the degenerate case, they can become additional sources of complications for the PC process. This is discussed in Subsection 4.4.

With these carrier-induced polarizations, the mode-amplitude coefficients of the multimode fields in Equations 84-87 satisfy the following coupled-mode equations.

$$\frac{dA_a^{(p)}}{dz} = \frac{i2\pi\omega}{c} \exp(-i\beta_a z) \iint dx dy P_F(\omega) \cdot \psi_a \tag{122}$$

$$\frac{dA_a^{(p')}}{dz} = - \frac{i2\pi\omega}{c} \exp(i\beta_a z) \iint dx dy P_B(\omega) \cdot \psi_a \tag{123}$$

$$\frac{dA_a^{(i)}}{dz} = \frac{i2\pi(\omega - \Omega)}{c} \exp(-i(\beta_a - \delta\beta_a)z) \iint dx dy P_F(\omega - \Omega) \cdot \psi_a \tag{124}$$

$$\frac{dA_a^{(s')}}{dz} = - \frac{i2\pi(\omega + \Omega)}{c} \exp(i(\beta_a + \delta\beta_a)z) \iint dx dy P_B(\omega + \Omega) \cdot \psi_a \tag{125}$$

In these equations, the total carrier-induced polarizations, $P_F = P_F^{(1)} + P_F^{(3)}$ and $P_B = P_B^{(1)} + P_B^{(3)}$, which include the carrier-contributed saturated optical gain in $P_F^{(1)}$ and $P_B^{(1)}$ were used. This is because the defined waveguide modes were in terms of the intrinsic waveguide structure without injection, as has

been discussed in the previous section. In the strong-pump approximation, if the pump intensities are kept constant, the carrier-induced background saturated susceptibility, $\chi_s^{(1)}$, does not vary with the mixing fields. Also included is $\chi_s^{(1)}$ in the total linear dielectric constant of the waveguide used to define the modes. Then P_F and P_B in each of Equations 122-125 should be replaced by $P_F^{(3)}$ and $P_B^{(3)}$, respectively. However, β_a and ψ_a then become complex since the total linear dielectric constant becomes complex with the linear gain included. Both approaches give the same result, but the first one is more convenient for the analysis in this report.

The nonlinear mixing terms in Equations 116-121 stem from various physical origins. There are four categories,

$$\langle E_p \cdot E_p^* \rangle, \langle E_p^* \cdot E_p \rangle \text{ standing grating } \sim \cos 2\beta z \quad (126)$$

$$\left. \begin{array}{l} \langle E_p^* \cdot E_i \rangle, \langle E_p \cdot E_s^* \rangle \\ \langle E_p \cdot E_i^* \rangle, \langle E_p^* \cdot E_s \rangle \end{array} \right\} \text{ moving grating } \sim \cos (2\beta z + \Omega t) \quad (127)$$

$$\langle E_p \cdot E_p^* \rangle, \langle E_p^* \cdot E_p \rangle \text{ transverse grating } \sim \text{constant in } z \text{ and } t \quad (128)$$

$$\left. \begin{array}{l} \langle E_p^* \cdot E_i \rangle, \langle E_p \cdot E_s^* \rangle \\ \langle E_p \cdot E_i^* \rangle, \langle E_p^* \cdot E_s \rangle \end{array} \right\} \text{ oscillating index } \sim \cos (\Omega t - \delta\beta z) \quad (129)$$

Notice that in addition to the z - and t -dependencies, every term has x - and y -dependencies which set up transverse standing gratings. For the $\langle E_p \cdot E_p^* \rangle$ and $\langle E_p^* \cdot E_p \rangle$ terms, the background saturation contributions, which do not depend on the spatial frequencies, have already been accounted for in $\chi_s^{(1)}$ and are included in $P_F^{(1)}$ and $P_B^{(1)}$. Therefore, these terms in $P_F^{(3)}$ and $P_B^{(3)}$ include only those transverse gratings set up by mixing between different modes in the pump fields. They disappear with single-mode pumps. The standing and moving gratings in Equations 126 and 127, respectively, are

created by interference between counterpropagating fields while the index-saturating transverse gratings and the time-dependent index oscillations, in Equations 128 and 129, respectively, are generated by copropagating fields.

In the absence of carrier diffusion, such as 4-wm in an optical fiber, the spatial-frequency dependencies of the mixing efficiency through the Lorentzian function in each term disappear completely. In this case, every term in these equations contributes and the symbols, \langle and \rangle , for the spatial-frequency dependence can be dropped. Where carrier diffusion is present, the spatial-frequency dependencies are important and the four categories of contributions have very different efficiencies. In a typical semiconductor waveguide, such as one of GaAs, $n_0 \sim 3.5$, $\lambda = 2\pi c/\omega \sim 0.8 \mu\text{m}$, and $L \sim 2 \mu\text{m}$. From Equation 89, this results in $2\beta L > 2k_0 L > 100$.

Therefore, the nonlinear terms contributed by the standing and moving gratings vanish in the presence of carrier diffusion because of their vanishingly small efficiency according to Equation 100. Notice, that unlike the conclusion derived from spatial averaging discussed by Bogatov, et al. (Ref. 48) and that the effect of the moving gratings depends on the detuning frequency Ω , the analysis shows that the moving gratings vanish irrespective of the detuning frequency, as can be seen from Equation 100. One conclusion can be immediately drawn from these discussions: In the presence of carrier diffusion, the copropagating fields in the 4-wm process cannot be orthogonally polarized, while the relative direction between polarizations of counterpropagating fields does not affect the wave-mixing efficiency at all. For maximum efficiency, the copropagating fields have to be polarized in the same direction.

Equations 124 and 125 describe the coupling between the probe image field and the conjugate signal. The relevant carrier-induced polarizations are $P_p(\omega - \Omega)$ and $P_s(\omega + \Omega)$ with the standing and moving grating terms dropped from Equations 117 and 121, respectively. For the signal field (E_s in Eq. 87) to be the PC of the image field (E_i in Eq. 86) with high fidelity, it is necessary that $A_a^{(s')} = K_a A_a^{(i)*}$ for every mode a with a mode-independent constant, $K_a = K$. The generation and development of the amplitude for each mode in the signal field is governed by

$$\begin{aligned}
\frac{dA_a^{(s')}}{dz} &= - \frac{i2\pi(\omega + \Omega)}{c} \exp(i(\beta_a + \delta\beta_a)z) \iint dx dy \psi_a \cdot \{ \chi_s^{(1)} \mathbf{E}_s \\
&+ \chi_s^{(3)} (\langle \mathbf{E}_p \cdot \mathbf{E}_p^* \rangle + \langle \mathbf{E}_{p'} \cdot \mathbf{E}_{p'}^* \rangle) \mathbf{E}_{s'} + \chi_m^{(3)} \langle \mathbf{E}_p \cdot \mathbf{E}_i^* \rangle \mathbf{E}_{p'} \\
&+ \chi_m^{(3)} \langle \mathbf{E}_{p'} \cdot \mathbf{E}_s^* \rangle \mathbf{E}_{p'} \} \\
&= - \frac{i2\pi(\omega + \Omega)}{c} \{ SG + SM + PC + SC \}
\end{aligned} \tag{130}$$

The signal is first generated by scattering off the backward-propagating pump by the oscillating index fluctuation created by interference between \mathbf{E}_p and \mathbf{E}_i^* . This process is described by the PC term. The first (SG) term provides the growth of the signal amplitude through the saturated gain, which is partially responsible for the very large signal efficiency in the 4-wm experiments with the semiconductor active medium (Refs. 14 and 17). The second and third terms (SM) account for the scattering and modulation of the signal induced by the transverse standing gratings created by the mixing between the modes of the strong forward- and backward-propagating pump fields, respectively. Once the signal is generated by the PC term, it is amplified and modulated by the SG and SM terms. In addition, it can beat with the backward-propagating pump field to create an oscillating index fluctuation which scatters off the backward pump field $\mathbf{E}_{p'}$ into the signal. This process is described by the last (SC) term. The SG and SM processes do not create complexities in cross coupling between different modes in the image and signal fields, while the PC and SC processes are the source of complexities. The effects for these two terms are similar. To understand the effect of carrier diffusion, it suffices to examine only the PC term.

With the multimode fields given in Equations 84-87, one has

$$\begin{aligned}
PC &= \iint dx dy \chi_m^{(3)} \langle \mathbf{E}_p \cdot \mathbf{E}_i^* \rangle \mathbf{E}_{p'} \cdot \psi_a \exp(i(\beta_a + \delta\beta_a)z) \\
&= C_{aaaa} A_a^{(p')} A_a^{(p)} A_a^{(1)*} \exp(i2\delta\beta_a z) + \sum_{b \neq a} C_{abba} A_b^{(p')} A_b^{(p)} A_a^{(1)*} \exp(i2\delta\beta_a z) \\
&+ \sum_{b \neq a} C_{aabb} A_a^{(p')} A_b^{(p)} A_b^{(1)*} \exp(i(\delta\beta_a + \delta\beta_b)z)
\end{aligned} \tag{131}$$

where only the nearly phase-matched terms are kept. The subscript indices of the nonlinear coupling coefficients, C_{abba} and C_{aabb} , correspond to the modes in the four mixing fields in the s'p'p i sequence. These nonlinear coupling coefficients are functions of spatial and temporal beat frequencies which depend strongly on the mixing modes,

$$C_{abba} = -\frac{\chi_s^{(1)}}{I_s} \iint dx dy \psi_a \cdot \psi_b \left\langle \frac{\mathcal{L}(\beta_b - \beta_a + \delta\beta_a; \Omega) \psi_b \cdot \psi_a}{1 + \mathcal{L}(\beta_b - \beta_a + \delta\beta_a; \Omega) \sum_a (I_a^{(p)} + I_a^{(p')}) / I_s} \right\rangle \quad (132)$$

$$C_{aabb} = -\frac{\chi_s^{(1)}}{I_s} \iint dx dy \psi_a \cdot \psi_a \left\langle \frac{\mathcal{L}(\delta\beta_b; \Omega) \psi_b \cdot \psi_b}{1 + \mathcal{L}(\delta\beta_b; \Omega) \sum_a (I_a^{(p)} + I_a^{(p')}) / I_s} \right\rangle \quad (133)$$

where Equation 115 was used and the transverse-spatial-frequency dependencies of \mathcal{L} are determined by the transverse patterns of the modes in the angle brackets. The dependence of \mathcal{L} on $\delta\beta$ in Equations 132 and 133 can be neglected since $\delta\beta L \sim n\Omega L/c \sim 10^{-5}$ for $\Omega\tau \sim 1$. C_{aaaa} can be obtained by setting $a = b$ in either Equation 132 or 133. Without loss of generality, it is also assumed that the injection current is uniformly distributed so that $\chi_s^{(1)}$ is a spatially-independent constant in the guiding region. To illustrate the full spatial-frequency dependencies of the nonlinear coupling coefficients, take the mode pattern of the strongly index-guided mode (Ref. 50) as an example. With the origins of the transverse x- and y-coordinates defined at the center of the waveguide, the transverse mode pattern in the guiding regions, $-w/2 \leq x \leq w/2$ and $-d/2 \leq y \leq d/2$, can be written (Ref. 50).

$$\psi_a(x, y) = \frac{2}{\sqrt{wd}} \cos(\xi_a x + \alpha_a) \cos(\eta_a y + \gamma_a) e_a \quad (134)$$

where e_a is the unit polarization vector of mode a , and w and d can be considered effective cross-sectional dimensions of the guiding region (Ref. 50). For simplicity, neglect the exponentially decaying fields outside the guiding region in the integration for C_{abba} and C_{aabb} . Since the interest is in multimode waveguides with many guided modes, most modes will be well

guided and this simplification will not change any general conclusions. It is also assumed that the copropagating fields are polarized in the same direction for maximum 4-wm efficiency.

4.3.1 Low Saturation, $\Sigma_a(I_a^{(p)} + I_a^{(p')})/I_s \ll 1$

In this case, since $|\mathcal{Q}| \leq 1$, $1 + \mathcal{Q}(\Omega) \Sigma_a(I_a^{(p)} + I_a^{(p')})/I_s \approx 1$. For $a \neq b$, one obtains

$$C_{aaaa} = - \frac{\chi_s^{(1)}}{4\omega d I_s} \left\{ \mathcal{Q}(2\xi_a, 2\eta_a, 0; \Omega) + 2\mathcal{Q}(2\xi_a, 0, 0; \Omega) + 2\mathcal{Q}(0, 2\eta_a, 0; \Omega) + 4 \right\} \quad (135)$$

$$C_{abba} = - \frac{\chi_s^{(1)}}{4\omega d I_s} \left\{ \mathcal{Q}(\xi_a + \xi_b, \eta_a + \eta_b, \beta_a - \beta_b; \Omega) + \mathcal{Q}(\xi_a + \xi_b, \eta_a - \eta_b, \beta_a - \beta_b; \Omega) (1 + \delta_{\eta_a, \eta_b}) + \mathcal{Q}(\xi_a - \xi_b, \eta_a + \eta_b, \beta_a - \beta_b; \Omega) (1 + \delta_{\xi_a, \xi_b}) + \mathcal{Q}(\xi_a - \xi_b, \eta_a - \eta_b, \beta_a - \beta_b; \Omega) (1 + \delta_{\xi_a, \xi_b}) (1 + \delta_{\eta_a, \eta_b}) \right\} \quad (136)$$

$$C_{aabb} = - \frac{\chi_s^{(1)}}{4\omega d I_s} \left\{ 2\mathcal{Q}(0, 2\eta_a, 0; \Omega) \delta_{\eta_a, \eta_b} + 2\mathcal{Q}(2\xi_a, 0, 0; \Omega) \delta_{\xi_a, \xi_b} + 4 \right\} \quad (137)$$

From Equations 130 and 131, the mode intensity in the conjugate signal $I_a^{(s')} \propto |A_a^{(s')}|^2 \propto |C|^2 \propto |\mathcal{Q}|^2$. From Equation 100, if any one of the following conditions,

$$(i) |\xi_a \pm \xi_b|L \leq 1, (ii) |\eta_a \pm \eta_b|L \leq 1, \text{ or } (iii) |\beta_a \pm \beta_b|L \leq 1 \quad (138)$$

is not valid, $|\mathcal{Q}|^2$ will be reduced to ≤ 0.25 . If any two of these three conditions are violated, then $|\mathcal{Q}|^2 \leq 0.1$. Using Equations 88 and 89, it can be shown that if Conditions (i) and (ii) are both satisfied, $|\beta_a - \beta_b|L < 1$. Since the \mathcal{Q} functions in Equations 135-137 depend only on $\beta_a - \beta_b$ and not on

$\beta_a + \beta_b$, only Conditions (i) and (ii) need to be considered in the evaluation of the contribution of each term C_{aaaa} , C_{abba} , and C_{aabb} to the conjugate signal.

For the strongly index-guided modes given in Equation 134, one has $\xi_a = q_a \pi / \omega$ and $\eta_a = m_a \pi / d$, where q_a and m_a are positive integers. The numbers of guided modes in the x- and y-directions are $Q \sim 2n\omega/\lambda$ and $M \sim 2nd/\lambda$, respectively, and the total number of guided modes is $N = QM$. With $n \sim 3.5$, $\lambda \sim 0.8 \mu\text{m}$, and $L \approx 2 \mu\text{m}$ Conditions (i) and (ii) in Equation 138 become

$$(i) \quad |q_a \pm q_b| \leq 0.018Q \quad \text{and} \quad (ii) \quad |m_a \pm m_b| \leq 0.018M \quad (139)$$

These conditions are hard to satisfy for the terms with spatial sum-frequency dependencies in Equations 135-137 unless Q and M are extremely large and a and b are modes of very low order. Therefore, except for a few low-order modes, one will expect

$$C_{aaaa} \sim C_{aabb} \sim - \frac{\chi_s^{(1)}}{wdI_s} \quad (140)$$

$$C_{abba} \sim - \frac{\chi_s^{(1)}}{4wdI_s} \mathcal{G}(\xi_a - \xi_b, \eta_a - \eta_b, \beta_a - \beta_b; \Omega) (1 + \delta_{\xi_a, \xi_b}) (1 + \delta_{\eta_a, \eta_b}) \quad (141)$$

Notice that for C_{abba} in Equations 131 and 141, the mode index a refers to the modes in the image and signal fields and the index b refers to the modes that exist simultaneously in the two pump fields. For the spatial difference-frequency dependencies in Equation 141, the conditions in Equation 139 can be satisfied only when a and b are neighboring modes. However, even when a and b are directly adjacent modes such that $|q_a - q_b| = 1$ or $|m_a - m_b| = 1$, Equation 139 requires a minimum number of guided modes, $Q_{\min} > 55$ or $M_{\min} > 55$, respectively.

From Equation 131, the desirable PC signal $A_s^{(s')} = K_s A_s^{(1)*}$ comes from the contributions of the first two terms associated with C_{aaaa} and C_{abba} , respectively. The third term associated with C_{aabb} actually creates cross-talk between different modes in the image and signal fields and is not desirable,

although it usually exists in the case of multimode pumps. The C_{aaaa} term accounts for the generation of the mode amplitude $A_a^{(s')}$ in the conjugate signal when both pumps are also coupled into the mode a . The term associated with C_{abba} describes the more general source of generation of $A_a^{(s')}$ by all the other modes in the pump fields. In the case without carrier diffusion, this term is the major source of contribution (Ref. 11). Then, either single-mode (Ref. 9) or multimode (Ref. 11) pumps will work well to generate a PC signal. With single-mode pumps, the complication due to the C_{aabb} term also disappears. These nice features are not available in the presence of carrier diffusion because of the requirement of Conditions (i) and (ii) in Equation 139 on C_{abba} . As an example, assume that both pumps are coupled into only one mode, say the fundamental mode, and the waveguide supports a large number of guided modes in both the x- and y-directions such that $N = QM \gg 55^2 \sim 3,000$. Then, out of the total N available modes, the signal will be generated through C_{abba} only within the $\sim 3 \times 10^{-4} N$ modes closest to the pump mode. With multimode pumps, the C_{abba} term only creates signal in modes around the pump modes. From Equation 140, $C_{aaaa} \sim \text{constant}$ and $K_a \propto A_a^{(p')} A_a^{(p)}$, except for a few very low-order modes. Therefore, although the C_{aaaa} term always exists, the signal amplitude $A_a^{(s')}$ in each mode depends on the amplitudes of the pump fields in the particular mode. From the discussions in this section, the conclusion is that the diffusion of carriers in a semiconductor waveguide severely complicates the coupling between various modes and limits the possibility of the generation of a high-fidelity PC signal. In fact, the only possibility of generating a high-fidelity PC signal with sufficient image resolution in a multimode semiconductor waveguide with carrier diffusion may be by coupling both pump fields into all the guided modes *uniformly*. Then the C_{aaaa} and C_{abba} terms will generate $A_a^{(s')} = KA_a^{(i)*}$ for all the guided modes a with K depending little on the mode index. However, even in this situation, the C_{aabb} term exists and contributes to some undesirable cross-talk coupling between modes.

4.3.2 High Saturation, $\Sigma_a(I_a^{(p)} + I_a^{(p')})/I_s > 1$

In semiconductor laser waveguides, it is common to have significant gain saturation. When $|\mathcal{L}(\Omega)\Sigma_a(I_a^{(p)} + I_a^{(p')})/I_s| \geq 1$, the \mathcal{L} functions in Equations 135-137 for C_{aaaa} , C_{abba} , and C_{aabb} , respectively, have to be replaced by $\mathcal{L}/(1 + \mathcal{L}\Sigma_a(I_a^{(p)} + I_a^{(p')})/I_s)$, as can be realized from Equations 132 and 133.

This makes C_{aaaa} , C_{abba} , and C_{aabb} look very complicated, but it does not change much of the conclusions obtained in the case of low saturation. However, since now $\Sigma_a(I_a^{(p)} + I_a^{(p')})/I_s > 1$, it is possible that $|\mathcal{L}\Sigma_a(I_a^{(p)} + I_a^{(p')})/I_s| > 1$ even when Conditions (i) and (ii) are not satisfied and $|\mathcal{L}|$ is small. The effect of gain saturation is to relax Conditions (i) and (ii) in Equation 138 to

$$\begin{aligned} \text{(iv)} \quad & |\xi_a \pm \xi_b|L \leq \left\{ \Sigma_a (I_a^{(p)} + I_a^{(p')}) / I_s \right\}^{1/2} \\ \text{(v)} \quad & |\eta_a \pm \eta_b|L \leq \left\{ \Sigma_a (I_a^{(p)} + I_a^{(p')}) / I_s \right\}^{1/2} \end{aligned} \quad (142)$$

This is equivalent to the following relaxed conditions in place of Equation 139,

$$\begin{aligned} \text{(iv)} \quad & |q_a \pm q_b| \leq 0.018Q \left\{ \Sigma_a (I_a^{(p)} + I_a^{(p')}) / I_s \right\}^{1/2} \\ \text{(v)} \quad & |m_a \pm m_b| \leq 0.018M \left\{ \Sigma_a (I_a^{(p)} + I_a^{(p')}) / I_s \right\}^{1/2} \end{aligned} \quad (143)$$

Therefore, for those terms in C_{aaaa} , C_{abba} , and C_{aabb} which have spatial frequencies satisfying Conditions (iv) and (v), $\mathcal{L}/(1 + \mathcal{L}\Sigma_a(I_a^{(p)} + I_a^{(p')})/I_s) \approx I_s/\Sigma_a(I_a^{(p)} + I_a^{(p')})$. They become independent of the spatial beat frequencies. If the waveguide becomes so severely saturated that $\Sigma_a(I_a^{(p)} + I_a^{(p')})/I_s \gg 1$ and Conditions (iv) and (v) are satisfied for the sum and difference beat frequencies between any two guided modes, the C_{abba} and C_{aabb} become totally independent of the spatial and temporal frequencies and, for $a \neq b$,

$$C_{aaaa} = - \frac{9\chi_s^{(1)}}{4\omega d \Sigma_a (I_a^{(p)} + I_a^{(p')})} \quad (144)$$

$$C_{abba} = C_{aabb} = - \frac{\chi_s^{(1)}}{4\omega d \Sigma_a (I_a^{(p)} + I_a^{(p')})} (2\delta_{\xi_a, \xi_b} + 2\delta_{\eta_a, \eta_b} + 4) \quad (145)$$

These are exactly what will be obtained in the case of no carrier diffusion. However, the nonlinear coupling coefficients and, therefore, the 4-wm efficiency are severely reduced by the increase of saturation. Notice that in

addition to the $(\Sigma_a(I_a^{(p)} + I_a^{(p')}))^{-1}$ dependence in Equations 144 and 145, $\chi_s^{(1)}$ is also inversely proportional to $\Sigma_a(I_a^{(p)} + I_a^{(p')})$ according to Equation 108. Therefore, although gain saturation relaxes the stringent limitation of coupling the power of a pump mode to other modes in the signal due to carrier diffusion, this comes at a price of severely reducing the overall nonlinear coupling efficiency. In fact, $|g|$ falls off quickly when either of Conditions (i) or (ii) is not satisfied. For the transverse gratings generated by beat frequencies which satisfy Conditions (iv) and (v) but not Conditions (i) or (ii), their contributions to the nonlinear coupling efficiency becomes unimportant although Equations 144 and 145 apply. The conclusion is that gain saturation can relax the limitation caused by carrier diffusion but in a very undesirable way. For Equations 144 and 145 to apply for a large enough mode so that a high-fidelity PC signal can be generated with sufficient resolution, the saturation needed would be so high that the nonlinear coupling coefficients become vanishingly small and the signal disappears altogether.

4.4 DEGENERATE FOUR-WAVE MIXING

In the degenerate case, when $\omega_p = \omega_{p'} = \omega_1 = \omega_{s'}$, $\Omega \rightarrow 0$ and $\delta\beta \rightarrow 0$. Then, the moving gratings identified in Equation 127 become standing gratings like those in Equation 126 and the time-dependent oscillating index terms in Equation 128 become only time-independent transverse gratings like those in Equation 129. In the presence of carrier diffusion, those terms with a longitudinal grating of spatial frequency 2β certainly do not contribute also in the degenerate case. Therefore, still only those terms identified in Equations 128 and 129 are kept for the carrier-induced polarizations.

As discussed earlier and expressed in Equations 124 and 125, in the nondegenerate case only $P_F(\omega - \Omega)$ and $P_B(\omega + \Omega)$ contribute to the generation, growth, and modulation of $A_s^{(i)}$ and $A_s^{(s')}$, respectively. The polarizations $P_F(\omega + \Omega)$ and $P_B(\omega - \Omega)$ are also generated in the 4-wm process, but they can be easily distinguished from the contributions of $P_F(\omega - \Omega)$ and $P_B(\omega + \Omega)$ and do not affect $A_s^{(i)}$ and $A_s^{(s')}$, directly. The major difference between the degenerate and nondegenerate cases is that in the degenerate case this distinction disappears and the coupling between $A_s^{(i)}$ and $A_s^{(s')}$ is complicated

by these two additional polarizations, $P_F(\omega+\Omega)$ and $P_B(\omega-\Omega)$, as $\Omega \rightarrow 0$. In the strong-pump approximation and in the presence of carrier diffusion, one can then write

$$P_F^{(p)}(\omega) = \chi_s^{(1)} E_p + \chi_s^{(3)} (\langle E_p \cdot E_p^* \rangle E_p + \langle E_{p'} \cdot E_p^* \rangle E_p) \quad (146)$$

$$\begin{aligned} P_F^{(i)}(\omega) = & \chi_s^{(1)} E_i + \chi_s^{(3)} (\langle E_p \cdot E_p^* \rangle E_i + \langle E_{p'} \cdot E_p^* \rangle E_i) \\ & + \chi_m^{(3)*} (\langle E_p^* \cdot E_i \rangle E_p + \langle E_{p'}^* \cdot E_i \rangle E_p) \\ & + \chi_m^{(3)} (\langle E_p \cdot E_i^* \rangle E_p + \langle E_{p'} \cdot E_i^* \rangle E_p) \end{aligned} \quad (147)$$

$$P_B^{(p')}(\omega) = \chi_s^{(1)} E_{p'} + \chi_s^{(3)} (\langle E_p \cdot E_p^* \rangle E_{p'} + \langle E_{p'} \cdot E_p^* \rangle E_{p'}) \quad (148)$$

$$\begin{aligned} P_B^{(s')}(\omega) = & \chi_s^{(1)} E_{s'} + \chi_s^{(3)} (\langle E_p \cdot E_p^* \rangle E_{s'} + \langle E_{p'} \cdot E_p^* \rangle E_{s'}) \\ & + \chi_m^{(3)} (\langle E_p \cdot E_i^* \rangle E_{p'} + \langle E_{p'}^* \cdot E_{s'} \rangle E_{p'}) \\ & + \chi_m^{(3)*} (\langle E_p^* \cdot E_i \rangle E_{p'} + \langle E_{p'} \cdot E_{s'}^* \rangle E_{p'}) \end{aligned} \quad (149)$$

Equations 146 and 148 are identical to Equations 116 and 119, respectively, except that the terms corresponding to the standing longitudinal gratings are dropped due to carrier diffusion. Equations 122 and 123 are still valid with $P_F(\omega)$ and $P_B(\omega)$ replaced by $P_F^{(f)}$ and $P_B^{(p')}(\omega)$, respectively. Therefore, in the strong-pump approximation, the pumps are not changed by frequency degeneracy. However, the coupled-mode equations for $A_a^{(i)}$ and $A_a^{(s)}$ given in Equations 124 and 125 have to be modified by replacing $P_F(\omega-\Omega)$ and $P_B(\omega+\Omega)$ with $P_F^{(i)}$ and $P_B^{(s')}(\omega)$, respectively, in addition to setting $\Omega = 0$ and $\delta\beta_a = 0$. Therefore, the generation, development, modulation, and coupling of $A_a^{(s')}$ is now described by

$$\frac{dA_a^{(s')}}{dz} = - \frac{i2\pi\omega}{c} \{SG + SM + PC + SC + AM\} \quad (150)$$

where the SG, SM, PC, and SC terms are the same as those defined in Equation 130.

They also provide the same contributions and limitations to the PC 4-wm process as described in Subsection 4.3 for the nondegenerate case. The existence of the anomalous mixing (AM) terms in Equation 150 is due to the fact that $P_B(\omega - \Omega)$ given in Equation 120 also contributes to $P_B^{(s')}(\omega)$ in the degenerate case,

$$AM = \iint dx dy \chi_m^{(3)*} \left(\langle E_p^* \cdot E_i \rangle E_{p'} + \langle E_{p'} \cdot E_s^* \rangle E_p \right) \cdot \psi_a \exp(i\beta_a z) \quad (151)$$

The effect of carrier diffusion on the multimode-field mixing of the AM terms in Equation 151 is similar to that discussed in Subsection 4.3 for the PC term.

From Equations 150 and 151, it is obvious that the effect of frequency degeneracy is to couple $A_a^{(s')}$ to the modes of E_i and E_s^* directly. As a consequence, one can expect that $A_a^{(s')}$ becomes a sum of many different contributions. In addition to the desirable PC contribution, $K_a A_a^{(i)*}$, discussed in Subsection 4.3, there is a non-PC contribution, $K'_a A_a^{(i)} + \sum_{b \neq a} K'_{ba} A_b^{(i)}$, to the backward-propagating signal amplitude $A_a^{(s')}$. There is also a backward-propagating amplitude proportional to $A_a^{(s')*}$ due to the second AM term in Equation 151. Obviously, these extra contributions in the degenerate case tend to destroy the PC signal. With a single-mode waveguide, it can be seen that the returned signal in a degenerate 4-wm process can never be the PC of the probe field because the AM terms are as effective as the PC term in generating the backward-propagating signal in this case. However, as is discussed earlier, in order to have sufficient image resolution in a PC image replication process, a multimode waveguide with a large number of guided modes is necessary. It can be shown through a more detailed study of the AM term that the non-PC backward-propagating signals proportional to E_i and E_s^* , are only generated in the modes where both pumps exist. Therefore, if the multimode waveguide is pumped with single-mode pump fields, all the modes in the signal will not be affected by the AM terms except the one mode where the pumps exist. However, this is only possible in a waveguide without carrier diffusion since carrier diffusion makes the coupling of the power from a pump mode to a different mode in the signal very inefficient, as has been discussed in Subsection 4.3.

On the other hand, it seems that even when the waveguide is pumped with multimode pump fields, the effect of the AM contributions is not to destroy the PC replica of the image but only to reduce the efficiency by coupling pump powers to a non-PC background noise signal. This is because only the PC components of the backward-propagating signal field can add together at a certain distance away from the waveguide entrance to reproduce the image, while the non-PC components, not having the correct total z -dependent phase relationship among the modes, tend to diverge and average out as a background noise at a distance. This probably explains why Jensen and Hellwarth (Ref. 10) could observe PC image replication through a degenerate 4-wm process in a waveguide pumped with multimode pump fields.

Finally, there is a question as to how small Ω should be when it can be considered degenerate. To our understanding, so long as there are externally applied strong pumps as the arrangement shown in Figure 2, Ω is limited only by the ability to resolve the frequencies. In other words, the frequency degeneracy is instrument-defined. However, with a semiconductor laser waveguide, it is possible to drive the laser above threshold and use the internal lasing fields as pumps. In this case, Ω has to be kept larger than the injection-locking range (Ref. 17). Otherwise, the laser waveguide can become injection-locked and the PC process no longer exists.

4.5 CONCLUSIONS

Four-wave mixing in a semiconductor waveguide under current injection has a very large signal gain due to the large carrier-induced optical gain and optical nonlinearity in the semiconductor medium. The interest is in the possibility of utilizing this large conjugate signal gain for optical PC image replication. For the generation of a PC replica image with a multimode waveguide, the participation of a large number of guided propagating modes is needed for sufficient image resolution. In addition, the PC efficiency has to be uniform across the modes in the image field for high-fidelity PC. Carrier diffusion in a semiconductor waveguide under current sets many limitations on these requirements.

The effect of carrier diffusion on PC 4-wm in multimode semiconductor waveguides has been studied. Several conclusions are obtained from the

analysis. First of all, the gratings set up by counterpropagating fields in a 4-wm arrangement are always washed out by carrier diffusion. The whole process relies on the transverse gratings and the time-dependent index oscillation set up by beating between copropagating fields to provide any conjugate signal reflectivity. Therefore, the copropagating fields cannot be orthogonally polarized. For maximum efficiency, they have to be polarized in parallel. On the other hand, the relative direction between polarizations of the counterpropagating fields does not affect the efficiency. The major effect of carrier diffusion is to severely limit the efficiency of coupling the power in a particular pump mode to other modes in the signal and image fields. In a typical semiconductor waveguide, the power in each pump mode can be coupled to only a very small fraction of all guided modes. Even in a waveguide with a very large number of guided propagating modes, only modes very closely neighboring a pump mode can be generated in the conjugate field. This makes it totally impossible to pump with single-mode pumps. The only possibility is to couple both pump fields into all the guided modes with uniform amplitudes across the pump modes, which is certainly very difficult if not impossible. Gain saturation by strong pumps, which is common in semiconductor waveguides, relaxes this limitation. The power in a pump mode can be coupled to more modes in the signal field as the saturation increases. In the limit of very high saturation, the effect of carrier diffusion becomes unimportant and the nonlinear mode-coupling coefficients reduce to those of no carrier diffusion. However, this does not solve the problem since gain saturation severely reduces the 4-wm efficiency. To the extent that saturation sufficiently removes the effect of carrier diffusion, the conjugate signal also disappears altogether.

The experimental observation of Lucente, *et al.* (Ref. 43) is consistent with our conclusions. In their experiment, PC 4-wm was performed with a noncollinear geometry in a broad-area semiconductor laser waveguide. The PC signal was observed to have spatial- and frequency-dependencies of a Lorentzian lineshape function. In this experimental setup, the pump and probe fields were obviously coupled into only one spatial mode but were separated by the noncollinear geometry. The grating responsible for the generation of the conjugate signal was created by the noncollinear wave vectors of the forward-propagating pump and the probe fields. This is equivalent to the last term in

C_{abba} . Among all the terms discussed in Subsection 4.3, only this term existed in their experiment because the noncollinear pump and probe fields were coupled into only one mode.

5.0 CONJUGATE GENERATION REQUIREMENTS IN MULTIMODE WAVEGUIDES AND THE UTILITY OF WAVEGUIDE ARRAYS

5.1 INTRODUCTION

The formalism developed in Sections 3.0 and 4.0 shows that some stringent requirements must be satisfied in order to generate a PC beam in a multimode waveguide. In the first part of the section, these requirements are discussed and placed in the context of previously published work. The additional constraints imposed when the nonlinear interaction is subject to diffusion effects are also considered. Finally, the idea of using 4-wm in an array of single mode waveguides as a means of overcoming the limitations imposed on multimode waveguides is introduced. The use of the array also allows optical control of the propagation direction of the conjugate wavefront, a feature not possible in multimode waveguides and only achievable in some bulk media using precise wavelength control of the interacting beams.

5.2 MULTIMODE WAVEGUIDE PHASE-CONJUGATION REQUIREMENTS

The first requirement for high fidelity phase conjugation is that the pump beams must not be depleted by the nonlinear interaction. As with bulk media, the "undepleted pump approximation" is necessary to keep the phase of the generated beam in each mode (or wave vector in the bulk case) from phase and amplitude variations due to the z-dependent amplitude coefficients of the pump beams. This is quite reasonable given the similarity between first-order differential equations for the coupled-wave and coupled-mode formalisms. Except for the overall proportionality factors and a replacement of the k-vector delta function in the bulk case with the transverse overlap integral of the mode patterns in the waveguide (Ref. 25), the two formalisms similarly relate the generated field amplitude to the input field amplitudes.

A second constraint that generally arises relates to the fact the P_z^{NL} must be treated differently from P_T^{NL} in the coupled-mode formalism. If the longitudinal nonlinear polarization plays a significant role, then the coupled-mode equations must be solved iteratively, as shown in Section 3.0. This iterative process will not retain the phase relationship between the conjugate of the input signal and the generated beam and, therefore, lead to a degrading of the

phase conjugation fidelity. Though there are specific cases where P_z^{NL} will not play a role due to the specific geometry or material properties, in general, phase conjugation in multimode waveguides is limited to those situations where it can be ignored. This requires that all modes involved in the nonlinear interaction be guided and that the condition of weak guiding hold (Ref. 29). Weak guiding requires that the modes vary slowly, with respect to the optical wavelength, in the transverse directions. Because the longitudinal component of the electric field is related to the transverse mode derivatives in Maxwell's equation, the z-components of the electric field and nonlinear polarization can generally be ignored when all modes involved in the interaction are weakly guided.

Assuming that P_z^{NL} can be neglected, the mode expansion for the electric field leads to overlap integrals,

$$C_{abcd} = \iint dx dy \psi_{-a} \cdot \chi^{(3)} : \psi_b \psi_c \psi_d \quad (152)$$

and phase factors, $\exp(-i(\beta_a - \beta_b - \beta_c - \beta_d)z)$, in the coupled-mode equations. In general, Equation 152 implies coupling among all combinations of modes in the mixing process. However, Hellwarth has pointed out that only pairwise mode combinations, e.g., $(a, b, c, d) = (a, b, -a, -b)$ or $(a, a, b, -b)$, etc., make significant contributions in the case where the waveguide length, l , is sufficiently large and the waveguide modes are nondegenerate (Ref. 11). In this case, the overlap integrals essentially become intensity overlap integrals plus a term which describes polarization overlap of the modes and $C_{abcd} = C_{ab}$. With a proper choice of input field polarization, all excited modes can be made collinearly polarized in the weakly guiding waveguide required for negligible P_z^{NL} (Ref. 29).

The coupled-mode equation for the PC can be written in the form,

$$\frac{dA_a^{(s')}}{dz} = - \frac{i4\pi(\omega + \Omega)}{c} \{SM + PC\} \quad (153)$$

where

$$\begin{aligned}
 SM = & 2C_{aa}(|A_a^{(p)}|^2 + |A_{-a}^{(p')}|^2)A_{-a}^{(s')} + \sum_{b \neq a} C_{ab}(|A_b^{(p)}|^2 + |A_{-b}^{(p')}|^2)A_{-a}^{(s')} \\
 & + (A_b^{(p)} A_a^{(p)*} + A_{-a}^{(p')} A_{-b}^{(p')*}) A_{-b}^{(s')} \exp(i(\delta\beta_a - \delta\beta_b)z) \}
 \end{aligned} \quad (154)$$

$$\begin{aligned}
 PC = & C_{aa}A_a^{(p)}A_{-a}^{(p')}A_a^{(i)*} \exp(i2\delta\beta_a Z) \\
 & + \sum_{b \neq a} C_{ab} \{ A_b^{(p)} A_{-b}^{(p')} A_a^{(i)*} \exp(i2\delta\beta_a z) \\
 & + A_b^{(p)} A_{-a}^{(p')} A_b^{(i)*} \exp(i(\delta\beta_a + \delta\beta_b)z) \}
 \end{aligned} \quad (155)$$

$\delta\beta_a$ and $\delta\beta_b$ in Equations 154 and 155 arise from the frequency detuning, Ω . Because intensity overlap integrals are not expected to show a strong mode-to-mode variation (Ref. 11), the first two terms in both SM and PC have the same form as the bulk case. The last term in SM and PC arise from the spatial overlap of pump and probe beams. Therefore, as in bulk media, phase conjugation by 4-wm in waveguides requires undepleted pumps and is only possible when P_z^{NL} can be ignored, i.e., the weak-guiding or slow transverse variation limit. If the image and pump beams occupy the same modes, then the image beam cannot be depleted in the 4-wm interaction. This is the case analyzed by Hellwarth (Ref. 11). Yariv, *et al.*, analyzed the case when the pump and probe beams occupy different modes and showed that image depletion and conjugate amplification may occur (Ref. 9). Phase conjugation spatial and temporal bandwidth in a multimode waveguide are limited by the requirements of sufficient guiding so that only pairwise spatial overlap integrals contribute, and no dephasing of the spread of pump and image frequency components over the interaction length. These two requirements can be summarized:

$$\frac{\lambda}{S} \ell > 1 \quad (156)$$

and

$$\frac{2\Omega}{c} \ell < 1 \quad (157)$$

where S is the effective cross section of the waveguide. It can be approximated (Ref. 29),

$$S \sim 2n \Delta n A \quad (158)$$

where A is the core cross-sectional area and Δn is the index mismatch between core and cladding. Putting Equations 156 and 157 together limits the number of modes to on the order of 10^3 at a gigahertz bandwidth. Jensen and Hellwarth observed phase conjugation in multimode waveguide containing on the order of 10^5 modes but the conjugate images they reported could have been formed from only the lower order modes of their waveguide (Ref. 10).

In addition to the above considerations, diffusion must be considered in those situations where the nonlinearity results from mobile particles, such as the free carriers in a semiconductor under current injection. In a rectangular waveguide, each transverse mode field pattern, $\psi(x,y)$, is characterized by two transverse wave numbers, ξ_a and η_a , associated with the transverse spatial frequencies of ψ_a in the x - and y -directions, respectively. These wave numbers satisfy the following condition (Ref. 50),

$$\xi_a^2 + \eta_a^2 + \beta_a^2 = \kappa^2 \quad (159)$$

Due to the carrier diffusion, the nonlinear susceptibilities depend on the spatial and temporal beat frequencies through a Lorentzian function,

$$\begin{aligned} \mathcal{L}(\xi_a \pm \xi_b, \eta_a \pm \eta_b, \beta_a \pm \beta_b; \Omega) \\ = \{1 + [(\xi_a \pm \xi_b)^2 + (\eta_a \pm \eta_b)^2 + (\beta_a \pm \beta_b)^2] L^2 - i\Omega\tau\}^{-1} \end{aligned} \quad (160)$$

where τ is the carrier lifetime and L is the carrier diffusion length.

As was discussed in Section 4.0, the contribution of a term in the nonlinear susceptibility becomes negligible unless the transverse beat frequencies in the \mathcal{L} function of this particular term satisfy (i) $|\xi_a \pm \xi_b|L \leq 1$ and (ii) $|\eta_a \pm \eta_b|L \leq 1$. These conditions set stringent limitations on the efficiency of coupling the power from a mode in the pump fields to other modes in the signal. As an example, in a typical semiconductor waveguide with

$n \sim 3.5$, $\lambda = 2\pi c/\omega \sim 0.8 \mu\text{m}$, and $L \sim 2 \mu\text{m}$, each pump mode can only couple to the nearest neighboring modes within $<0.024/\sqrt{\Delta n}$ of the total guided modes in both x- and y-directions. This means that in a truly two-dimensional waveguide with a sufficiently large number of modes for image resolution, each pump mode will couple to only $<6 \times 10^{-4}/\Delta n$ of the total two-dimensional guided modes. As a result, to uniformly couple all the guided modes, the index step, Δn , cannot be $>6 \times 10^{-4}$. This results in a very weakly guiding waveguide with a small acceptance angle of ~ 7 deg at the input from the free space and a very small number of guided modes in the waveguide. When the index step is increased to improve the pixel resolution and the acceptance angle, the multimode coupling becomes highly nonuniform in a waveguide with carrier diffusion.

5.3 FOUR-WAVE MIXING IN A WAVEGUIDE ARRAY

To avoid the problems involved in a multimode waveguide while still keeping the advantages of a waveguide, 4-wm in an array of single-mode waveguides is proposed. The geometry of such an arrangement is shown in Figure 4.

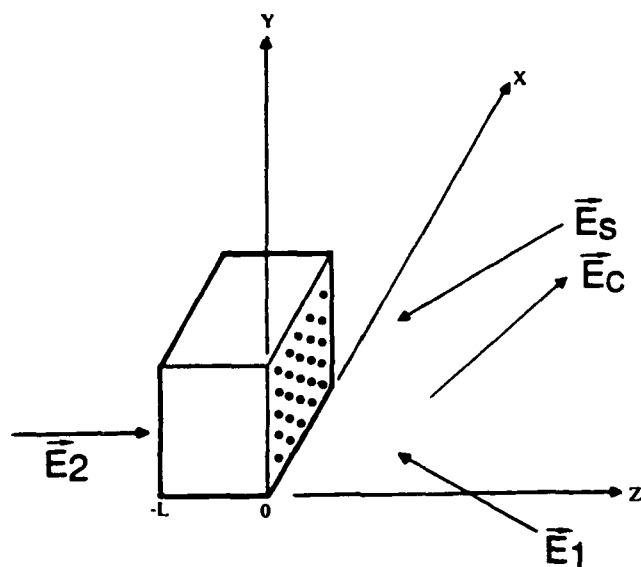


Figure 4. Geometry for 4-wm in a waveguide array with incident pump beams E_1 and E_2 , signal beam E_s , and generated beam E_c .

A periodic array of identical waveguides is located with faces in the x-y plane at $z = 0$ and $z = -L$ and with confined propagation along the z axis. Each waveguide supports only one mode with a propagation constant β , which may

be complex, and an electric-field pattern with the transverse component $\psi(x,y)$ polarized along the y axis. Three beams are incident upon the array; two on the $z = 0$ face and one on the opposite face, with the constraints that their propagation directions fall within the acceptance angle of the waveguide and that their amplitudes are slowly varying across the array face with respect to the interwaveguide spacing. Two of the beams, one on each face, are pump beams at the same frequency, ω_0 , while the third is shifted by an amount Ω . Within the waveguide mode all beams are spatially degenerate, but 4-wm involving the probe beam is frequency shifted from the nonlinear mixing of the two pump beams.

Coupling between the guided mode of each waveguide and the radiation fields is completely determined by the continuity of the tangential electric-field components at the interface and the constraints on the propagation constants in the guided region and free space. If all three incident fields have their tangential polarization along the y axis, to match the guided-mode polarization, then the coupling of the three fields into the waveguides will be determined by their angles of incidence. The angle of incidence will also determine the phase relation between the fields incident at each waveguide.

The three input waves are decomposed into a linear superposition of plane waves,

$$\mathbf{E}_j(x, y, z) = \iint dk_{jx} dk_{jy} \exp[i\mathbf{k}_j \cdot \mathbf{r}] \mathcal{E}_j(k_{jx}, k_{jy}) \quad (161)$$

where the subscript j is s , 1 or 2 for the signal and first and second pump waves, respectively. In free space,

$$|\mathbf{k}_j|^2 = k_{jx}^2 + k_{jz}^2 + = \frac{\omega_j^2}{c^2} \quad (162)$$

and

$$\mathcal{E}_j \cdot \mathbf{k}_j = 0 \quad (163)$$

allowing the z components of \mathcal{E}_j and k_j to be determined in terms of the x and y components. If the surface reflection can be ignored because of, for example, an antireflection coating, then the electric field from the signal beam coupled into the waveguide array at the interface will be (Ref. 51),

$$\begin{aligned} E_s(x, y, 0) &= \sum_{m, n} E_{smn}(x, y, 0) \\ &= \sum_{m, n} A_{smn}(0) \psi(x - mx_0, y - ny_0) \end{aligned} \quad (164)$$

where x_0 and y_0 are the center-to-center element spacing in the array and m and n denote the individual waveguides. The amplitude coefficients are determined by the mode-plane wave overlap,

$$\begin{aligned} A_{smn}(0) &= \iint dk_{sx} dk_{sy} \mathcal{E}_{sy}(k_{sx}, k_{sy}) \\ &\quad \times \iint dx dy \psi(x - mx_0, y - ny_0) \\ &\quad \times \exp[i(k_{sx}x + k_{sy}y)] \end{aligned} \quad (165)$$

$$\begin{aligned} &= \iint dk_{sx} dk_{sy} \mathcal{E}_{sy}(k_{sx}, k_{sy}) \\ &\quad \times \exp[i(mk_{sx}x_0 + nk_{sy}y_0)] \gamma(k_{sx}, k_{sy}) \end{aligned} \quad (166)$$

$$\gamma(k_{sx}, k_{sy}) = \iint dx dy \psi(x, y) \exp[i(k_{sx}x + k_{sy}y)] \quad (167)$$

where \mathcal{E}_{sy} is the tangential component of the input plane wave. Similar expressions hold for the two pump waves. Note that the phase of each plane wave at all waveguides is explicitly retained and that waves ranging over the waveguide acceptance angle are all coupled into the mode. Propagation of the coupled light within the waveguide is determined by the propagation constant, β , and the nonlinear interaction. All light not coupled into a waveguide mode is assumed to be absorbed.

The usual approximations can be made for a nearly degenerate 4-wm interaction, slowly varying amplitudes and undepleted pump beams (Ref. 1). In the waveguide, the nonlinear susceptibility $\chi^{(3)}$ is weak enough that the linear mode

pattern $\psi(x,y)$ describes the TE-field patterns. The frequency range, Ω , is small enough so that both $\chi^{(3)}$ and ψ are constant over the interval $\omega_0 \pm \Omega$. The 4-wm interaction for a single-mode waveguide has been solved to show that the generated field E_c is proportional to the conjugate of the input field (Ref. 41). If there is negligible coupling between waveguides in the arrays, then

$$E_{cmn}(x,y,0) = A_{cmn}(0) \psi(x - mx_0, y - ny_0) \quad (168)$$

$$\begin{aligned} A_{cmn}(0) &= F(A_{1mn}, A_{2mn}, \omega_0, \Omega, \beta, L, \Gamma) A_{smn}^*(0) \\ &= F_{mn} A_{smn}^*(0) \end{aligned} \quad (169)$$

Field confinement effects are contained in the parameter Γ ,

$$\Gamma(\Omega) = \iint dx dy \chi^{(3)}(x,y,\omega_0,\Omega) |\psi(x,y)|^4 \quad (170)$$

To determine the generated field propagating in free space, the previous procedure was followed, expanding the output mode patterns as a superposition of plane waves (Ref. 51).

$$\begin{aligned} E_c(x,y,z) &= \iint dk_{cx} dk_{cy} \\ &\quad \times \exp(i\mathbf{k}_c \cdot \mathbf{r}) \sum_{m,n} \mathcal{E}_{cmn}(k_{cx}, k_{cy}) \end{aligned} \quad (171)$$

$$\begin{aligned} \mathcal{E}_{cmn}(k_{cx}, k_{cy}) &= \frac{1}{4\pi^2} \iint E_{cmn}(x,y,0) \\ &\quad \times \exp[-i(k_{cx}x + k_{cy}y)] dx dy \end{aligned} \quad (172)$$

Insertion of Equations 168 and 169 into Equations 171 and 172 yields,

$$\begin{aligned}
 E_c(x, y, z) = & \frac{1}{4\pi^2} \iint dk_{cx} dk_{cy} \exp(ik_c \cdot r) \\
 & \times \iint dk_{sx} dk_{sy} \gamma^*(k_{sx}, k_{sy}) \gamma(-k_{cx}, -k_{cy}) \\
 & \times \mathcal{E}_s^*(k_{sx}, k_{sy}) \sum_{m,n} F_{mn} \exp[-i(mk_{sx}x_0 \\
 & + nk_{sy}y_0 + mk_{cx}x_0 + nk_{cy}y_0)]
 \end{aligned} \tag{173}$$

If F_{mn} is a constant, then the summation over waveguides reduces to a set of angularly separated δ functions, corresponding to the diffraction orders of the array, when the array sufficiently samples the plane-wave components of the signal beam. Therefore, within an angle defined by the separation of diffraction orders, $k_{cx} = -k_{sx}$, $k_{cy} = -k_{sy}$, and

$$\begin{aligned}
 E_c(x, y, z) = & F \iint dk_{sx} dk_{sy} \\
 & \times \exp(-ik'_s \cdot r) |\gamma(k_{sx}, k_{sy})|^2 \mathcal{E}_s^*(k_{sx}, k_{sy})
 \end{aligned} \tag{174}$$

where the propagation vector, k'_s , is slightly shifted relative to k_s caused by the frequency difference, 2Ω , between the signal and generated beams. E_c is an essentially counterpropagating, high-quality conjugate of the input field pattern if γ is a constant when \mathcal{E}_s is nonzero. To a good approximation, this condition will be met if the spread of the incident wave vectors is small compared to the acceptance angle of the waveguide. A constant F requires identical waveguides and pump beams that look like counterpropagating plane waves, not necessarily at normal incidence. The transverse polarization of each waveguide mode in the array and all input beams must be aligned to prevent excitation of orthogonal polarization components.

To quantify the conditions for a high-quality conjugate image, consider, as an example, an array where each waveguide element has a Gaussian profile with a beam waist of $\omega_0 = 10\pi k^{-1}$. Using Equations 156 and 174 limits the spread of k vectors to ~ 10 mrad for beams no more than 175 mrad (10 deg) from normal incidence. The angular separation of array diffraction orders is increased by

decreasing the interelement spacing (Ref. 52). A $3\omega_0$ spacing yields an angular separation of ~ 70 mrad. The required number of elements in the array depends on the length scale of phase-front and amplitude variations in the signal beam. The array must be large enough to generate a diffraction-limited spot size equal to the inverse of twice the highest spatial frequency in the signal beam (Ref. 53). In this example, 1-mrad resolution requires $\approx 2 \times 10^4$ elements. For 1- μm -wavelength light, these numbers correspond to 5- μm waveguides on centers of $\leq 50 \mu\text{m}$, yielding a total array area of $\leq 0.5 \text{ cm}^2$. A signal beam generated by an object of 1 mm^2 in area, located 10 cm from the array and containing ≈ 100 emitting area elements, would be imaged by the backpropagating conjugate beam. This image is also replicated in the multiple orders of the array output that fall within the acceptance angle, $\sim 4\pi(k\omega_0)^{-1}$, of the waveguides.

If the pump waves are plane waves but are not counterpropagating, then an additional phase between waveguides is introduced. For instance, if pump beam 1 is not at normal incidence and pump beam 2 is, then the amplitude coefficient A_{lmn} will have the phase term $\exp[i(mk_{1x}x_0 + nk_{1y}y_0)]$, as can be seen by examining Equation 166. By absorbing the phases into the amplitude coefficients,

$$A'_{cmn} = A_{cmn} \exp\left[-\frac{i}{2}(mk_{1x}x_0 + nk_{1y}y_0)\right] \quad (175)$$

$$A'^*_{smn} = A^*_{smn} \exp\left[\frac{i}{2}(mk_{1x}x_0 + nk_{1y}y_0)\right] \quad (176)$$

the coupled equations describing the 4-wm interaction in a single-mode waveguide return to their original form, but the phase relation between the signal and generated beams is changed. This changes the location of the δ function that occurs when the summation over waveguides is made in Equation 173. Now $k_{cx} = -k_{sx} + k_{1x}$ and $k_{cy} = -k_{sy} + k_{1y}$, changing the propagation direction of the generated field but not the fidelity of the replication. The conjugate beam generated in a multimode waveguide by 4-wm remains counter-propagating when a pump beam angle of incidence is changed (Ref. 11).

In conclusion, it has been shown that nearly degenerate 4-wm in an array of identical waveguides can yield a high-quality conjugate beam. However, the range of wave vectors present in the signal beam must be small enough so that there is nearly equal coupling into the waveguides. Stringent phase-matching conditions that apply to the 4-wm interaction in bulk media are lifted by the ability to couple light into a waveguide mode over an acceptance angle. Beam steering of the generated beam can be achieved by changing the propagation direction of one of the pump beams, without destroying the 4-wm interaction and while maintaining the spatial coherence of the generated field pattern.

6.0 EXPERIMENTS ON OPTICAL FIBERS AND LASER DIODES

6.1 INTRODUCTION

Experimentally testing much of the theoretical framework developed in Sections 3.0 to 5.0 is impractical given the current minimal availability of complex nonlinear waveguiding structures. In this program, two key points have been illustrated using a nonpolarization-preserving, single-mode optical fiber and GaAs-AlGaAs heterostructure and quantum well laser diodes. The first point is the importance of removing degeneracy between the waveguide propagating modes (Ref. 11). A nonpolarization preserving single-mode optical fiber actually contains two degenerate, orthogonal, linearly polarized modes in the weak-guiding limit (Ref. 29). The experiments show that polarization scrambling between the two modes can be as strong a nonlinear effect as phase modulation. The second set of experiments, using the laser diodes, measures the amplitudes and relative phases of the output beams generated in the nearly degenerate 4-wm interaction. The experiments show that, in the weak probe limit, the nonlinear interaction in a laser diode acts as a phase modulation of the laser diode and that the generated conjugate beam acts to minimize the free carrier population pulsations responsible for the third-order nonlinearity.

6.2 FIBER NONLINEAR BIREFRINGENCE EXPERIMENT

Nonpolarization-preserving, single-mode optical fibers are an example of a weakly guiding nonlinear waveguide with degenerate modes. The circularly symmetric core leads to two orthogonally polarized modes with identical propagation constants. Small inhomogeneities or temperature and stress effects can cause coupling of the two modes even in the linear regime. The purpose of this experiment is to show that the fiber nonlinearity causes further modification to the polarization of a beam after propagating through the fiber. A schematic of the experimental apparatus is shown in Figure 5. A continuous-wave (cw) mode-locked Nd:YLF laser, producing ≈ 72 -ps pulses, is used. The beam is passed through a quarter-wave plate and two polarizing beamsplitters to produce temporally-spaced, orthogonally polarized pulses which could be injected into a 215-m-long silica fiber. A variable beamsplitter is used to adjust input intensity. The light transmitted through the fiber was passed through a polarizer before detection with a Si-photodiode.

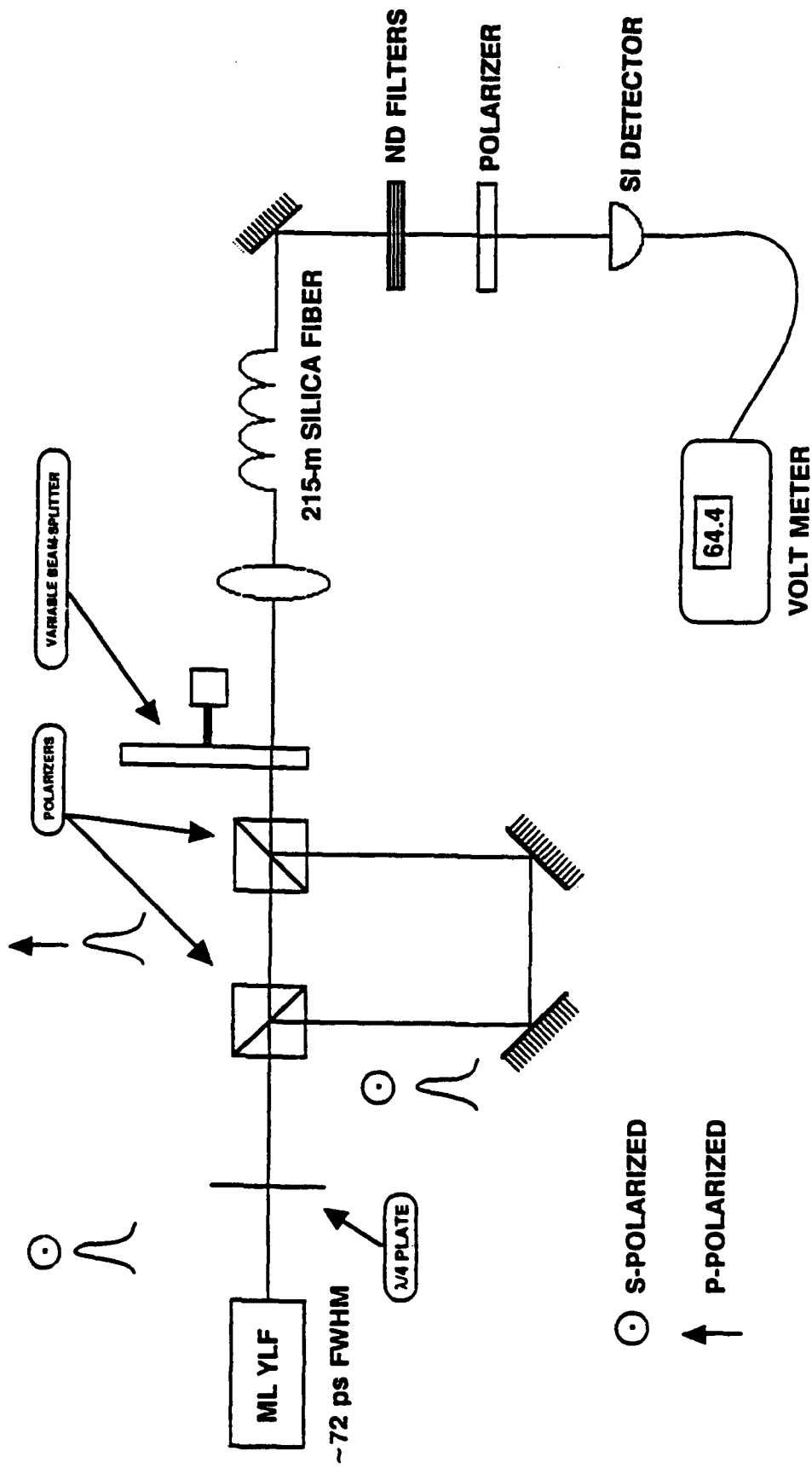


Figure 5. Schematic of the experimental configuration investigating polarization effects in single-mode fibers.

Initially, the s-polarized path through the beamsplitters was blocked and the p-polarized input was detected as a function of power. The polarizer was rotated to determine the intensity ratio at the orthogonal angles of maximum and minimum transmitted intensity. Figure 6 shows the behavior for two consecutive runs. At low intensities the ratio is large. An infinite ratio signifies linear polarization. As the intensity increases, the polarization ratio tends to oscillate. While the general oscillation trend is clear, there are clear differences between the two consecutive runs that are plotted. The s-polarized light displays a similar intensity dependence, as shown in Figure 7. Note that this third displayed p-polarized data run differs slightly from the two plotted in Figure 6.

In addition to the polarization ratio, the angle of the polarization ellipse is important. Figure 8 shows the angle of the polarizer at maximum transmission intensity, the major axis of the polarization ellipse, for the two orthogonal input polarizations as a function of laser power. The reference plane is laboratory horizontal and the low-power angle is arbitrary due to fiber inhomogeneities so that the relative rotation with increasing power is the important measured parameter. The oscillating features of the polarization ratio data are somewhat mimicked in the ellipse rotation data. Note, that the orthogonal polarization relation is not maintained at many power levels.

The importance of the scrambling of polarization on the interpretation of other measurements is illustrated by a second set of experiments. The modified experimental apparatus is shown in Figure 9. The output optical train from the fiber now includes a Mach-Zehnder interferometer. One arm of the interferometer has a variable delay so that the delayed s-polarized pulse in one arm can be made to temporally overlap with the p-polarized pulse of the second arm. In this case, three pulses will arrive at the detector, with the output displayed using a sampling oscilloscope. Without polarization scrambling there would be no interference between the overlapping s and p pulses. However, interference effects can be shown with small displacements of the optical delay line. Two cases of relatively large interference effects at different power levels are shown in Figures 10 and 11. The interference is quite strong at 100 mW/pulse less so at 300 mW/pulse. Referring back to Figure 7, the polarization ratio is closest to one near 100 and 300 mW and,

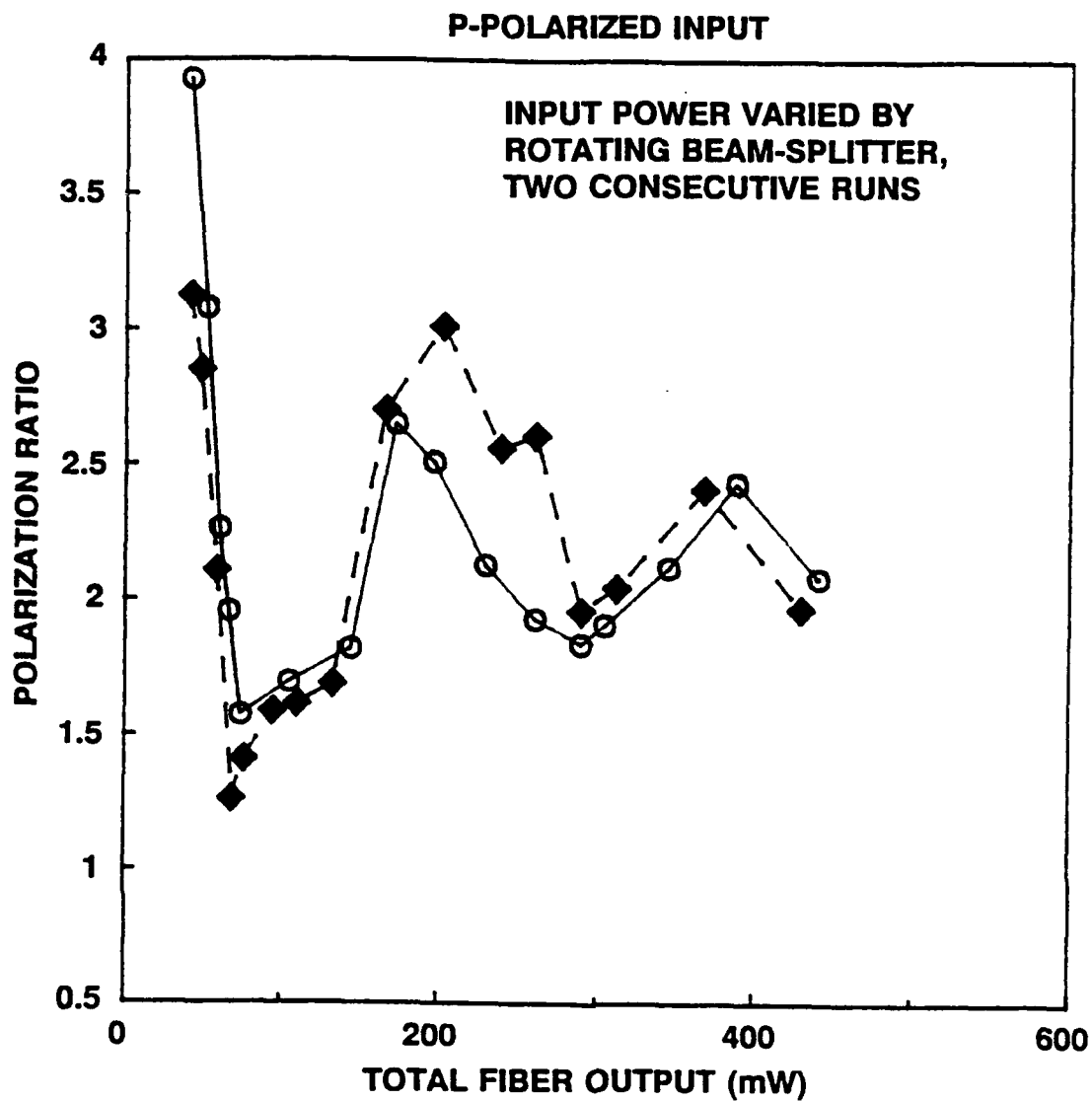


Figure 6. The polarization ratio as a function of output power from the fiber for the p-polarized input light.

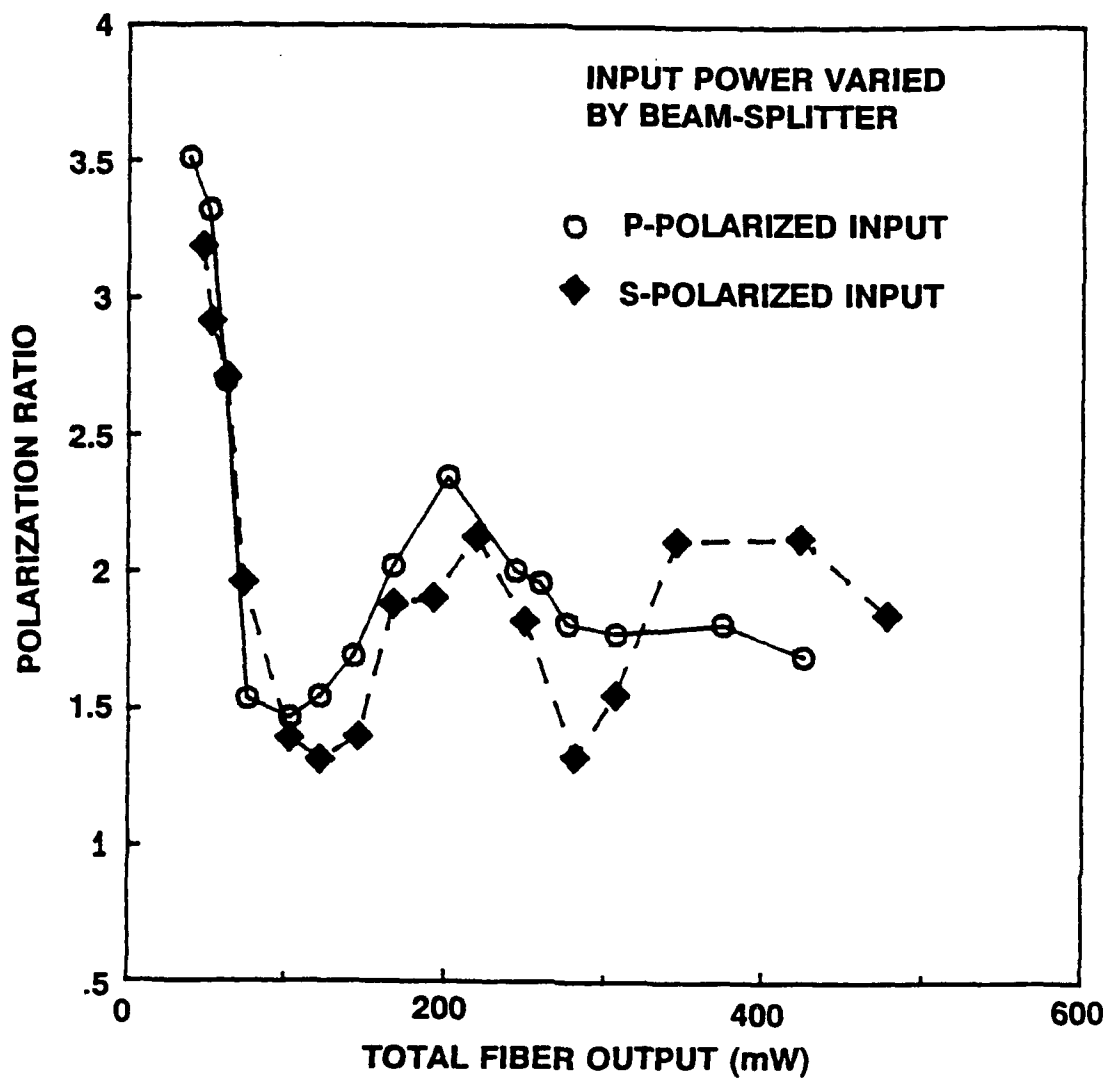


Figure 7. The polarization ratio, the maximum to minimum transmitted intensity ratio determined by rotating a polarizer, as a function of input power.

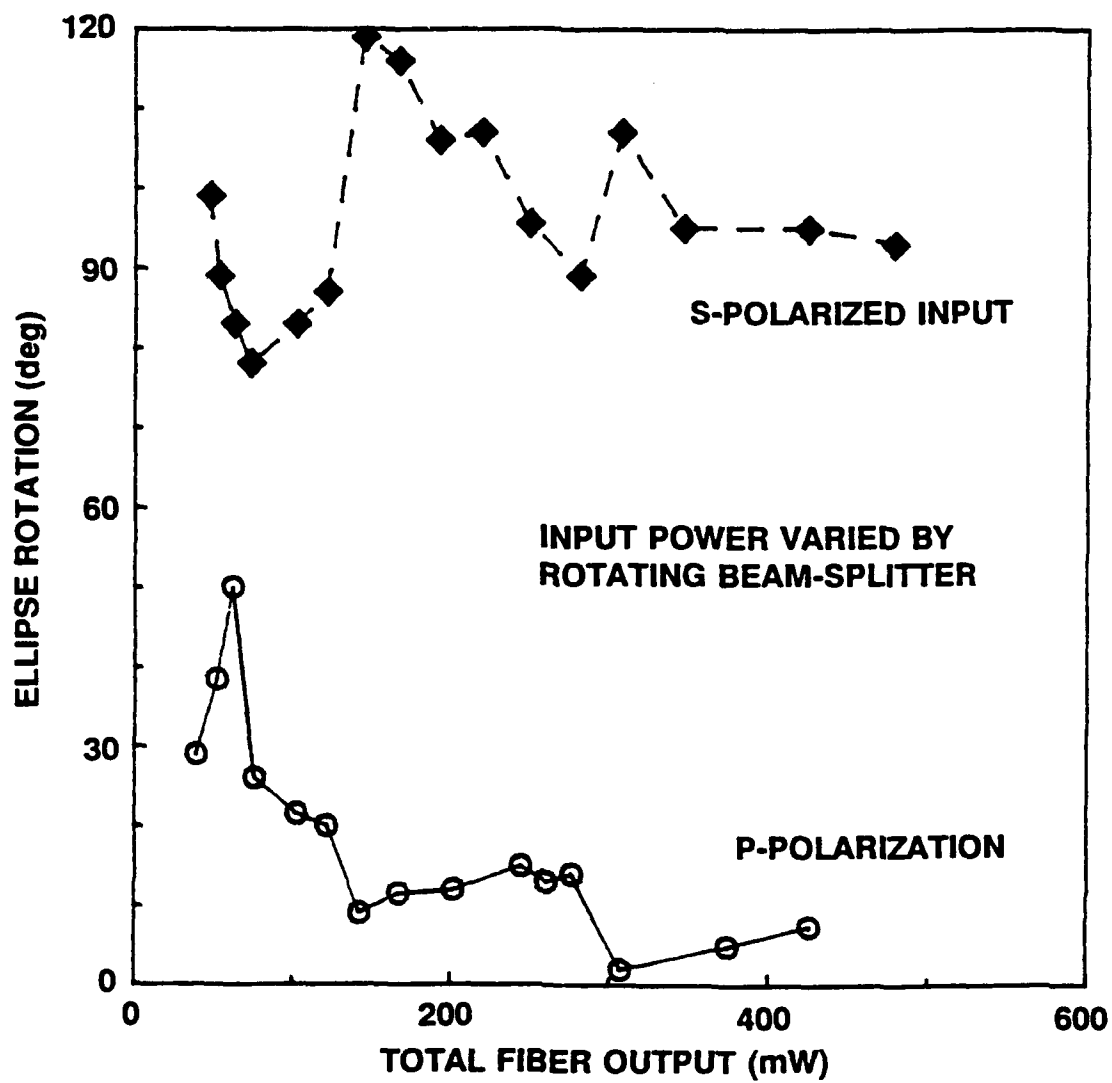


Figure 8. The ellipse rotation as a function of output power for orthogonally polarized inputs.

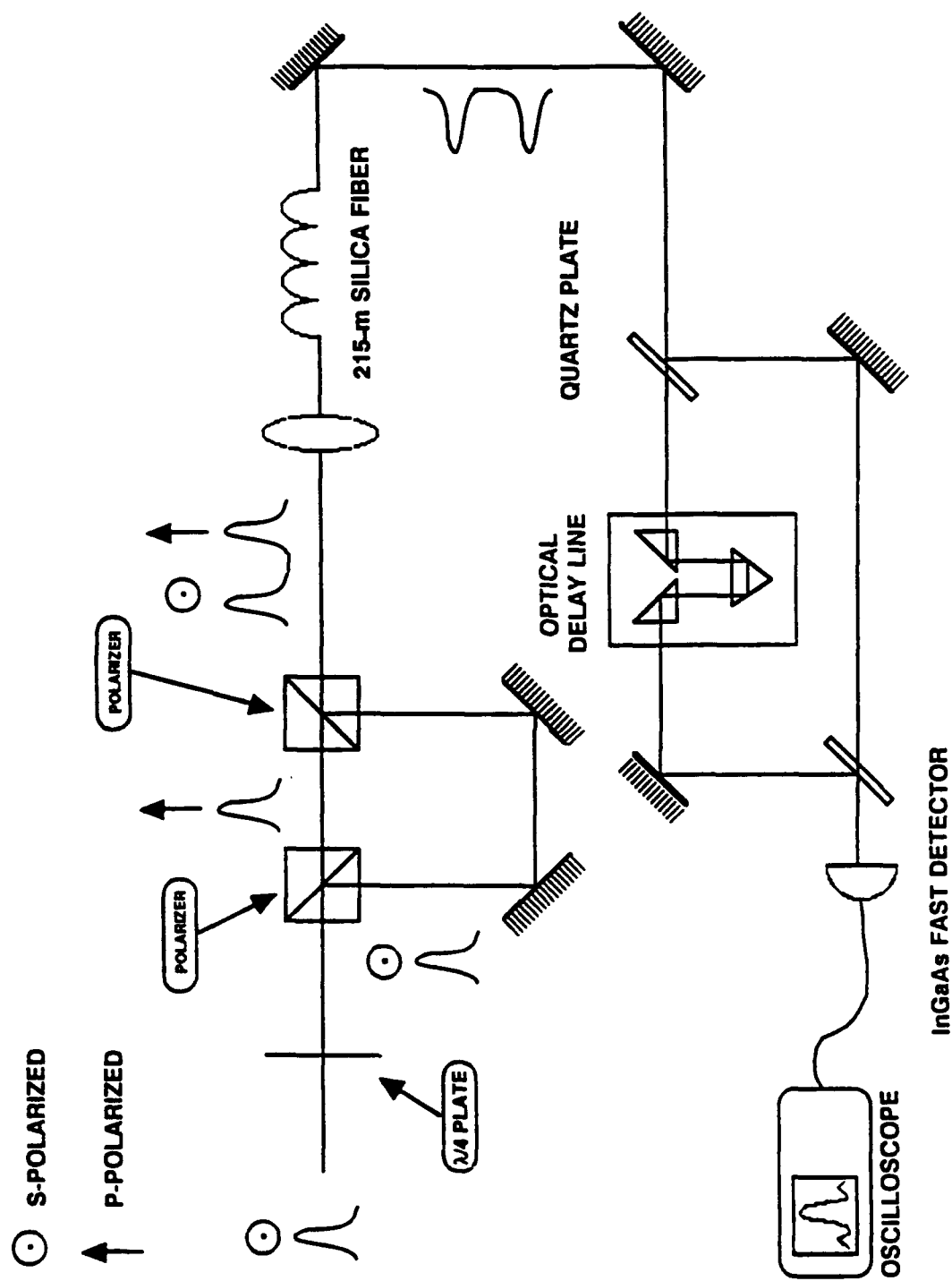


Figure 9. A schematic of the modified experimental apparatus used to illustrate the effects of polarization scrambling on interference measurements.

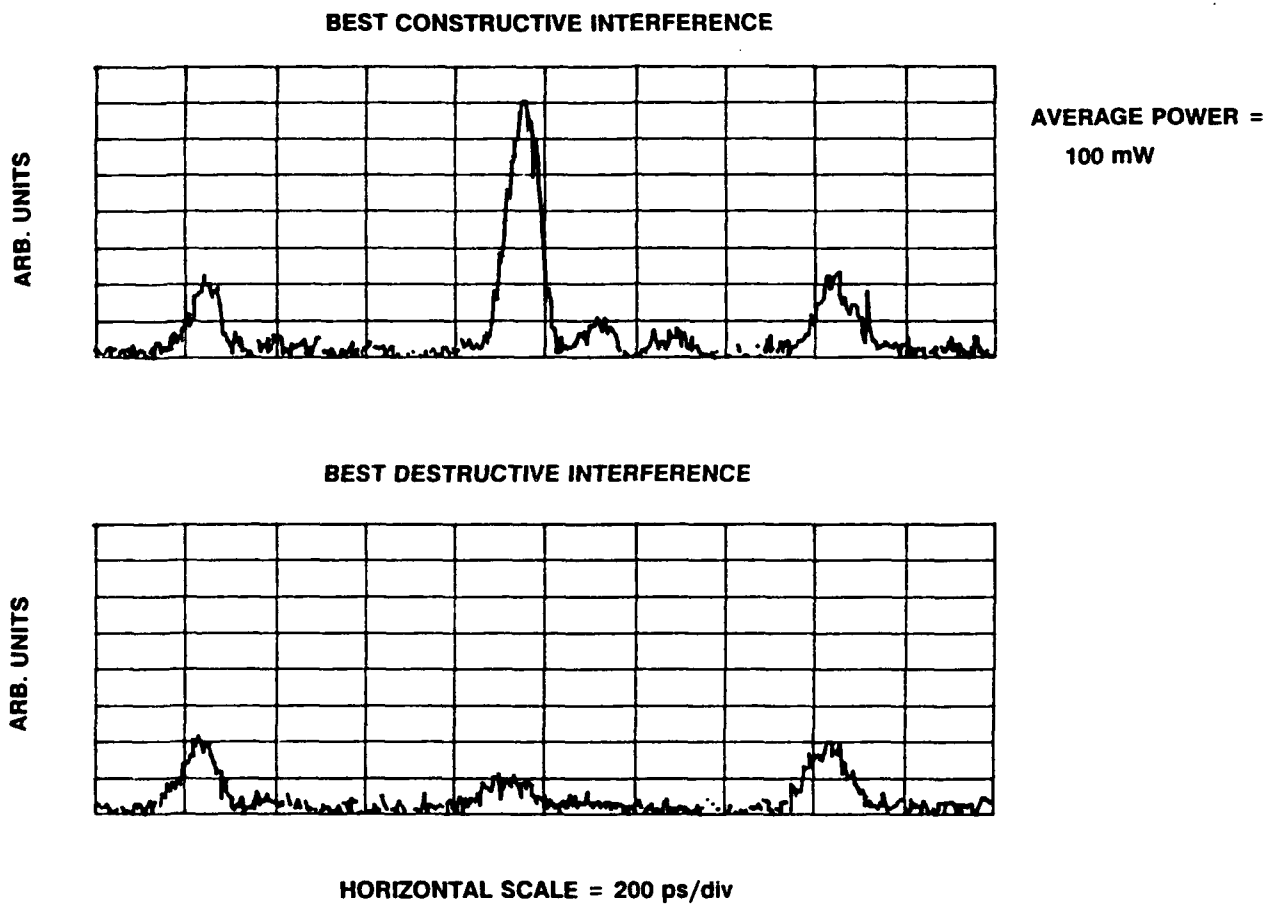


Figure 10. Oscilloscope trace of the fast photodiode output using the apparatus shown in Figure 9. Average power through the fiber is 100 mW.

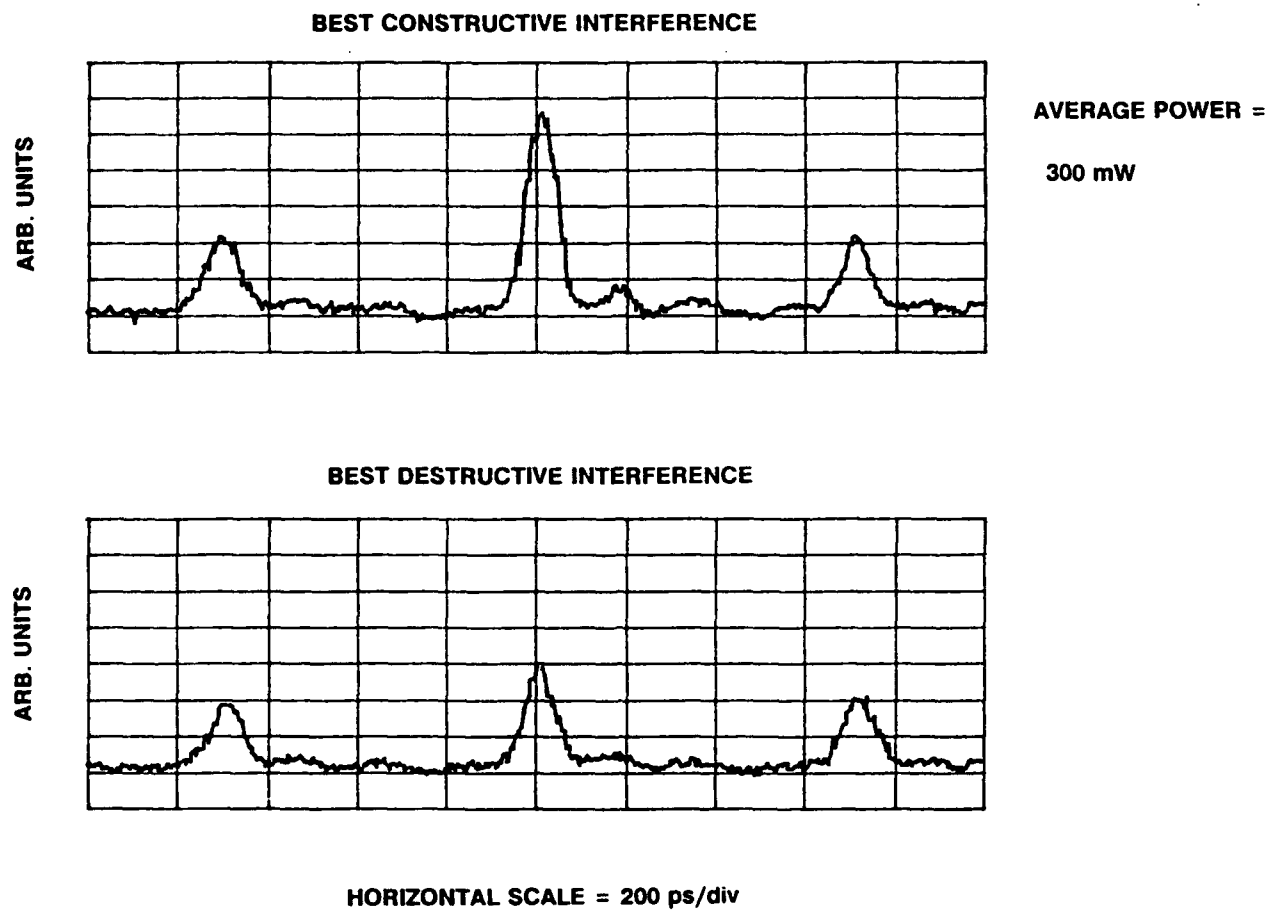


Figure 11. Oscilloscope trace of the fast photodiode output using the apparatus shown in Figure 9. Average power through the fiber is 300 mW.

using Figure 8, the ellipse rotation angle is more nearly orthogonal at the higher power level. This explains the relatively strong interference effects at both power levels and the greater interference at 100 mW/pulse.

Polarization changes obscure phase changes due to the degeneracy of the two orthogonal modes. Clearly, such nonlinear polarization coupling of modes would destroy the fidelity of a PC beam. Deciphering these effects is further hindered by the sensitivity of the polarization behavior to external factors such as temperature and stress. These types of effects account for the variability between the data of Figures 6 and 7. Though displaying interesting behavior, interpretation of effects in basic optical fibers is less straightforward than the highly nondegenerate slab geometry of semiconductor waveguides.

6.3 LASER DIODE EXPERIMENTS

Four-wave mixing experiments have been performed in single-mode laser diodes (Refs. 17, 54 and 55), traveling wave amplifiers (Refs. 40 and 56), and broad-area Fabry-Perot devices (Ref. 43). The traveling wave amplifier interaction has also been theoretically modeled (Refs. 16 and 41). To date, the measurements of 4-wm have concentrated on the amplitude of the amplified input, or probe, beam and generated 4-wm signal with little investigation of the phase relations between the interacting optical beams. In this work, nearly-degenerate 4-wm measurements have been performed in the weak injection limit of a laser diode. In this regime, the optical phase of the counter-propagating pump beams (φ_0), the amplified input signal (φ_1), and conjugate 4-wm signal (φ_2), satisfy the relation,

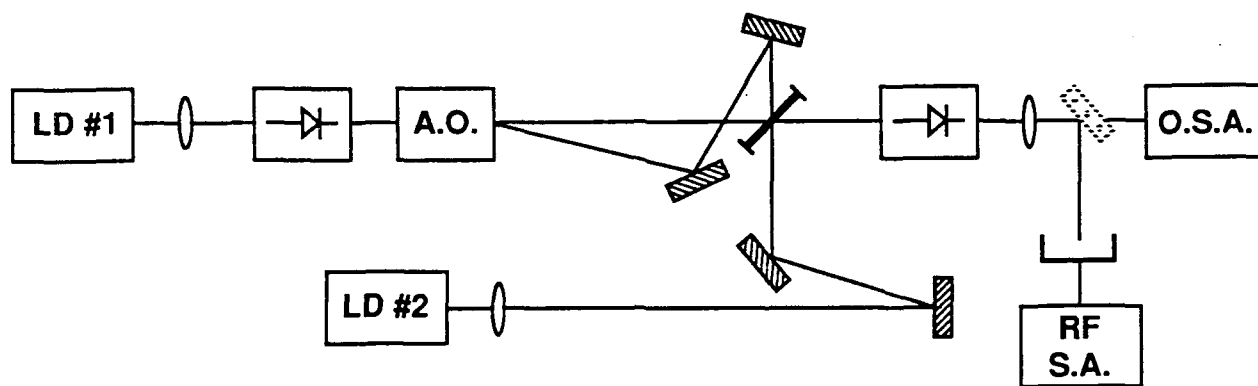
$$\varphi_2 \pm \pi = 2\varphi_0 - \varphi_1 \quad (177)$$

Further, the amplitudes of the electric fields E_1 and E_2 , corresponding to the amplified input and generated 4-wm mixing fields, respectively, are nearly equal. This is equivalent to saying that injecting a near-resonant optical signal, offset by frequency Ω , induces a phase modulation of the laser diode at Ω . Because of nonlinear interaction results from modulations of the

carrier density (Ref. 41), this phase relation means that the generated 4- μm beam acts to minimize the density modulations induced by the amplified, injected probe.

A schematic of the experimental apparatus is shown in Figure 12. One laser diode acts as a probe. It is optically isolated against back-reflected light from any components in the optical train. The output is then passed through an acousto-optic modulator where a small fraction, on the order of 10 percent, of the beam is deflected and shifted in frequency by 80 MHz. The main beam, at an optical frequency ν_1 , passes through a variable attenuator and a second optical isolator to the measurement apparatus. The shifted beam is injected into a second laser diode, operating at a frequency ν_0 , slightly shifted from ν_1 by an amount Ω . The output from the second laser diode is partially reflected off of the variable beamsplitter so as to become collinear with the ν_1 beam. Both laser diodes are temperature and current stabilized. To bring them to nearly degenerate operating frequencies, the temperature is adjusted for gross frequency changes and then the current is adjusted for fine tuning. Three different laser diodes were used in the measurements. Two are commercially available GaAs-AlGaAs heterostructure lasers, the Sharp LT015MD (with an output power of 30 mW and operating wavelength near 830 nm), and the Hitachi HL 7838G (operated at ≈ 10 mW and 784 nm). The third type of laser was a GaAs-AlGaAs quantum well laser operating near 830 nm and 5-mW output power. This laser had a Fabry-Perot cavity length of 600 μm , more than twice as long as the commercially available diodes, which gave it greater frequency stability (Ref. 57).

To measure the spectrum of the emitted light, two spectrum analyzers were used. The first was a Newport SR-240 high-finesse scanning Fabry-Perot with detector. This instrument had a free spectral range of 8 THz and finesse of 20,000, giving an optical frequency resolution of 400 MHz. Alternatively, the laser diode output was detected by a fast photodiode, 3-dB point at 2 GHz, and the photodiode signal was displayed on a radio frequency (RF) spectrum analyzer. Because the photodiode is a square-law detector, its output will have a spectrum corresponding to the difference in frequencies between various optical frequency components.



LD = LASER DIODE

○ = LENS

—|> = FARADAY OPTICAL ISOLATOR

A.O. = ACOUSTO-OPTIC MODULATOR (80 MHz)

▨ = MIRROR

┌ = BEAMSPLITTER

└ = PHOTODIODE

O.S.A. = OPTICAL SPECTRUM ANALYZER

RF S.A. = RF SPECTRUM ANALYZER

Figure 12. Schematic of the experimental arrangement for 4-wm in laser diodes.

Detection of four optical frequency components can be expected. They are the two diode operating frequencies, ν_0 and ν_1 , the acousto-optically shifted frequency, $\nu_1 + 80$ MHz, and the 4-wm frequency, $2\nu_0 - (\nu_1 + 80$ MHz). However, 80 MHz is an insufficient frequency shift to be resolved by the Fabry-Perot. With the RF spectrum analyzer, there will be potentially many mixing components, but assuming that the optical frequency components at ν_0 and ν_1 are strong compared to the others, the primary frequency components should be at 80 MHz, Ω , $2\Omega \pm 80$ MHz, and $\Omega \pm 80$ MHz. The plus or minus sign will depend on the magnitude of ν_1 , with respect to ν_0 . The first three radio

frequencies result from the mixing of the three output frequencies from laser diode #2 with ν_1 , while the fourth is the beat frequency between ν_0 and its two sideband frequencies.

Figure 13 displays the output of the optical spectrum analyzer when the two laser diodes are tuned to near degeneracy. The main peak is at ν_0 and the larger side-peak is primarily at ν_1 . Oppositely shifted from ν_0 is the generated nearly-degenerate 4-wm signal. If the ν_1 beam is blocked just before the variable attenuator, only the output from laser diode #2 is displayed. This is shown in Figure 14. Now the amplified version of the beam injected at $\nu_1 + 80$ MHz is shown to the left of the ν_0 signal. Note that it is at approximately the same magnitude as the 4-wm signal.

When the fast photodiode and RF spectrum analyzer are used, a typical RF spectrum is shown in Figure 15. The frequency range that could be measured was limited by a 500-MHz bandwidth amplifier that followed the photodiode. There are three RF features that result from the mixing of optical frequencies. The two small peaks near zero frequency are noise artifacts. An instrument resolution limited feature at 80 MHz is generated by ν_1 and the amplified probe signal at $\nu_1 + 80$ MHz. This signal does not result from reflections off of optical components. This was verified by tuning the current of laser diode #2 which moved the operating frequencies. Unless ν_1 and ν_0 were nearly degenerate, the 80-MHz signal disappeared. The tuning range will be discussed further. The second, and largest, feature in the RF spectrum is due to the mixing of ν_0 and ν_1 . It is broadened due to the inherent frequency jitter of the free-running diodes. Finally, at higher frequency, there is a second broadened feature at a frequency corresponding to 2 Ω to 80 MHz. Therefore, it is the mixing signal between ν_1 and the generated 4-wm frequency.

Significantly, there is no RF feature at the difference frequency $\Omega - 80$ MHz, though there are certainly optical frequency components with this spacing. This is even more surprising given that the strength of the optical power detected at ν_0 is more than an order of magnitude larger than at ν_1 . Referring back to Figure 14, note again that the two sideband components are of nearly equal amplitude. The photodiode signal, measuring optical power rather than field amplitude, shows no power modulation at $\Omega - 80$ MHz. This point

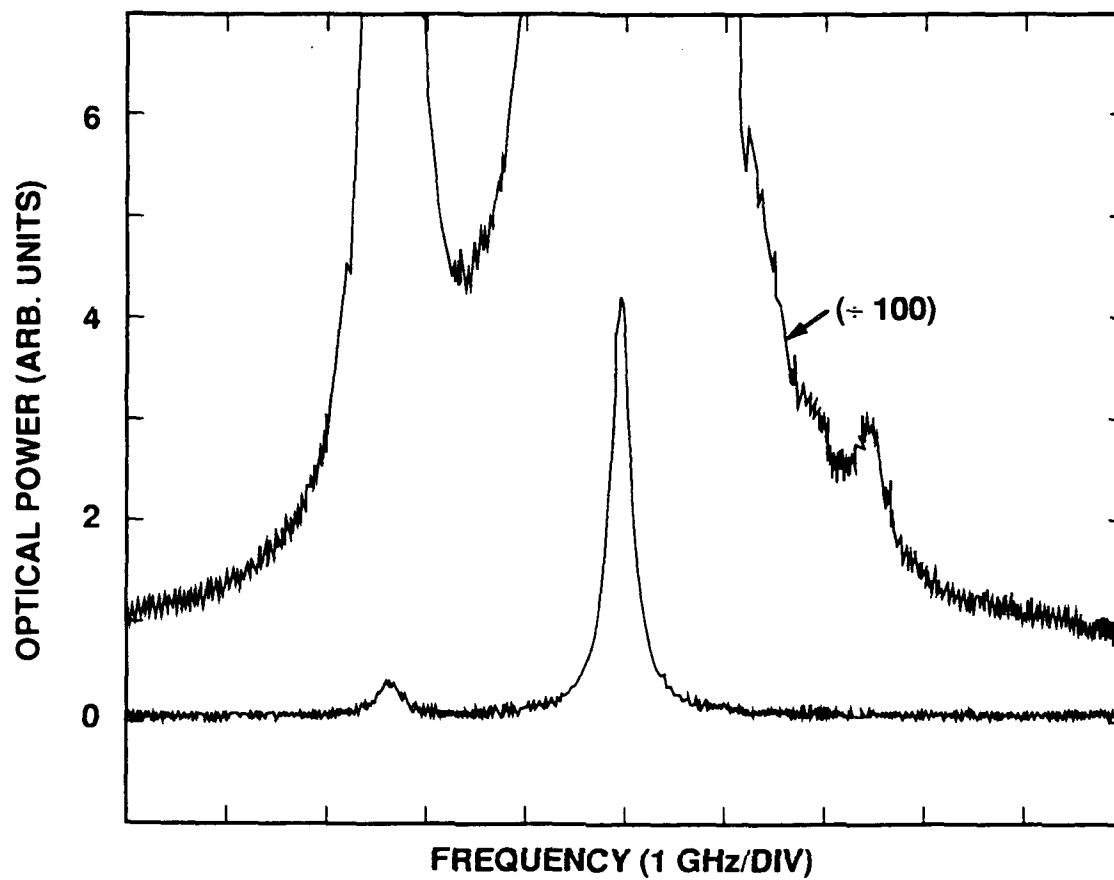


Figure 13. Optical spectrum analyzer trace using the apparatus shown in Figure 12. The upper trace is an offset, 100x expansion of the lower trace.

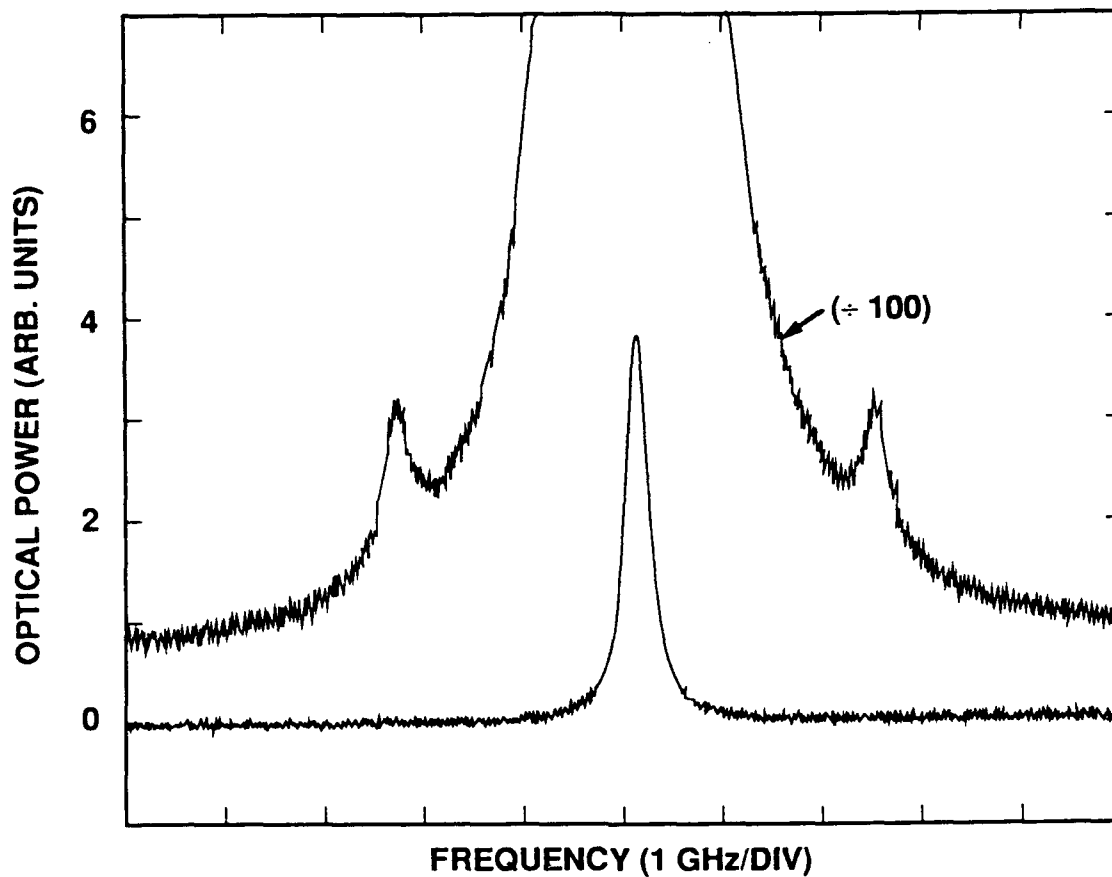


Figure 14. Optical spectrum analyzer trace using the apparatus shown in Figure 12, except that the direct optical path from laser diode #1 to the beamsplitter has been blocked. The upper trace is an offset, 100x expansion of the lower trace.

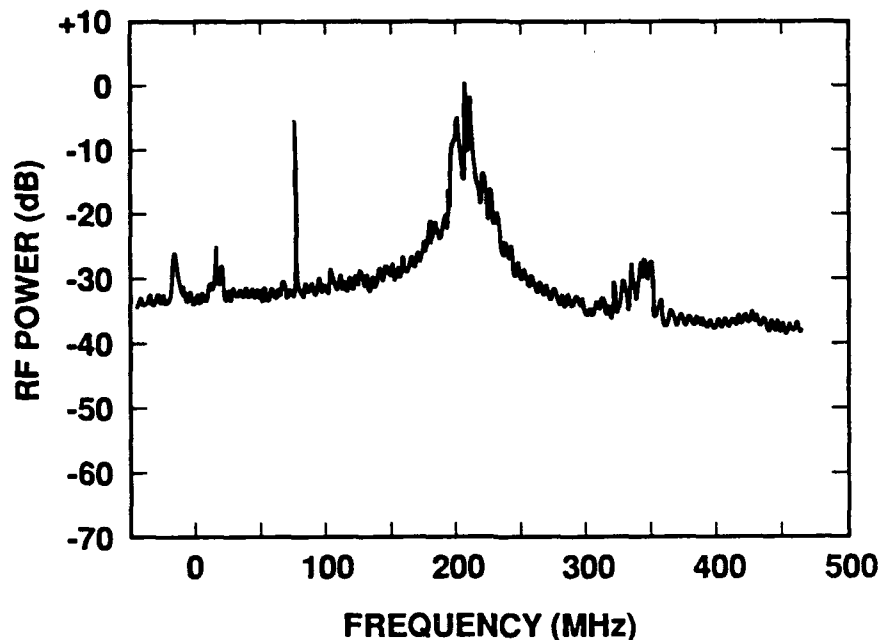


Figure 15. Radio frequency spectrum analyzer trace using the apparatus shown in Figure 12.

requires that the optical sidebands represent a phase modulation of ν_0 and that the phases of the three frequency components generated by laser diode #2 be related according to Equation 177. The fact that the RF feature at 80 MHz is resolution limited means that the amplified input signal remains injection-locked, while the broadening of the other two features shows that the two lasers remain unlocked.

It is now generally accepted that the 4- μm signal in laser diodes results from free-carrier population pulsations in single-mode devices and gratings in broad-area devices (Refs. 41 and 43). The pulsations and gratings are assumed to be set up by modulation of the carrier density at Ω due to the injected beam. The phase relation between the three optical beams means that the nonlinear interaction acts to limit the population pulsations induced by the injected signal. Using Agrawal's theory (Ref. 41), if the amplified injected signal were absolutely equal in amplitude, there would be no free-carrier or refractive index modulations. The generated beam acts to cancel the intensity modulations experienced in the laser diode and keep the carrier pulsations to a minimum. Previous work has shown that the generated 4- μm signal saturates

with increasing injected signal power (Ref. 54). This implies that the amplified injected signal becomes less efficient at modulating the carrier density as it tends toward saturation.

A requirement of an optically-induced real population pulsation or grating through 4-wm is that the beams involved in the mixing have collinear polarization components. There is no field mixing with orthogonal polarizations. Using a half-wave plate inserted in the ν_1 - 80 MHz beam path, the amplified injected beam signal and 4-wm signal were verified and resulted only from the polarization component injected parallel to the circulating laser field polarization in laser diode #2. As the half-wave plate was rotated, the amplified injected signal and 4-wm signal scale proportional to the intensity of the component parallel to the circulating laser-field polarization. The orthogonal (vertical) polarization was neither amplified nor did it induce a signal in the parallel (horizontal) polarization direction.

There are several interesting effects which appear as the frequency of the signal injected into the diode is varied. Figures 16-18, along with Figure 15 are a sequence of RF spectra showing changes as the injection laser is scanned through the oscillation frequency of the second laser diode. In all cases, the injected signal is very weak so that the 4-wm signal is $\approx 10^{-3}$ of the main signal strength. Continuing the convention, the laser diode #1 is at ν_1 , the acousto-optic modulator generates a beam at $\nu_1 + 80$ MHz and the second laser diode operates at ν_0 . Figure 15 is the spectrum with ν_1 tuned well below ν_0 . As the frequency of ν_1 is increased, the $\nu_0 - \nu_1$, and $2(\nu_0 - \nu_1) - 80$ MHz features shift to lower frequencies until the injected signal locks the second laser diode. An injection-locked spectrum is shown in Figure 16. There is a single, sharp feature at 80 MHz, the acousto-optic frequency shift. The feature sits atop a pedestal that is broadened by the phase and amplitude noise of the two diodes. Continuing to increase the frequency of ν_1 , now $> \nu_0$, the injection-locking range is less than ≈ 50 MHz with this weak signal, so that when $\nu_1 \sim \nu_0$ there are simultaneously narrow and broad features, at 80 MHz, as shown in Figure 17. The narrow feature is the amplified-injected signal and the broad feature is the symmetrically offset 4-wm signal with the frequency inverted. There are two weak features at 160 and 240 MHz which are electronic noise generated by the acousto-optic modulator power supply. Finally, as ν_1 is increased further, the $\nu_1 - \nu_0$ peak and 4-wm peaks move to

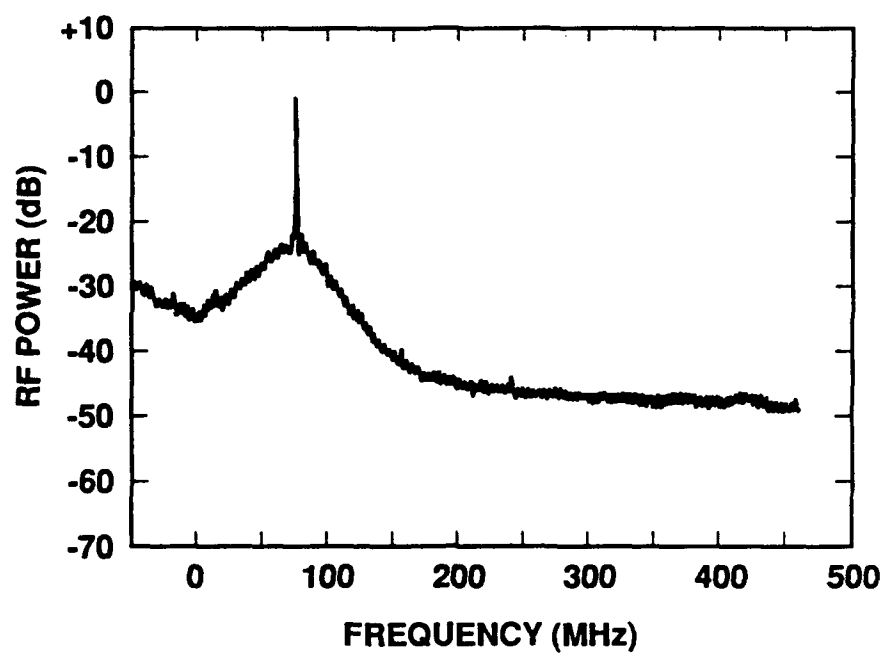


Figure 16. Radio frequency spectrum analyzer trace using the apparatus shown in Figure 12 when the two laser diodes are phase locked.

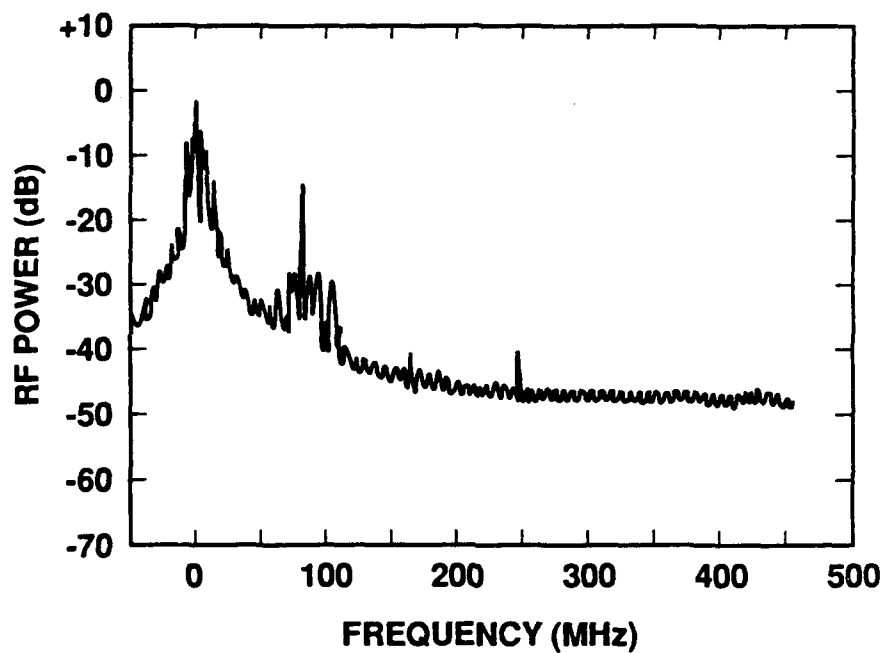


Figure 17. Radio frequency spectrum analyzer trace using the apparatus shown in Figure 12 when the two laser diodes have a frequency difference of ~ 80 MHz.

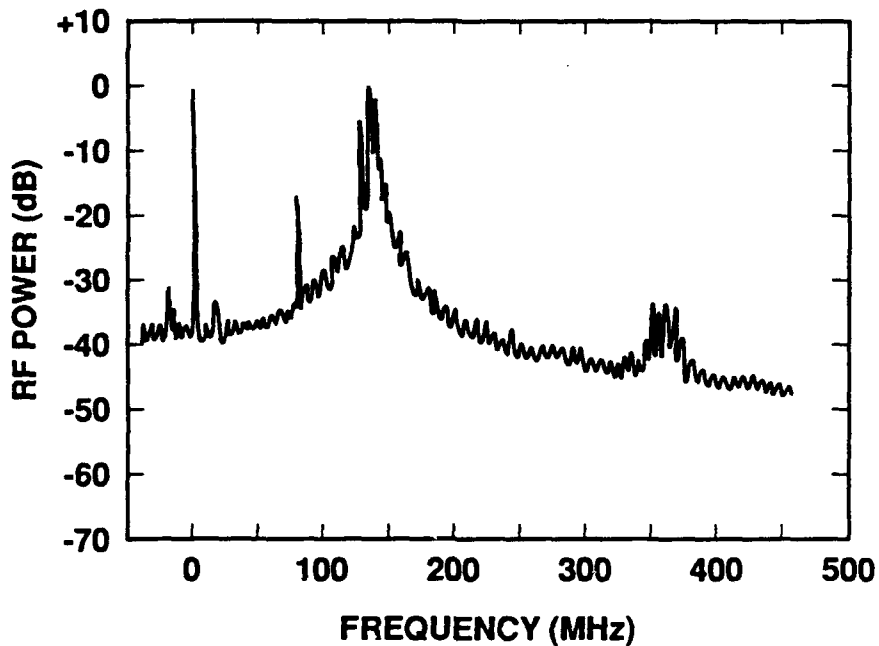


Figure 18. Radio frequency spectrum analyzer trace using the apparatus shown in Figure 12 when laser diode #2 operates at a higher frequency than laser diode #1.

higher radio frequencies, again reflecting the RF spectra display of the absolute frequency difference. In this case, however, the 4-wm signal is now at $2(\nu_1 - \nu_0) + 80$ MHz, as shown in Figure 18. Except over the narrow injection-locked frequency range, the spectra are qualitatively similar.

A second series of spectra, taken with the optical spectrum analyzer, are shown in Figures 19-23. The injected power is approximately a factor of 5 larger than in Figure 15 in this series. Again, frequency increases from left to right and only the output from laser diode #2 reaches the detector. In Figure 19, the injected signal is the small peak ≈ 8 GHz below the main feature. Also, there is an even smaller, oppositely-shifted 4-wm signal. There are also symmetric shoulders on the main peak that correspond to the relaxation oscillation resonance (Refs. 17 and 18). The resonance results from the photon-free carrier coupling and is at a frequency between the inverse laser cavity photon lifetime, on the order of a few picoseconds, and

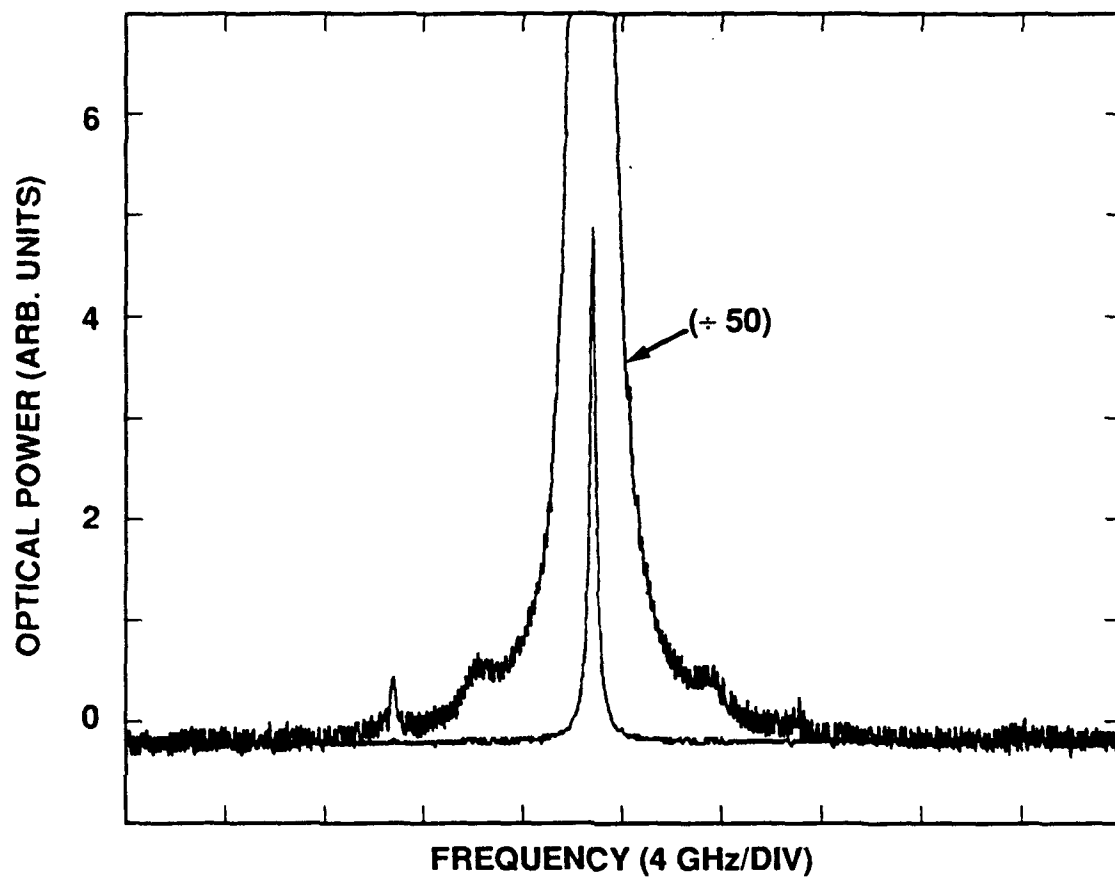


Figure 19. Optical spectrum analyzer trace of the output from laser diode #2 when the injection frequency is offset by ~8 GHz. The upper trace is a 50x expansion of the lower trace.

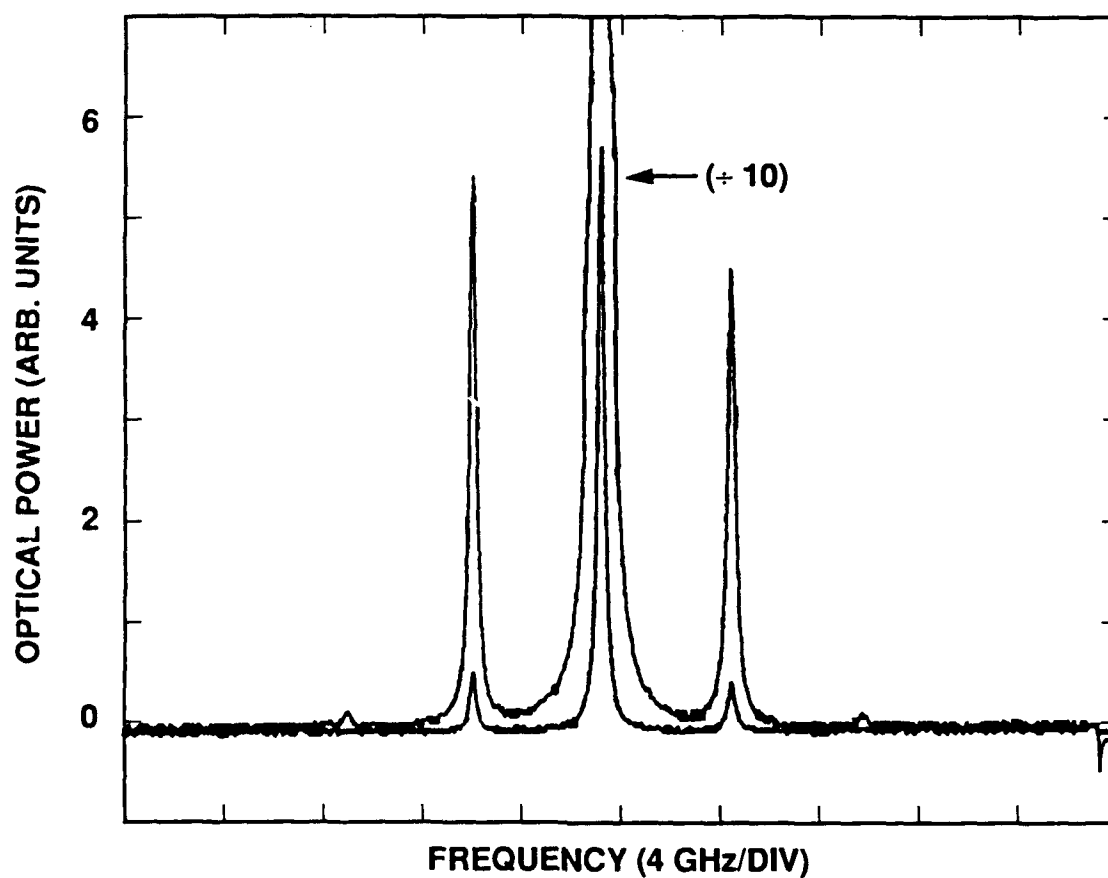


Figure 20. Optical spectrum analyzer trace of the output from laser diode #2 when the injection frequency is offset by the relaxation resonance frequency. The upper trace is a 10x expansion of the lower trace.

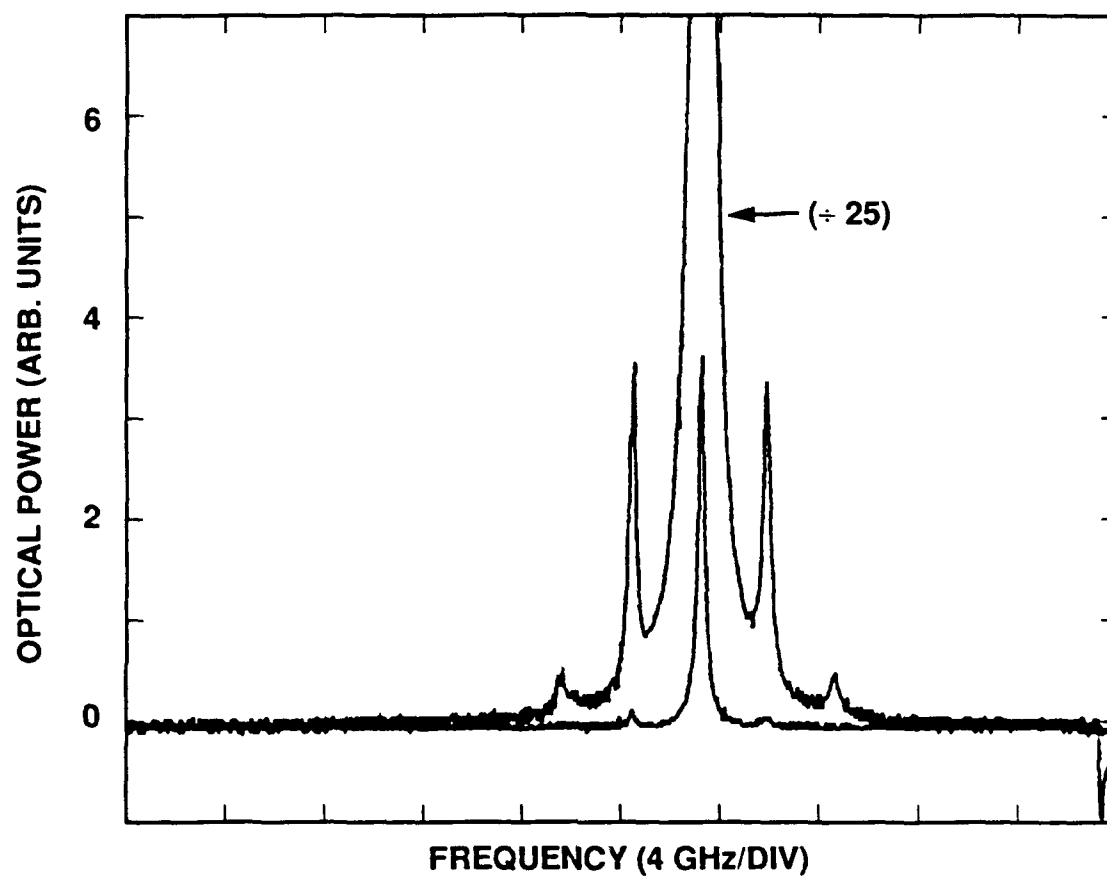


Figure 21. Optical spectrum analyzer trace of the output from laser diode #2 when the injection frequency is offset by ~3 GHz. The upper trace is a 25x expansion of the lower trace.

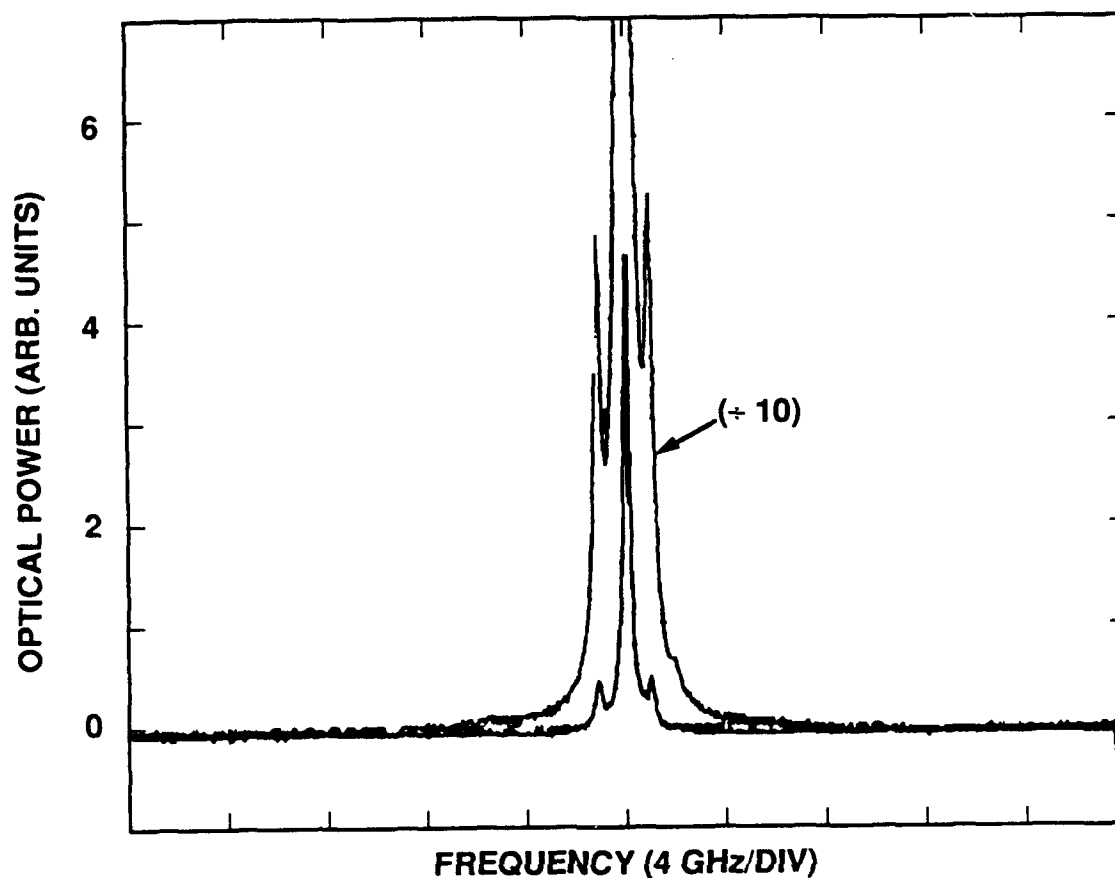


Figure 22. Optical spectrum analyzer trace of the output from laser diode #2 when the injection frequency is offset by ~ 1 GHz. The upper trace is a 10x expansion of the lower trace.

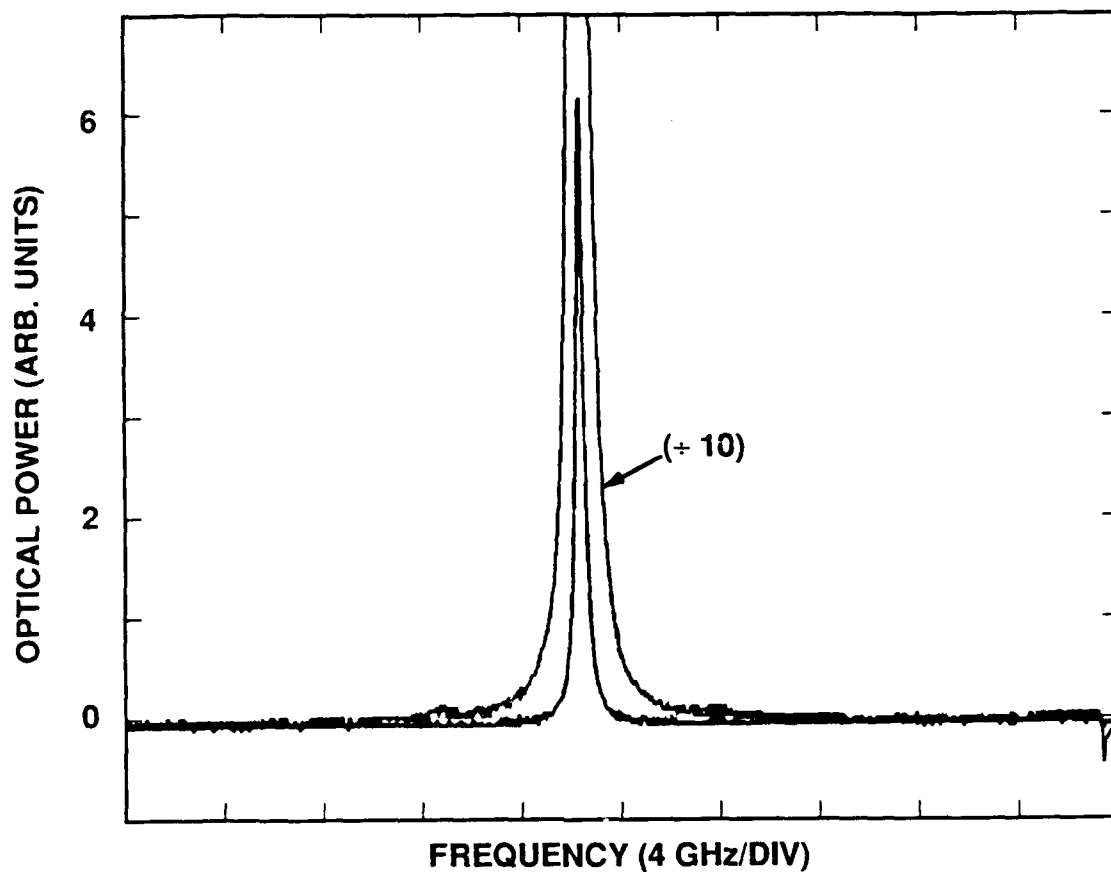


Figure 23. Optical spectrum analyzer trace of the output from laser diode #2 when it is phase locked. The upper trace is a 10x expansion of the lower trace.

inverse free carrier lifetime, on the order of a nanosecond. When the injection frequency is offset from the free-running frequency by greater than the relaxation frequency, as shown in Figure 19, the 4-wm interaction and the amplification of the injected signal are quite weak. At the relaxation resonance, these signals are nearly a factor of 50 larger, as shown in Figure 20. Peaks at twice the relaxation frequency, due to the relaxation peaks of the injected signal mixing with the sidebands of laser diode #2, are also visible. The signals are reduced by somewhat more than a factor of 3 at half the relaxation frequency (Fig. 21) and only become as strong again when the offset is reduced to ≈ 1 GHz, as shown in Figure 22. Also note that there is some asymmetry in the amplitude of the two sidebands, indicating that amplitude as well as phase modulation is playing a role in the laser diode operation. Figure 23 shows injection-locked operation. These results are consistent with those previously reported (Ref. 17).

A final series of spectra taken with the optical spectrum analyzer are shown in Figures 24-28. These were made using the Sharp laser diodes, which had a much stronger relaxation oscillation than the Hitachi diodes measured in Figures 19-23. For these spectra, the injected signal was quite strong, approximately an order of magnitude larger than the previous series. The free-running output of laser diode #2 is shown in Figure 24, and a weakly amplified input signal well offset is shown in Figure 25.

As ν_1 is tuned toward the relaxation resonance peak, the frequency spectra change dramatically. Representative spectra are shown in Figures 26-28. The offsets are ≈ -6 , -3 , and $+3$ GHz, respectively. Figures 27 and 28 show strong evidence of a set of closely-spaced or continuous-frequency components over a range of the spectra. This could be evidence of coherence collapse and/or chaotic phenomena, but verification requires a more detailed study with higher frequency resolution than was available in the current program.

The spectra identify several key features. First, there are at least three operating ranges of injection intensity. At low levels, the injected signal acts as a phase modulator generating symmetric sidebands. At intermediate levels, the sidebands become asymmetric while at high levels spectral broadening and multiple asymmetric features dominate the optical spectrum. A key parameter in determining signal strength is the relaxation resonance. This is to be expected given the basis of the 4-wm signal as the coupling between the photon and free carrier densities. Finally, it should be noted the two lasers could never be stably injection-locked by the 4-wm sidebands. When the two lasers showed locking behavior, the output frequencies of the two laser diodes were always degenerate.

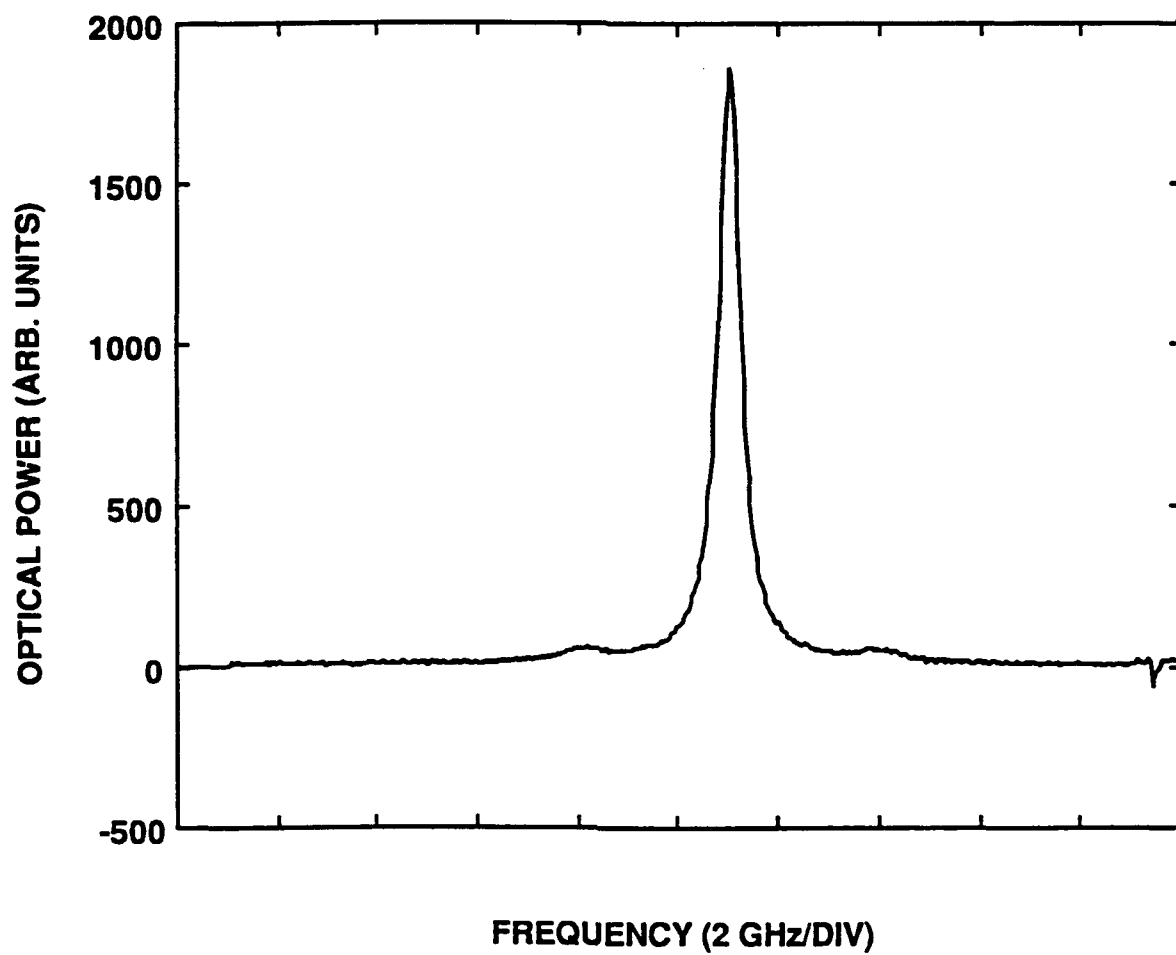


Figure 24. Optical spectrum analyzer trace showing the free-running output of the Sharp LT015 laser diode with its relatively strong resonance sidebands at $\sim \pm 3$ GHz.

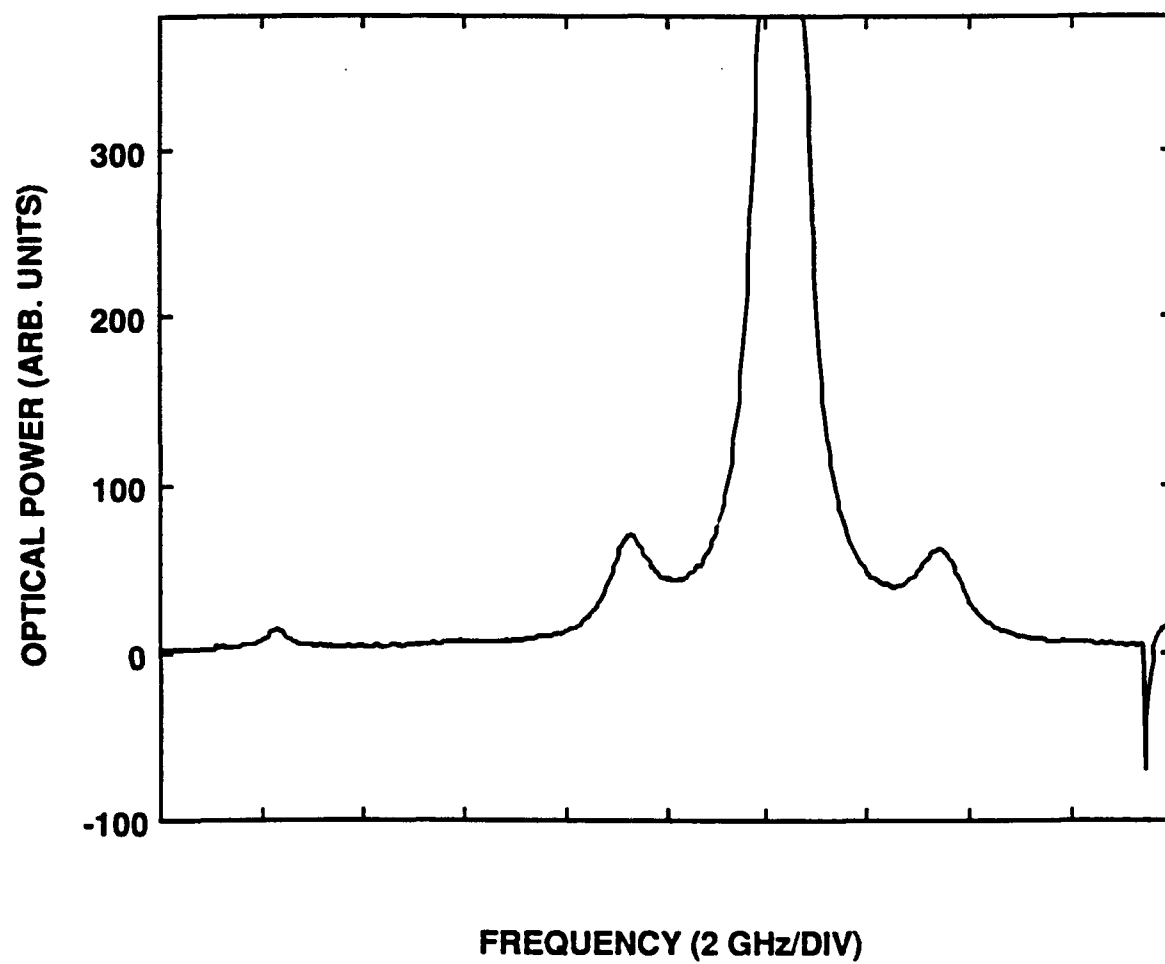


Figure 25. Optical spectrum analyzer trace showing the LT015 laser diode under strong optical injection ~10 GHz below the main peak.

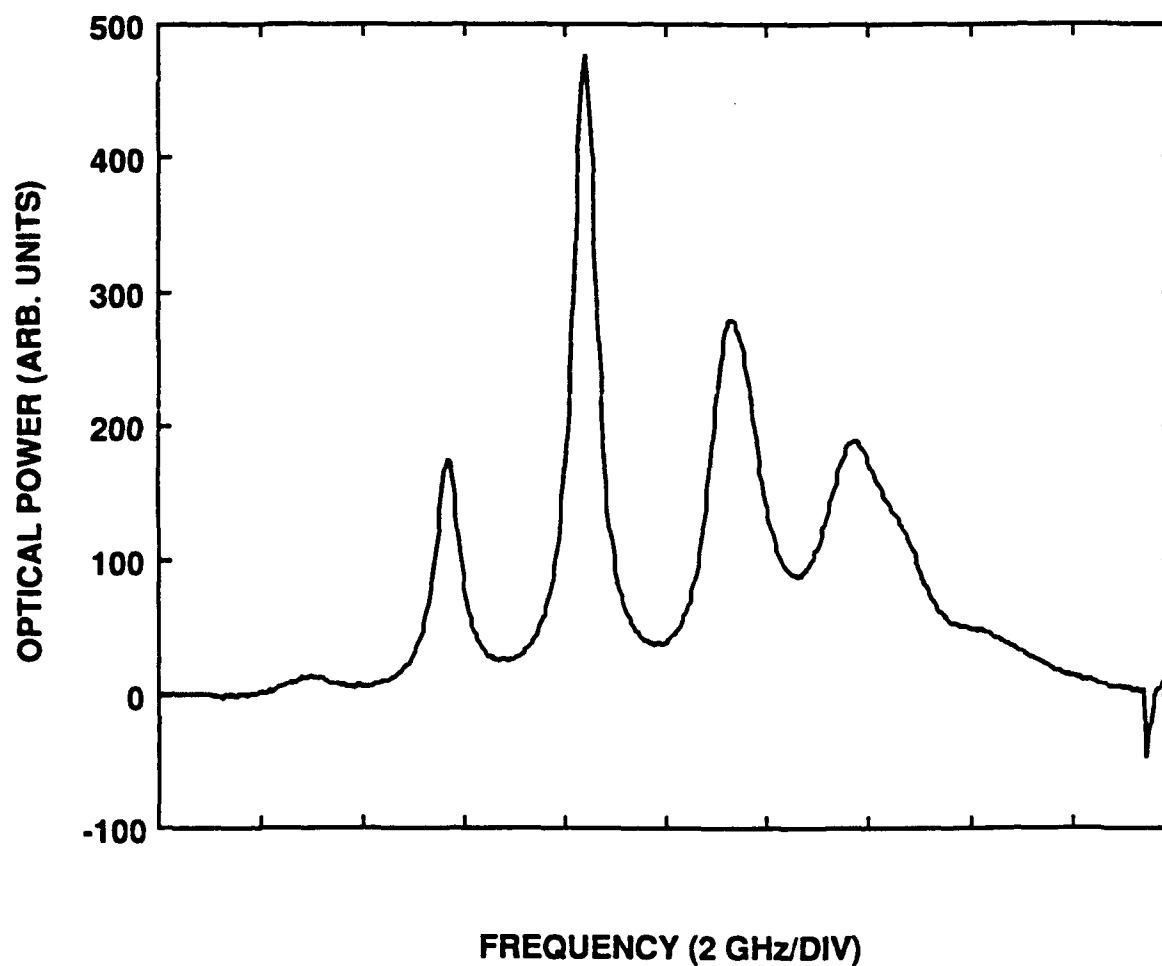


Figure 26. Optical spectrum analyzer trace showing the LT015 laser diode under strong optical injection ~6 GHz below the free-running frequency.

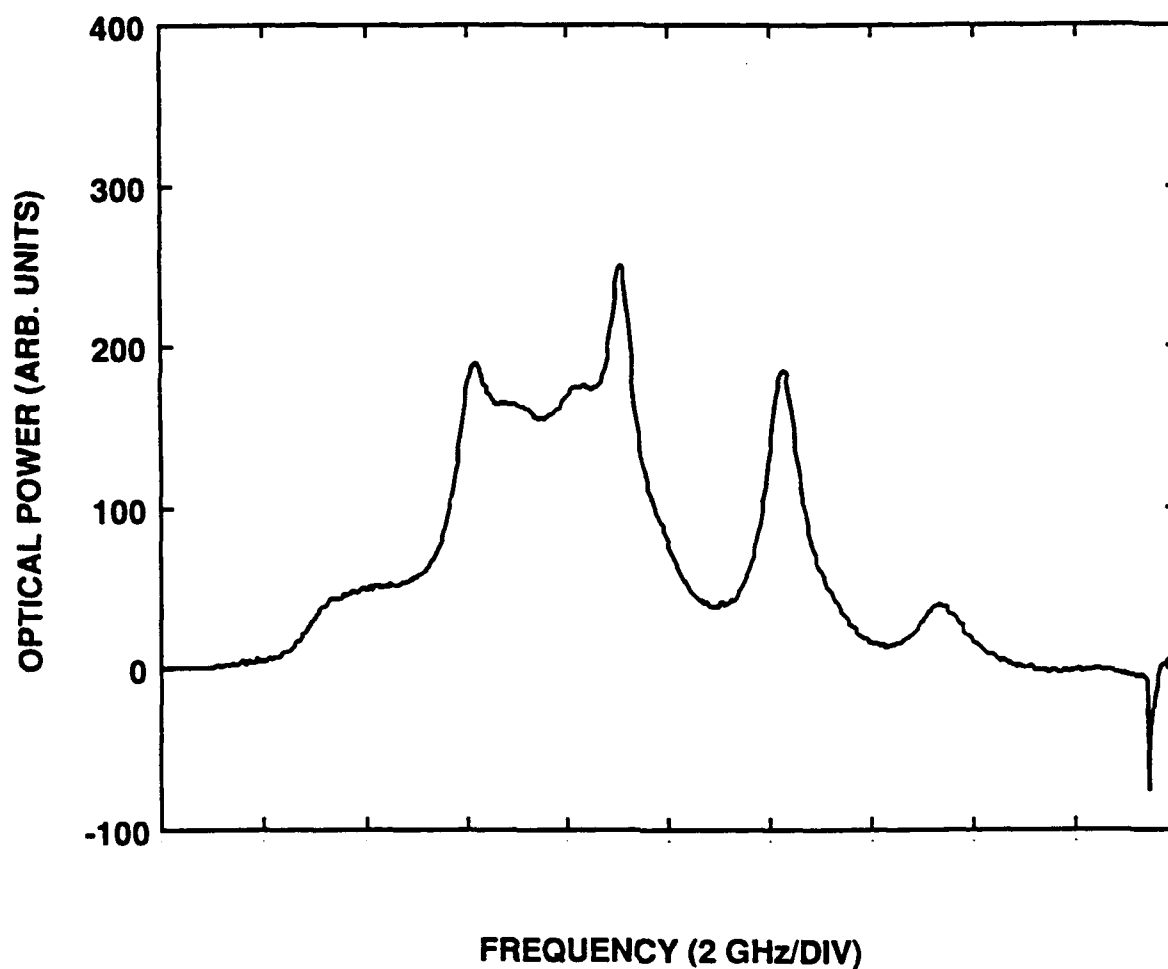


Figure 27. Optical spectrum analyzer trace showing the LT015 laser diode under strong optical injection ~3 GHz below the free-running frequency.

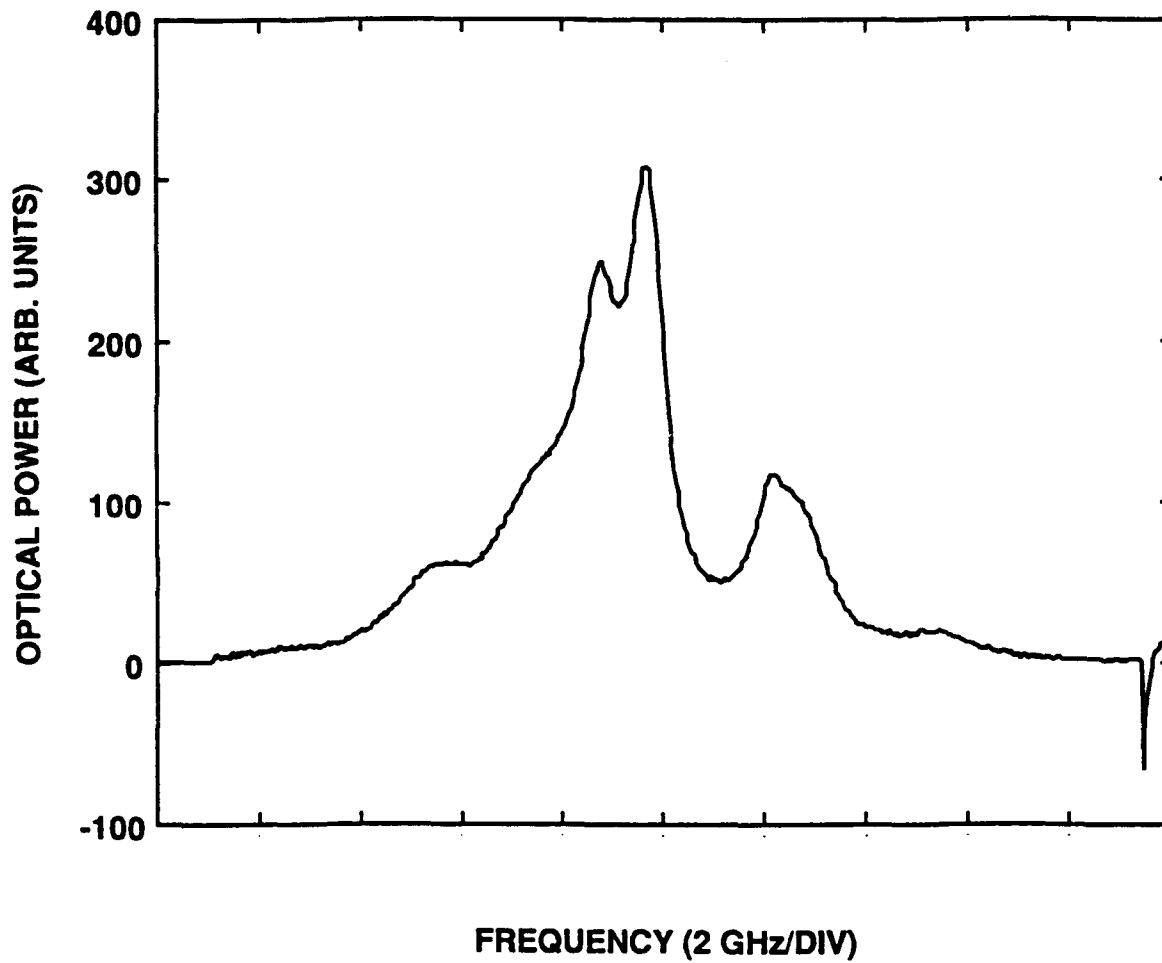


Figure 28. Optical spectrum analyzer trace showing the LT015 laser diode under strong optical injection ~3 GHz above the free-running frequency.

7.0 CONCLUSIONS

This program has investigated 4-wm in nonlinear waveguides, with a concentration on generation of a conjugate output beam in materials that exhibit both a strong nonlinearity and resonance with linear gain. The coupled-mode theory was used to develop a general formalism to describe nonlinear optical interactions in a waveguide. Under a wide range of experimentally and technologically relevant configurations, the basic result can be summarized:

$$\frac{dA_a}{dz} = \pm i \frac{2\pi\omega}{c} \exp(i\beta_a z) \iint dx dy P^{NL}(\mathbf{r}, \omega) \cdot \psi_a(x, y) \quad (178)$$

Here, the \pm refers to propagation along the $\pm z$ (waveguide) direction, the $\psi_a(x, y)$ and β_a are the linear mode transverse field patterns and propagation constants, respectively, and the A_a are the amplitude coefficients for each mode, which vary due to the nonlinearity. The modes are used to describe the electric field patterns:

$$\mathbf{E}(\mathbf{r}, t) = \sum_a A_a(z) \psi_a(x, y) \exp[i(\beta_a z - \omega t)] \quad (179)$$

The mode amplitudes become coupled through the effect of the nonlinear polarization:

$$\begin{aligned} P^{NL}(\mathbf{r}, \omega_0) &= \chi^{(2)}(\mathbf{r}, \omega = \omega_1 + \omega_2) : \mathbf{E}(\mathbf{r}, \omega_1) \mathbf{E}(\mathbf{r}, \omega_2) \\ &+ \chi^{(3)}(\mathbf{r}, \omega = \omega_1 + \omega_2 + \omega_3) : \mathbf{E}(\mathbf{r}, \omega_1) \mathbf{E}(\mathbf{r}, \omega_2) \mathbf{E}(\mathbf{r}, \omega_3) \\ &+ \dots \end{aligned} \quad (180)$$

An important feature of Equation 178 is its similarity to the coupled-wave formalism which has been used to successfully model nonlinear optical interactions in bulk media. Nonlinear phenomena in waveguides, such as 4-wm, can be modeled similarly to the bulk interaction, with the overlap integral of Equation 178 accounting for the spatial confinement effects. An important requirement for the use of a single amplitude coefficient, A_a , with each guided mode is that all fields involved in the nonlinear interaction can be

described by the propagating modes of a weakly guiding system. Though the coupled-mode theory can handle situations where all modes are not confined and the weakly guiding approximation does not hold, these situations will almost always tend toward reduced fidelity in replication of an input beam through the 4-wm process. This result, in combination with results of Hellwarth's earlier analysis (Ref. 11), puts strict limits on the speed and image fidelity of PC generation by 4-wm in nonlinear waveguides.

Of particular interest in this study are materials where the nonlinearity results from density gradients of mobile particles, such as semiconductors under current injection. In these materials, carrier diffusion acts to limit gradients of high-spatial frequency. Semiconductor waveguides generally have rectangular cross sections and transverse mode patterns which are, in general, described by two transverse spatial frequencies (Ref. 50). Nonlinear optical coupling will only occur between those modes where the spatial frequency difference is, approximately, less than the inverse diffusion length. This limits the divergence angle of an optical beam, or the angle between two incident beams, to a few degrees in a typical III-V semiconductor material. The experimental results of Lucente, *et al.* (Ref. 43) are consistent with this analysis.

To overcome these limitations in multimode waveguides, the use of an array of uncoupled, identical, single-mode waveguides was proposed. In addition to offering the potential of high-fidelity phase conjugation, the array can produce conjugate wavefronts whose propagation direction can be controlled by the pump beams. Unfortunately, a suitable array cannot be obtained to test the predictions of the model. In fact, understanding of 4-wm using two or three single-mode waveguides has yet to be achieved.

A particularly important waveguide is the laser diode. A variety of nonlinear phenomena, from saturation to chaotic behavior, have been observed. Specifically, 4-wm in laser diodes and traveling wave amplifiers has been investigated experimentally (Refs. 17, 43, 54 and 55) and theoretically (Refs. 16 and 41). Past work has shown large nonlinear amplification due to optically-generated, free-carrier density pulsations or gratings. The nearly degenerate 4-wm interaction has been shown to cause the laser diode to respond as a phase

modulated device, in the limit of a weak injection signal. In effect, the laser diode acts to minimize carrier modulations by generating a new frequency components.

This result, when compared with previously published results on 4- μm in laser diodes, raises several tantalizing questions. First, all previous results were made outside of the weak injection signal limit and show asymmetric sidebands on an optical spectrum analyzer. Because no RF spectra have been taken, carrier response in this regime has not been determined. The influence of two or n input beams on the diode output has not been measured, nor has the influence of the transverse coupling that exists, for example, in a diode array. Further, the nonlinear interaction medium is a Fabry-Perot. Placing a material with a strong nonlinear optical response within an optical cavity couples the amplitudes and phases of the circulating optical fields. While the importance of the optical feedback on the 4- μm has been recognized, the specific effects, particularly on phase relations between interacting beams, are not clearly understood. Recently, it has been demonstrated that a diode laser can be mode-locked when it is coupled to a linear, empty external cavity which provides direct feedback to the laser.* This implies strong nonlinear interactions between the laser modes under self-feedback. Because of the importance of optical phase relations to problems of technological interest, including the generation of a coherent optical output by arrays of laser diodes, further investigation of the basic physics of multiwave mixing in active nonlinear waveguides is an important task.

* G. Yao, P. Wang, Y.C. Chen, C.M. Harding, R.J. Dalby, R.G. Waters, J.M. Liu, and K.K. Lee, "Self-Starting Additive-Pulse Mode Locking in Semiconductor Lasers with Linear External Cavity," submitted to Opt. Lett.

REFERENCES

1. Optical Phase Conjugation, R.A. Fisher, Ed., New York: Academic (1982).
2. J. Feinberg and G.D. Bacher, Appl. Phys. Lett. **48**, 570 (1986).
3. J.O. White, G.C. Valley and R.A. McFarlane, Appl. Phys. Lett. **50**, 880 (1987).
4. M. Segev, S. Weiss and B. Fischer, Appl. Phys. Lett. **50**, 1397 (1987).
5. B. Fischer and S. Sternklar, Appl. Phys. Lett. **51**, 74 (1987).
6. Y. Owechko, G.J. Dunning, E. Marom, and B.H. Soffer, Appl. Opt. **26**, 1900 (1987).
7. D.Z. Anderson, Opt. Lett. **11**, 56 (1986).
8. P. Yeh, Appl. Opt. **26**, 602 (1987) and subsequent comments by A.M. Glass, et al. and P. Yeh, Appl. Opt. **26**, 3189 (1987).
9. A. Yariv, J.A. Yeung, D. Fekete, and D.M. Pepper, Appl. Phys. Lett. **32**, 635 (1978).
10. S.M. Jensen and R.W. Hellwarth, Appl. Phys. Lett. **33**, 404 (1978).
11. R.W. Hellwarth, IEEE J. Quantum Electronics **QE-15**, 101 (1979).
12. J.A. Yeung, D. Fekete, D.M. Pepper, A. Yariv, and R.K. Jain, Opt. Lett. **4**, 42 (1979).
13. G.I. Stegeman, C.T. Seaton and C. Karaguleff, IEEE J. Quantum Electronics **QE-22**, 1344 (1986).
14. H. Nakajima and R. Frey, Appl. Phys. Lett. **47**, 769 (1985).
15. D.S. Chemla, D.A. B. Miller, P.W. Smith, A.C. Gossard, and W. Wiegmann, IEEE J. Quantum Electronics **QE-20**, 265 (1984).
16. R. Frey, Opt. Lett. **11**, 91 (1986).
17. H. Nakajima and R. Frey, IEEE J. Quantum Electronics **QE-22**, 1349 (1986).
18. G.P. Agrawal, Opt. Lett. **12**, 260 (1987).
19. G.P. Agrawal, Appl. Phys. Lett. **51**, 302 (1987).
20. C. Karaguleff, G.I. Stegeman, R. Fortenberry, R. Zanoni, and C.T. Seaton, Appl. Phys. Lett. **46**, 621 (1985).
21. T.B. Simpson and J.M. Liu, in Resonances, A Volume in Honor of the 70th Birthday of Nicolaas Bloembergen, edited by M.D. Levinson, E. Mazur, P.S. Pershan, and Y.R. Shen, World Scientific Publishing, 221 (1990).
22. J.M. Liu and T.B. Simpson, Proc. SPIE **1220**, 32 (1990).

23. T.B. Simpson and J.M. Liu, Opt. Lett. **14**, 1383 (1990).
24. See, for example, a review by G.I. Stegeman and C.T. Seaton, J. Appl. Phys. **58**, R57 (1985).
25. Y.R. Shen, The Principles of Nonlinear Optics, Wiley, New York (1984).
26. B. Crosignani, A. Cutolo, and P. Di Porto, J. Opt. Soc. Am. **72**, 1136 (1982).
27. S.M. Jensen, IEEE J. Quantum Electronics **OE-18**, 1580 (1982).
28. Y. Kimura, M. Nakazawa, and S. Seikai, IEEE J. Quantum Electronics **OE-23**, 1261 (1987).
29. D. Marcuse, Theory of Dielectric Optical Waveguides, Academic, New York (1974).
30. A.W. Snyder, J. Opt. Soc. Am. **62**, 1267 (1972).
31. A. Yariv, IEEE J. Quantum Electronics **OE-9**, 919 (1973).
32. M.D. Feit and J.A. Fleck, Jr., Appl. Opt. **17**, 3990 (1978).
33. C. Yeh, W.P. Brown, and R. Szejn, Appl. Opt. **18**, 489 (1979).
34. J. Van Roey, J. van der Donk, and P.E. Lagasse, J. Opt. Soc. Am. **71**, 803 (1981).
35. R. Nietzke, P. Fenz, W. Elsässer, and E.O. Göbel, Appl. Phys. Lett. **51**, 1298 (1987).
36. L.D. Landau and E.M. Lifshitz, Electrodynamics of Continuous Media, Addison-Wesley, Reading, MA (1968).
37. R.F. Harrington, Time-Harmonic Electromagnetic Fields, McGraw-Hill, New York, p. 117 (1977).
38. D. Marcuse, Light Transmission Optics, Van Nostrand Reinhold, Princeton, NJ (1972).
39. H. Nakajima and R. Frey, Phys. Rev. Lett. **54**, 98 (1985).
40. K. Inoue, T. Mukai, and T. Saitoh, Appl. Phys. Lett. **51**, 1051 (1987).
41. G.P. Agrawal, J. Opt. Soc. Am. B **5**, 147 (1988).
42. M. Lucente, G.M. Carter, and J.G. Fujimoto, Appl. Phys. Lett. **53**, 467 (1988).
43. M. Lucente, J.G. Fujimoto, G.M. Carter, Appl. Phys. Lett. **53**, 1897 (1988).
44. M. Sargent III, F. Zhou, and S.W. Koch, Phys Rev A **38**, 4673 (1988).

45. W. Streifer, R.D. Burnham, and D.R. Scifres, IEEE J. Quantum Electronics QE-18, 856 (1982).
46. K. Otsuka and H. Iwamura, IEEE J. Quantum Electronics QE-19, 1184 (1983).
47. J.G. Provost and R. Frey, Appl. Phys. Lett. 55, 519 (1989).
48. A.P. Bogatov, P.G. Eliseev, and B.N. Sverdlov, IEEE J. Quantum Electronics QE-11, 510 (1975).
49. J.M. Liu and C. Yeh, Appl. Phys. Lett. 50, 1625 (1987).
50. E.A.J. Marcatili, Bell Sys. Tech. J. 48, 2071 (1969).
51. The waveguide propagating beam-coupling analysis is derived from H. Kressel and J.K. Butler, Semiconductor Lasers and Heterojunction LEDs, Academic, New York, p. 192 (1977).
52. M. Born and E. Wolf, Principles of Optics, 6th ed., p. 401 and following Pergamon, Oxford, UK (1980).
53. J.W. Goodman, Introduction to Fourier Optics, McGraw-Hill, New York, Chap. 2 (1968).
54. I. McMichael, M. Khoshnevisan, P. Yeh, Proc. SPIE 739, 7 (1987).
55. R. Nietzke, P. Panknin, W. Elsässer, E.O. Göbel, IEEE J. Quantum Electronics 25, 1399 (1989).
56. F. Favre and D. LeGuen, Electron. Lett. 25, 1053 (1989).
57. M.W. Hamilton, Contemporary Physics 30, 21 (1989).
58. K. Vahala, Ch. Harder, and A. Yariv, Appl. Phys. Lett. 42, 211 (1983).

APPENDIX A
DOT PRODUCT OTHOGONALITY RELATIONS

A simple set of dot-product orthogonality relations can be derived for CASES 2 and 3, when the propagation axis is an axis of symmetry for ϵ . This follows from the identity

$$\nabla \cdot (\mathbf{E}_a \times \mathbf{H}_b) = \frac{i\omega}{c} \mathbf{H}_a \cdot \mathbf{H}_b + \frac{i\omega}{c} \mathbf{E}_a \cdot \epsilon \cdot \mathbf{E}_b \quad (\text{A-1})$$

Integrating the equation over the transverse cross-sectional area and using Equations 52 and 53 in Subsection 3.3.2, the left-hand side of the equation vanishes for $\beta_a \neq \beta_b$. This leaves

$$\iint dx dy (\psi_a \cdot \epsilon \cdot \psi_b + \varphi_a \cdot \varphi_b) = \frac{2c\beta_a}{\omega} \delta_{a,b} \quad (\text{A-2})$$

Using the relations between the forward- and backward-propagating modes in Subsection 3.3.1 yields

$$\iint dx dy (\psi_{aT} \cdot \epsilon_T \cdot \psi_{bT} + \varphi_{az} \varphi_{bz}) = \frac{c\beta_a}{\omega} (\delta_{a,b} + \delta_{a,-b}) \quad (\text{A-3})$$

$$\iint dx dy (\epsilon_{zz} \psi_{az} \psi_{bz} + \varphi_{aT} \cdot \varphi_{bT}) = \frac{c\beta_a}{\omega} (\delta_{a,b} - \delta_{a,-b}) \quad (\text{A-4})$$

Equations A-3 and A-4 hold for both real and complex $\epsilon(\omega)$ so long as z is a symmetry axis for ϵ . No such simple relations are possible when z is not a symmetry axis.

It is important to note from Equations A-3 and A-4 that, in general,

$$\iint dx dy \psi_a \cdot \epsilon \cdot \psi_b \neq 0 \text{ and } \iint dx dy \psi_{aT} \cdot \epsilon_T \cdot \psi_{bT} \neq 0 \quad (\text{A-5})$$

$$\iint dx dy \varphi_a \cdot \varphi_b \neq 0 \text{ and } \iint dx dy \varphi_{aT} \cdot \varphi_{bT} \neq 0 \quad (\text{A-6})$$

When the transverse variation of the mode fields is slow on the scale of β^{-1} , then the z-component will be small relative to the transverse part of the fields. In this case, the integrated transverse dot product of different modes will be approximately zero. Alternatively, this term will be zero in specific geometries even though the z-component exists, such as the slab geometry where there is no dielectric variation along a transverse direction. For systems with cylindrical symmetry in general, the relations in Equations A-3 and A-4 complement the cross-product relations derived in Subsection 3.3.2.

APPENDIX B

ITERATIVE PROCEDURE FOR E WHEN $P_z^{NL} \neq 0$

When $P_z^{NL} \neq 0$, Equations 62 to 65 have to be used to expand the nonlinear field components in a waveguide. The mode coefficients, $A_a(z)$, cannot be solved directly through the coupled-mode equations. Instead, they can be solved self-consistently through an iterative procedure outlined below.

1. Initially set $P_z^{NL} = 0$.

2. Write

$$E_T = \sum_a A_a(z) \psi_{aT}(x, y) \exp(i\beta_a z) \quad (B-1)$$

$$E_z = \sum_a A_a(z) \psi_{az}(x, y) \exp(i\beta_a z) - \frac{4\pi}{\epsilon_{zz}} P_z^{NL} \quad (B-2)$$

In this step, $A_a(z)$ are unknown coefficients to be solved later, but an explicitly known P_z^{NL} given by the initial condition or calculated from the last iteration is used.

3. Using Equation 15, express P_T^{NL} and P_z^{NL} for the current iteration in terms of $A_a(z)$.

4. Write coupled-mode equations using Equation 81 and solve for $A_a(z)$.

5. Calculate P_T^{NL} and P_z^{NL} explicitly using expressions obtained in Step 3. Calculate E_T and E_z using the newly calculated values of $A_a(z)$ and P_z^{NL} .

6. Compare the new values of E and P^{NL} with those of the last iteration.
 - a. If significant difference exists, go to Step 2 using the newly calculated value of P_2^{NL} for the input.
 - b. Otherwise, a self-consistent solution for E and P^{NL} is obtained.